HERON is jointly edited by:
STEVIN-LABORATORY of the faculty of Civil Engineering, Delft University of Technology, Delft, The Netherlands
and
TNO BUILDING AND CONSTRUCTION RESEARCH. Rijswijk (ZH), The Netherlands
HERON contains contributions based mainly on research work performed in these laboratories on strength of materials, structures and materials science.

ISSN 0046-7316

This publication has been issued with the financial support from the Netherlands Technology Foundation (STW)

Secretary:
J. G. M. van Mier
Stevinweg 1
P.O. Box 5048
2600 GA Delft, The Netherlands
Tel. 0031-15-784578
Fax 0031-15-611465
Telex 38151 BUTUD

HERON vol. 38 1993 no. 3

Contents

A MICROMECHNICAL INVESTIGATION OF SOLFTENING OF CONCRETE LOADED IN COMPRESSION

R. A. Vonk
Eindhoven University of Technology
Faculty of Architecture and Building Science
Department of Structural Design
The Netherlands

Publication in HERON since 1970

Abstract

In this work softening of concrete specimens loaded in uniaxial compression is investigated by simulations with a micromechanical model. The simulation results are compared with experimental results. The micromechanical model calculates the mechanical response of the heterogeneous composite structure of concrete by simulating the crack-growth process. This is done by means of finite element analysis and fracture mechanics. Both distributed crack growth and localization into macrocracks is described by the model. The dependence of crack growth and softening response on the internal heterogeneous composite structure, the dimensions and the boundary conditions is shown.

Keywords
Concrete, uniaxial compression test, cracking, failure, softening, micromechanical model, finite element analysis, fracture mechanics.

A micromechanical investigation of softening of concrete loaded in compression

1 Introduction

1.1 *Subject of research*

Softening of concrete

This work deals with research into softening of concrete loaded in compression. Softening is a gradual decrease of mechanical resistance due to a continuous increase of deformation forced upon a material specimen or structure. It is a salient feature of quasi-brittle materials like concrete and rock, which fail due to a process of internal crack growth. Softening of concrete is important in the assessment of structural safety due to the fact that well-designed structures show considerable crack growth before attaining peak load.

Finite element analysis

During the last few decades, computer power has increased enormously. This has stimulated the use of finite element analysis in research and design of concrete structures. It has become possible to calculate the total load-deformation relation up to failure in the case of arbitrary structures. The nonlinear behaviour due to crack growth under multiaxial stress states can be taken into account. This has created the demand for knowledge of nonlinear material behaviour and numerical techniques to take into account the nonlinear behaviour. Knowledge in both has progressed significantly and has resulted in adequate models and methods.

Fracture mechanics

Fracture mechanics, studying the behaviour of cracks under load, was given a new impulse by the growing possibilities of numerical analysis of concrete structures. It concentrated mainly on the description of the growth of cracks under tensile loading. Although concrete loaded in compression fails due to crack growth too, knowledge on tensile failure did not yet include compressive failure, possibly because tensile cracking was considered more important, because compressive failure was not recognized to be a fracture-mechanics problem and because compressive failure is a much more complex phenomenon than tensile failure. In 1984, test results of Van Mier at Eindhoven University of Technology gave the first strong indication that fracture mechanics governs compressive failure of concrete and that it can not be described adequately by continuum mechanics. Therefore the present work is directed to a fracture-mechanics approach to compressive failure of concrete.

Structural behaviour

Recently, the statement "compressive failure is a structural behaviour" (Van Mier

[1984]) is encountered more and more in literature. Two reasons can be mentioned. First, it is caused by the fact that continuum mechanics falls short of adequately describing softening of concrete. The mechanical response of a softening concrete specimen is governed by a local fracture process which dominates the behaviour of the surrounding continuum. The heterogeneity of concrete plays an important role in this process. The response of the specimen is a combined action by several components, which can be looked upon as the behaviour of a structure. Second, compressive softening of concrete proves to be highly dependent on the boundary conditions. They play an essential role in the softening process, which should not be overlooked. Our knowledge of the structural behaviour is limited, which has made test results ambiguous and their interpretation difficult. Therefore, the present work gives special attention to the structural behaviour found for compressive softening.

Growing interest

Progress in the field of fracture mechanics has generated a growing interest in the subject and its applications in structural design. Results are finding their way to the building codes (ACI [1990], CEB-FIP [1991]). For the moment, this is mainly as far as the application of tensile properties of concrete are concerned. In the case of compressive failure the CEB-FIP Model Code states that there is a lack of experimental data and lays down a "conservative" stress-strain relation. However, if fracture mechanics is applicable to compressive softening, no such softening stress-strain relation is correct. Then the softening depends on the size of the structure. In the worst case no softening will be found and a highly brittle failure will occur at peak stress. Investigators have recently published work to show the importance of a better knowledge of the real nature of compressive failure for the rotational capacity of beams (Hillerborg [1988, 1991], Rokugo & Koyanagi [1992]). It appears that an exact knowledge of compressive softening is as important in the failure of concrete structures as that of tensile softening. Both peak load and rotational capacity of beams are influenced by the assumptions of compressive softening.

"Concrete Mechanics" project

Research into the nonlinear analysis of mechanical behaviour of concrete structures is organized in The Netherlands in the CUR "Concrete Mechanics" project. It aims at the development of numerical tools for the analysis of the behaviour of concrete structures and fundamental research towards the formulation of reliable constitutive models. The research described in this work is part of the CUR "Concrete Mechanics" project. The Technical Universities of Delft and Eindhoven, TNO Building and Construction Research, Dutch building companies and structural engineering consultants cooperate in this project, which is coordinated by the CUR (Centre for Civil Engineering Research and Codes).

1.2 *Aim, scope and method*

Aim

The aim of this research is to increase the knowledge of compressive failure of concrete in order to enable reliable modelling of this phenomenon.

Scope

This research concentrates on mechanical analysis and modelling of the structural behaviour of softening concrete loaded in compression. A link is made between fracture mechanics and compressive softening of concrete. The three-dimensional process of crack formation is analysed as it is governed by the heterogeneity of concrete, the boundary conditions and dimensions of concrete specimens. The behaviour of normal-strength concrete with relatively stiff and strong aggregates is considered. The influence of drying shrinkage, creep or loading rate is left out of consideration, although these aspects certainly play an important role in concrete softening.

Method

Compressive softening of concrete specimens is investigated by simulating the crack-growth process inside these specimens by means of a micromechanical model. In this model the heterogeneous structure of concrete and its influence on crack growth are simulated by means of finite element analysis and fracture mechanics. This approach has recently proven to be promising for the research into tensile softening of concrete. The advantage of the micromechanical approach is that the crack-growth process inside the concrete, causing the structural behaviour, can be followed continuously in time and in space and that the influence of the composition of the material, the dimensions and boundary conditions can easily be varied to investigate their influence. Further, a micromechanical model can be a first step to a more simple model to describe concrete behaviour for use in structural engineering.

The results of the micromechanical simulations are compared with test results. In the test the dimensions and boundary conditions of the specimens have been varied to be able to study their influence on the structural behaviour of the specimens. Extensive deformation measurements have been carried out and a simple but effective method has been developed to record the crack patterns inside the specimens after a test.

1.3 *Compressive softening of concrete*

Definition of softening

Softening is a gradual decrease of mechanical resistance due to a continuous increase of deformation forced upon a material specimen or structure.

Softening is found in a deformation-controlled test on a specimen of concrete. A characteristic nominal stress-deformation relation found in such a test is shown in Fig. 1. Under increasing deformation, the tangential stiffness of the specimen K_t shows

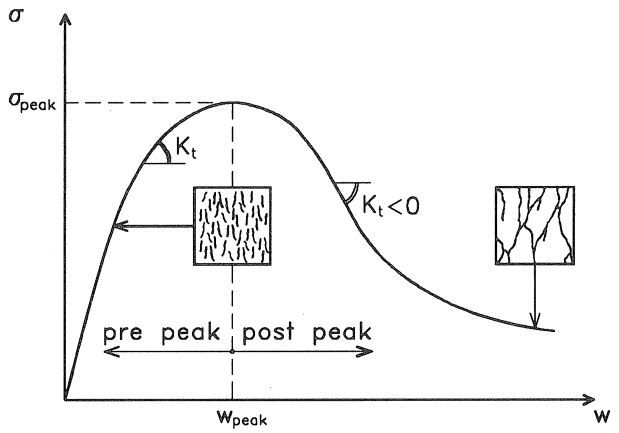

Fig. 1. Characteristic nominal stress-deformation relation of a concrete specimen loaded in compression under deformation control.

a continuous decrease until it is zero for peak stress. The post-peak decrease of mechanical resistance due to the continuous increase of deformation is called softening. It is characterized by the descending branch of the nominal stress-deformation curve which has a negative tangential stiffness K_t. In this work K_t will be used as the measure for brittleness. The behaviour of a specimen will be called more brittle, when the minimum value of the tangential stiffness K_t during softening is smaller.

Cause of softening

Concrete is a heterogeneous material comprising hardened cement paste, aggregates and voids. Internal stiffness and strength show a significant variation. Moreover, initial stresses and cracks are already present before loading. This causes that a progressive crack growth is found in a concrete specimen when it is subjected to a progressive deformation. Especially the weak interface between the large aggregates and the mortar plays an important role in this process of crack growth (Hsu et al. [1963]). The material is gradually weakened because a continuously diminishing number of internal bonds is capable of opposing the externally applied deformation. This finally results in softening of the specimen.

Localization of cracking and deformations

In view of the progressive crack growth, there seems to be no use in distinguishing between pre-peak nonlinear behaviour and post-peak softening. There seems to be a continuous process. Initially, the cracking starts as distributed microcracking. The microcracks are stable, which means that they grow only when the load is increased. Around peak load an acceleration of cracking takes place and the formation of macrocracks starts. The macrocracks are unstable, which means that the load has to

decrease to avoid an uncontrolled growth. In a deformation-controlled test, this macrocrack growth results in softening and localization of cracking, which is the most salient feature connected to softening. Localization of cracking means that all further cracking, but also deformations, concentrate in a small zone, while the concrete parts in series with this zone show no further cracking, but a decrease of deformations due to unloading. This phenomenon is quite clear for tensile failure.

Localization in tension

Bazant [1976] has shown that strain softening in a homogeneous continuum prefers to localize in the smallest volume possible, a straight plane. The heterogeneity of concrete prevents this. Localization of cracking and deformations in tensile tests on concrete comes close to localization of deformations in a zero volume (Gopalaratnam & Shah [1985], Cornelissen et al. [1986], Hordijk [1991]). Therefore, it has become common use to describe tensile cracking by means of a crack model with no volume (see Chapter 1.4, Hillerborg et al. [1976], Elfgren (ed.) [1989]). The behaviour of this crack is described by means of a stress-crack-opening relation including softening. This model will be used to demonstrate the consequences of localization of deformations for the behaviour of a concrete specimen. In this example the continuum behaviour will be described as linear elastic.

The consequences of localization at peak stress are shown in Fig. 2. The main consequence is that the behaviour of a concrete specimen becomes size dependent. The crack stress-opening relation is given in Fig. 2a as curve 0. It shows a gradual softening with crack opening, which starts when the tensile strength f_t is reached. The figure shows further the influence of the measuring length on the shape of the measured stress-deformation curve. For increasing measuring length, or specimen size, the elastic deformations of the continuum around the crack become more and more important, both in the pre-peak region and in the post-peak region. The post-peak curve becomes steeper due to the increasing influence of unloading of the continuum for an increasing measuring length. Even snap-back behaviour is found. In Fig. 2b the influence of localization of deformations on the measured stress-strain behaviour is given. In contrast with the pre-peak behaviour, it is found that the post-peak behaviour is size dependent. The observed behaviour becomes more brittle when the measuring length increases. This cannot be described by a continuum model. It is the most important consequence of localization of cracking and deformations.

Localization in compression

In the last few years researchers have started to realize that softening of concrete loaded in compression is probably also accompanied by localization like softening of concrete loaded in tension. Very little is known about this localization. An important indication that localization is present in uniaxial compression is found in experimental results of Van Mier [1984, 1986ab]. He carried out compression tests on specimens of different height and found that the softening depends on the height of the specimen (Fig. 3a). On

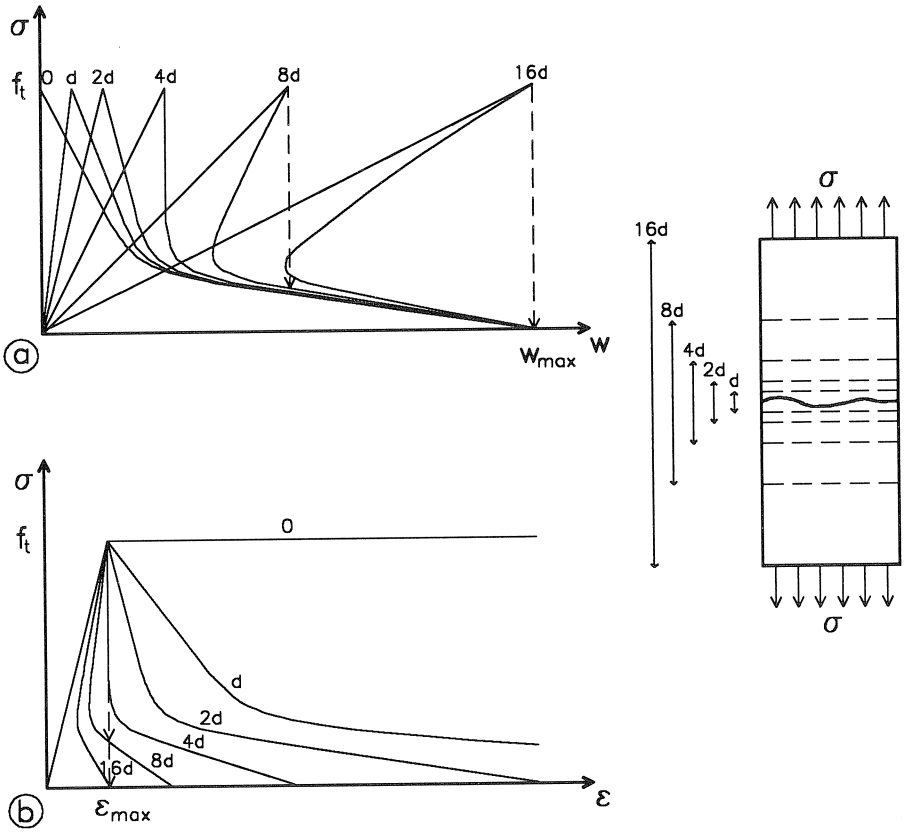

Fig. 2. Consequences of localization of deformations in a tensile test on (a) stress-deformation relation and (b) stress-strain relation.

comparing the post-peak stress-deformation curves, a striking resemblance was found (Fig. 3b). This indicates that post-peak behaviour of concrete loaded in uniaxial compression is also governed by a local fracturing process as found in uniaxial tension.

Material property or structural property?

In a homogeneous continuum every part of the volume has the same properties and reacts in the same way to an external action. The notions stress and strain then have a meaning. The stress can then be determined from the response of a test specimen by dividing the force by the total area transmitting this force and the strain by dividing the deformation by the distance over which the deformation is found. When the loading is uniform and the boundary conditions are chosen correctly, the relation between stress and strain is unique and does not depend on the size and shape of the specimen. This unique relation can then be called a *material property.*

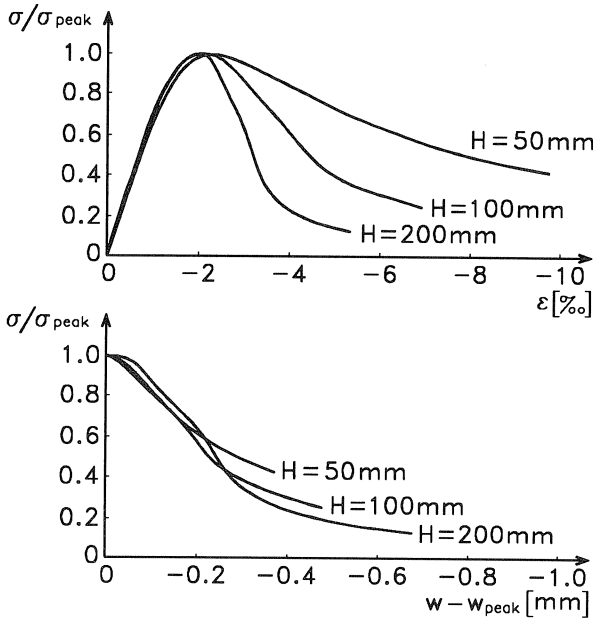

Fig. 3. (a) Stress-strain curves and (b) post-peak stress-deformation curves for concrete specimens of different height loaded in uniaxial compression (Van Mier [1984, 1986ab]).

The theory of the homogeneous continuum is applicable to concrete, even though it is a heterogeneous material, when the size of the concrete volume is much greater than the characteristic size of the heterogeneity. Within a small stochastic scatter, the relation between stress and strain can be determined as a material property. Sometimes the terms nominal stress and nominal strain are used to remind one that concrete is a heterogeneous material and that the calculated values are only average values for the total specimen.

During microcrack growth, the theory of the homogeneous continuum is still applicable to concrete because the microcracks are at the scale level of the heterogeneity of concrete. When macrocracks start to grow, the scale level of the cracks quickly rises to the scale level of the structure. The continuum theory is no longer applicable. Stress and strain lose their meaning. The cracks have to be taken into account as discontinuities which, together with the continuum, determine the behaviour of the structure. Due to the discontinuity, the response of the structure becomes dependent on its size. This is why softening has been termed to be a *structural response* (Bieniawski [1967], Van Mier [1984, 1986ab]). As a fact, softening cannot be measured as a property of concrete irrespective of the dimensions. It is a combined response of a local and a continuous process. The local process is governed by fracture mechanics, which describes the behaviour of cracks. The structural response can only be analysed by making assumptions as to the local and the continuum components of the behaviour

and verifying whether they give the correct response for the total structure. It is important that this is done by taking the correct boundary conditions into account. It has been found that compressive softening is highly sensitive to the boundary conditions. They have bedevilled the discussion about softening being a structural property owing to their dominant and often unexpected role in test results.

Structural behaviour observed in tests

To be able to model correctly the structural behaviour of concrete loaded in compression, it is important to know where and when localization of cracking takes place. This is not yet well-known, due to the fact that tests have proven to be very sensitive to the present boundary conditions.

Lateral expansion is essential to compressive failure of concrete. A lateral confinement makes concrete stronger and more ductile (Gerstle et al. [1978, 1980]) and delays (Jamet et al. [1984]) or even prevents (Bazant et al. [1986]) softening and macrocrack formation. It is a well-known fact that the restraint of lateral deformations by loading platens influences peak stress in a compression test (Schickert [1980]). The shear stresses induced in the concrete specimen cause triaxial compressive stress states near the loading platens, which prevent or slow down cracking there. When plain steel platens are used, this results in the well-known hour-glass failure mode (Fig. 4a). Softening is caused by the growth of cracks from the outside to the inside, which causes a constant reduction of the load-bearing core of the specimen (Hudson et al. [1972], Read & Hegemier [1984]).

When the boundary restraint to the lateral deformations is reduced, a distributed type of failure mode is found, which shows a significant amount of prominent vertical splitting cracks besides a number of shear cracks (Fig. 4b, Van Mier [1984], Shah & Sankar [1987]). The distributed character of the crack pattern has caused the lack of

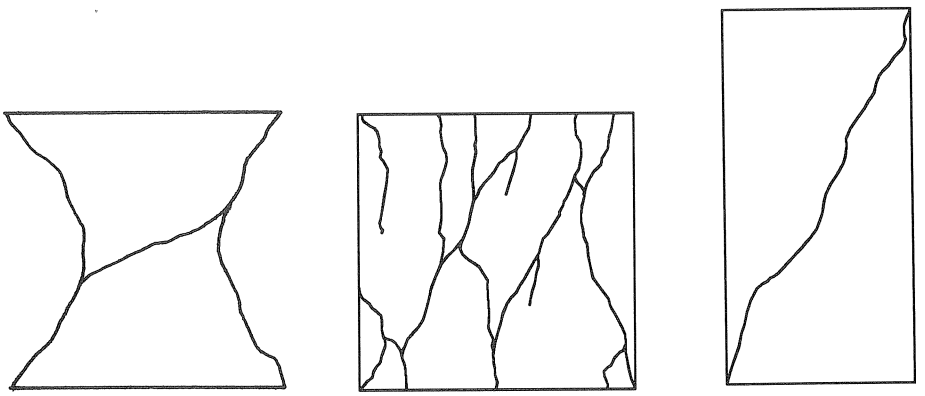

(a) (b) (c)

Fig. 4. Failure modes found in uniaxial compression.

agreement about localization of cracking and deformations in uniaxial compressive softening. Also for these tests with a small lateral boundary restraint a growth of cracks from the outside to the inside is reported. It is not clear whether this is still due to the small lateral boundary restraint or that it is due to shrinkage stresses present in the specimens, the wall effect as a result of casting or the discontinuity found at the edge of the specimen.
The influence of the loading platens on peak stress can be made negligible by increasing the slenderness of the specimen (Schickert [1980], Kotsovos [1983]). Tests carried out by Kotsovos [1983] show that the influence of the lateral boundary restraint in compressive softening tests is hard to eliminate. Kotsovos assumes that cracks are initiated in the central uniaxially stressed zone of the specimen and that their propagation is delayed by the triaxial compressive stress state near the loading platens. Based upon these test results, Kotsovos comes to the conclusion that the compressive softening found in tests is probably almost completely due to the boundary restraint and that it would be most realistic to describe concrete post-peak behaviour by a complete and immediate loss of load-carrying capacity.

Localization of deformations in one shear crack is found in tests on slender specimens which are loaded with a hinged loading platen (Fig. 4c, Newman and Sigvaldason [1965–1966], Kotsovos [1983], Van Mier [1984, Torrenti et al. [1989]). Newman and Sigvaldason showed that the use of one hinged loading platen can change a more distributed failure mode into a failure mode with one shear crack. Van Mier [1984] found that the increase of the height of the specimen increases the chance of finding a failure mode with one shear crack. The tests by Kotsovos [1983] show that the inclination of the shear crack decreases when the lateral boundary restraint decreases.

Generally, it is assumed that the process of localization starts around peak stress. Cracks larger than the maximum aggregate size are already found before peak stress is reached (Hsu et al. [1963], Carrasquillo et al. [1981]). Tests carried out by Torrenti et al. [1989] indicate that the formation of the shear crack starts before peak stress is reached. Then, the crack grows slowly during softening. This constant crack growth during softening has also been observed in tensile tests (Hordijk et al. [1987]). The localization and crack growth observed by Torrenti et al. can probably be explained by the nonuniform stress state in the specimen caused by the lateral restraint by the loading platens and the rotation of the hinged loading platen. An extensive analysis of the influence of a hinged loading platen on compressive testing can be found in Vonk [1992].

Besides Van Mier [1984, 1986ab] others have also carried out tests on specimens of different height for rock (Hudson et al. [1972]) and concrete (Rokugo & Koyanagi [1992]). However, these researchers did use loading platens which are known to influence compressive failure significantly, depending on the shape of the specimen. In these tests the size effect caused by the influence of the loading platens is much more

significant than the size effect caused by softening. It is very difficult to unravel the influence of both size effects. The brush platens used by Van Mier were known to influence compressive failure significantly less.

Failure mechanism

The crack growth in concrete loaded in compression results finally in a continuous crack pattern, which divides the concrete volume into a number of triangular or conical pieces which can shear off. This is schematically shown in Fig. 5. This kind of mechanism was reported by Van Mier [1984] for both uniaxial and multiaxial compression. A single shear fracture dividing a slender specimen in two has also been reported (Newman & Sigvaldason [1965–1966], Kotsovos [1983], Torrenti et al. [1989]).

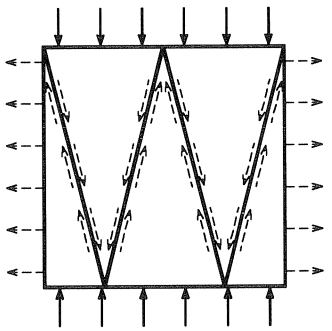

Fig. 5. Schematized failure mechanisms of concrete loaded in compression.

Tensile splitting cannot account for the inclined cracks needed for the formation of the mechanism shown in Fig. 5. Splitting cracks can have a slight inclination to the direction of the maximum compressive load, but will mainly grow in the direction of this load or otherwise be arrested by this load. However, often only the splitting cracks are reported by researchers, without questioning the kinematics of the failure mechanism. It can be argued that, after the concrete is split up into many slender columns, failure will take place due to bending and buckling of these columns. This failure mode is not likely to be found when lateral compression is present and cannot account for failure in multiaxial compression. It is more likely that the shear failure, which is found in multiaxial compression tests, is also present in uniaxial compression tests, but is modified by the formation of many splitting cracks. The tests on slender specimens, which fail due to the formation of one shear crack, indicate that the formation of splitting cracks is not essential to failure in uniaxial compression.

Shear cracking

The above indicates that a shear-crack mechanism is present in concrete compressive failure. Observations on crack formation in rock (Paterson [1978], Read & Hegemier [1984]) show that in this type of material shear cracks are formed through an array of

"en echelon" splitting cracks, which becomes unstable at a certain load (Fig. 6a). It is not unlikely that this kind of mechanism can also account for concrete compressive failure, because rock and concrete show many features in common in their failure behaviour. Stroeven [1973] reported the same arrays of splitting cracks on top of the large aggregates in concrete loaded in compression at the location where splitting cracks along the aggregate surface grow into shear cracks through the mortar (Fig. 6b). When the density of these splitting cracks is critical for the state of loading, failure occurs by a complex process of bending, buckling and crushing. This process is not well known. Horii & Nemat-Nasser [1985, 1986] have shown by model calculations and model tests on brittle resin specimens that weakening of a material by splitting cracks can result in shear failure under compressive loading.

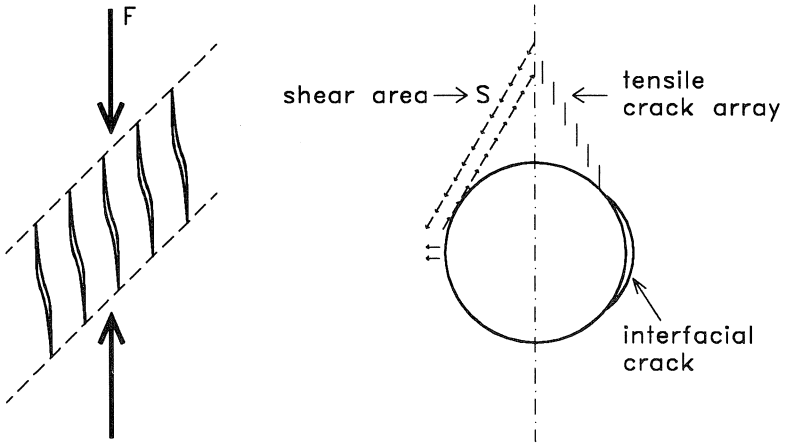

Fig. 6. (a) Shear loading of an array of splitting cracks in a compression test and (b) crack pattern reported by Stroeven [1973].

"Direct" shear tests

Recent "direct" shear tests (Hordijk et al. [1989]) have shown that it is difficult, if not impossible, to create pure shear loading without introducing any tension into the test specimen. Concrete is so much more sensitive to tensile failure than to shear failure that tensile failure always seems to dominate as soon as the slightest tensile stress is present. Finite element analysis of the tests carried out have shown that they can be simulated well by only using tensile crack models with crude assumptions for the behaviour under shear loading (Ingraffea & Panthaki [1985], De Borst [1986], Rots [1988]). It is now clear that these tests can not be used to investigate shear failure.

1.4 *Modelling of softening*

Continuum models

The development of finite element analysis has been a great stimulus to the formulation of nonlinear material models. Since the method was initially fully directed to the

description of continuum behaviour a large number of continuum models has been formulated (Vonk [1992]). It seems that these models are basically able to describe any nonlinear triaxial continuum behaviour under monotonic loading including softening. Unloading or cyclic loading can also be covered. However, the complexity of a model would be enormous when all these features are covered and no such model is to be found in literature.

Drawbacks of continuum models

1 Rotation of axes of principal stress and strain

A severe limitation is that the models are restricted to the principal stress or strain space. They do not take into account a rotation of the axes of principal stress or strain, which can lead to significant errors (Bazant [1983]), especially for softening when the orientation of damage changes the material from isotropic to highly anisotropic. This is no imaginary problem, because nonlinear structural behaviour causes these changes in principal stress or strain direction easily (see for example Rots [1988]). The correct approach is to link the state of damage with its orientation to the material and to calculate the response of the material to some kind of loading out of this state of damage. This is done in the concept of the microplane model (Bazant & Gambarova [1984], Bazant & Oh [1985], Ozbolt & Bazant [1991], Ozbolt & Eligehausen [1991]). The application of this model in finite element analysis, has been limited because of the significant demand for calculation time.

2 Localization of deformations

For this research the most severe limitation of the continuum models is found in the fact that they do not take into account the localization of deformations caused by strain softening. Some of the continuum models have been fitted directly to test results including softening, thus neglecting the phenomenon of localization. This means that the predicted behaviour will not be correct for any specimen of different size than the one used in the test or broadly speaking for any other concrete structure. Localization of deformations due to softening is incompatible with the classical continuum approach used up to now in modelling or interpreting test results. New ways have to be found to take the localization of deformations into account.

Fracture mechanics

Because softening of concrete is due to crack formation, many researchers have directed their efforts to the formulation of models for crack initiation and propagation. The most popular has become the cohesive-crack model, because it can predict both crack initiation and crack propagation and is easy to incorporate in finite element programs (Elfgren (ed.) [1989]). Linear-elastic calculations show that in front of the crack tip the stresses go to infinity, which will cause microcracking in that zone (Fig. 7). In a cohesive-crack model this zone is modelled as a part of the crack, which is not stress free but contains cohesive stresses. Hillerborg et al. [1976] were the first to apply a cohesive-crack model for the description of concrete cracking. Their "fictitious crack

model", which models a crack as a line crack, assumes that the cohesive stresses in the microcracked zone soften gradually as a function of the deformation of this zone (Fig. 8). The model predicts microcrack formation, which initializes softening, when the tensile strength f_t is reached. A stress-free macrocrack is formed when the opening of the fictitious crack is equal to w_{max}. These two parameters, together with the shape of the softening curve and the surface underneath it, the fracture energy G_f, are assumed to be material properties.

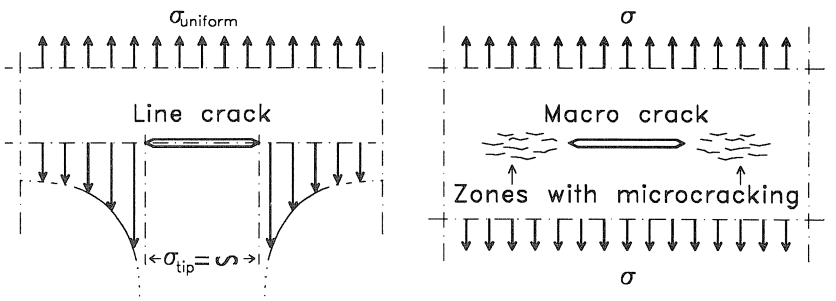

Fig. 7. (a) Stresses around a crack tip in an elastic medium and (b) microcracked zone in front of a crack tip.

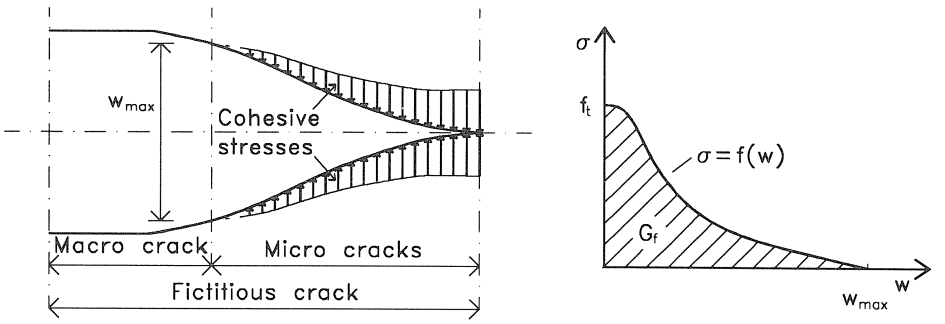

Fig. 8. Fictitious crack model (Hillerborg et al. [1976]).

Finite element analysis

Three concepts can be distinguished to describe cracking and softening in finite element analysis:

1. discrete-crack concept
2. smeared-crack concept
3. enriched-continuum concept

Discrete-crack concept

When the discrete-crack concept is used, each crack is modelled separately and is taken

into account as a discontinuity in the finite element mesh. Three important approaches can be distuiguished:

1 Crack path known in advance

When the crack path is known in advance, it is easily incorporated in the initial mesh of continuum elements as a series of interface elements, which represents the crack path (Fig. 9a, Rots [1988], Hillerborg & Rots [1989]). The need to know the crack path in advance is of course a severe limitation of this approach.

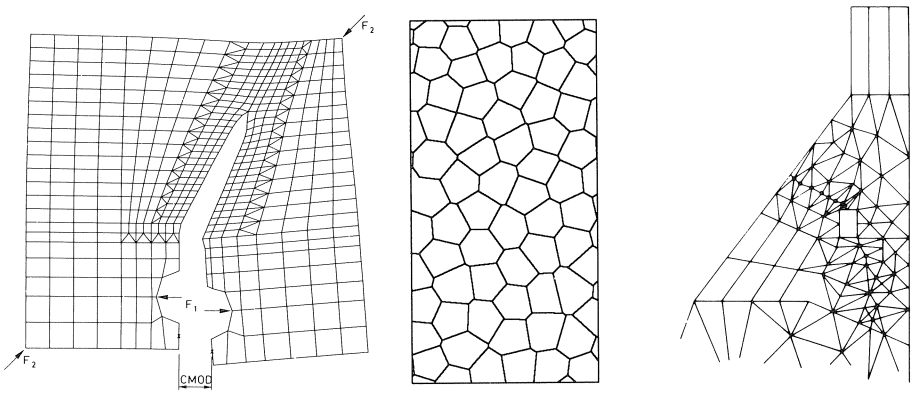

(a) (b) (c)

Fig. 9. Examples of discrete modelling of cracks: (a) crack path known in advance (Rots [1988]), (b) discontinuum (Lorig & Cundall [1987]), (c) remeshing (Ingraffea & Saouma [1985]).

2 Remeshing

When it is desired to keep crack propagation independent of the initially chosen finite element mesh, a technique of remeshing can be applied (Fig. 9b, Ingraffea and Saouma [1985]). Based on calculated continuum stresses, a prediction can be made for the extension of the crack, which determines the new configuration of the mesh incorporating the crack as a discontinuity. For implicit methods this means that the set of equations governing the problem must be reformulated and solved again completely from the start. It is clear that this takes a lot of computer time.

3 Discontinuum

When the crack path is not known in advance, it is possible to model a continuum separated by a continuous mesh of interface elements, which represents all potential crack paths (Fig. 9c). Then it is better termed a discontinuum than a continuum. The mesh of interfaces can be fully random, but can also be modelled taking into account the actual internal structure of the material. In rock mechanics it is an accepted method to model joints and discontinuities in this way. This method is used also in the Distinct Element Method (Cundall [1971], Cundall & Strack [1979], Lorig & Cundall [1987]), which is applied to the micromechanical simulations in the present investigation. A

drawback of this approach can be that the exact configuration of the mesh is not known or can not be established.

Smeared-crack concept

The smeared-crack concept was developed to overcome the problems of incorporating discontinuities in the finite element mesh and to have perfect freedom of crack initiation and growth (Bazant [1986], De Borst [1986], Rots [1988]). This concept soon became more popular than the discrete-crack concept adopted earlier, because it fits in better with the nature of the finite element method, which was directed initially only to the description of continuum behaviour. In the smeared-crack concept, the behaviour of the cracks in the concrete is translated to an equivalent stress-strain behaviour of the finite element containing the cracks. To obtain mesh-independent results (Bazant [1986]), the fracture energy of the element is made independent of the element size. It has been used mainly for simple tensile failure.

Problems with strain softening

Recently is was discovered that it is very difficult to incorporate softening correctly in the classical concept of the finite element method by means of strain softening as described by continuum models and smeared-crack models. The finite element method was entirely conceived and developed to the discretization of continuum behaviour on the assumption of displacement continuity. The displacement discontinuity due to crack formation, which is described by softening, seems to be incompatible with this method. It has been shown that the use of strain softening leads to dependency of calculation results on the size, shape, orientation and type of the finite elements (Bazant [1986], De Borst [1986], Rots [1988], Steinmann & Willam [1991]). Further, spurious local kinematic modes are found, which lead to instabilities hampering the solution procedure for the total structure (De Borst [1989]).

Characteristic length

Keeping the fracture energy independent of the size of the finite element by making strain softening dependent on the size of the finite element only solves the problem of mesh dependency in a few simple cases. A more general method is needed. Simple dimensional analysis shows that a parameter representing a length is needed to change strain-softening in a local fracture behaviour. Therefore, researchers have turned to enrichment of the classical continuum formulation with a characteristic length, which is used to control the localization of strain softening in a certain area (De Borst [1991]). This characteristic length is usually assumed to be related to the heterogeneity of concrete. It is a common assumption that the heterogeneity dominated by the large aggregates controls the spread of microcracking and macrocracking and thus the area which shows softening. Most important from a mathematical point of view is that enriching the governing field equations for the continuum with terms incorporating a characteristic length, prevents the system of equations from losing its elliptic character.

Comment

The enriched-continuum approaches can technically control strain localization under general loading conditions. What approach is most effective and how well concrete behaviour under all loading conditions can be described by these methods is not yet clear. The methods are very new and a thorough verification has not yet been carried out. They are a logical extension from an existing method which has proved its effectivity. The characteristic length introduces some notion of heterogeneity in the homogeneous continuum. How this characteristic length is related to the heterogeneity of concrete, whether it depends on the state of loading, what it really represents and how it can be identified or measured is not yet known.

Fracture mechanics and shear cracking

Tensile cracking is the most important and perhaps the sole cause of concrete softening. Still, it is difficult to model shear softening or compressive softening with tensile models. Perhaps this can be done when the heterogeneity of concrete is modelled down to a very low scale level. By means of linear-elastic fracture mechanics (LEFM) it can be shown that tensile cracking can take place in heterogeneous materials under shear loading or compressive loading (Di Tomasso [1984], Van Mier [1984], Horii & Nemat-Nasser [1985, 1986]). Even under triaxial compression tensile stresses can be found around a void or crack (El-Rahman & Shrive [1984]). However, LEFM has not brought forward a practical model for the description of shear cracking or compressive cracking.

Mohr-Coulomb type models

Up to now, the most practical models have been the Mohr-Coulomb type models, which limit and control the shear stress at a plane as a function of the normal stress on that plane (Fig. 10a). Many of the continuum models feature this limitation too. Though they are formulated in principal-stress space, they actually limit the shear stress on certain planes. How a shear band in a specimen loaded in compression is predicted by the use of a Mohr-Coulomb continuum model is illustrative (Fig. 10b, De Borst [1986]). When the shear plane is known, it is also possible to use a Mohr-Coulomb type of model for the description of interface behaviour. Simple interface models of this type have been used by Roelfstra et al. (Roelfstra & Sadouki [1986], Roelfstra [1989]) and

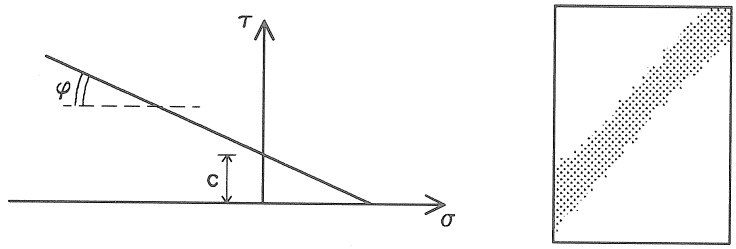

(a) (b)

Fig. 10. (a) Mohr-Coulomb criterion and (b) shear band predicted with a Mohr-Coulomb continuum criterion formulated in principal stress space (De Borst [1986]).

Lorig & Cundall [1987]. In these models a tension cut-off criterion is added to the shear-failure criterion. Recently, a more complex model for combinations of tensile and shear loading including softening has been proposed by Stankowski [1990].

Aggregate interlock models
It has long been recognized that the shear resistance of tensile cracks, which have opened and are subsequently subjected to a shear deformation, still can have a significant value. This is due to the irregular shape of the crack faces, caused by the fact that the cracks have to curve around the aggregates in the concrete. Under shear loading, the irregularly shaped crack faces make contact and cause the shear resistance. This phenomenon is called aggregate interlock. Adequate models have been proposed to describe this behaviour (Walraven [1980], Bazant and Gambarova [1985]). A complete model for crack behaviour should of course cover both the behaviour of a crack under tensile and shear loading during initiation and after opening.

2 Micromechanical model

2.1 *Introduction*

In a micromechanical model the microstructure of a material is modelled to be able to analyse the behaviour of the material as a composite. It has recently been shown that micromechanical models are a powerful tool for analyzing softening of concrete. For the description of concrete behaviour two types of micromechanical models can be distinguished: the truss models and the finite element models. Truss models have been developed by Zubelewicz & Bazant [1987], Bazant et al. [1990] and Schlangen & Van Mier [1991, 1992]. The properties of the truss models are modelled in such a way that the microstructure of concrete is described as close as possible. Finite element models have been developed by Roelfstra et al. (Roelfstra & Sadouki [1986], Roelfstra [1989]) and Willam et al. (Willam et al. [1989], Stankowski [1990]). In these models the heterogeneous microstructure of concrete is modelled very realistically by means of finite elements. The truss models are purely based on fracture mechanics, while the finite element models are still partly based on a strain-softening continuum description.

For tensile loading these models have shown to be able to describe:
1. crack patterns;
2. softening as a result of crack growth;
3. localization of cracking;
4. the size effect in peak stress and softening.

Willam et al. have also carried out simulations of compressive failure, which looked quite realistic.

2.2 *Idea behind the micromechanical model*

Two-phase model

The first and most logical step in modelling the heterogeneity of concrete is modelling it as a two-phase material existing of aggregates in a hardened cement-paste matrix. The aggregates act as the most important stress concentrators and define for normal concrete an area where no cracking is found. Hsu et al. [1963] conclude from their research that:

1. cracking in normal concrete starts at the interfaces between coarse aggregates and mortar because the bond between these components is the weakest link and;
2. continuous crack patterns are created by the growth of cracks through the mortar forming bridges between the bond cracks.

This means that the aggregates determine the shape and spacing of the cracks and that the interfaces between the aggregates and mortar play a very important role in the crack-formation process.

Discrete-crack approach

To be able to describe the above mentioned process, it was decided to model crack formation by means of a discrete-crack approach as done in the Distinct Element Method (Cundall [1971], Cundall and Strack [1979], Lorig and Cundall [1987]). In this way the problems of the smeared-crack approach are avoided. It was expected that the heterogeneity of the model would determine localization of cracking and deformations. The material between the discrete cracks, represented by continuum elements, is not allowed to crack in the model.

Interface pattern

A random mesh generator was built to generate a continuous pattern of interfaces representing all potential crack paths in concrete. Based on the conclusions of the research of Hsu et al. [1963], the pattern exists of two sets of interfaces, that is:

1. one set of interfaces representing all potential bond cracks along the boundaries of the aggregates and;
2. one set of interfaces representing all potential mortar cracks connecting all potential bond cracks in a logical and systematic manner.

The basic structure of the interface pattern is shown in Fig. 11a. The aggregates are schematized as regular hexagons. Only the coarse aggregates are modelled, because it is beyond computational means to model all aggregates. This means that the matrix around the aggregates represents mortar.

Simulation heterogeneity

The heterogeneity of concrete is simulated further by:

1. giving different elastic properties to the aggregates and the mortar;
2. giving different strength to the potential bond cracks and mortar cracks and;
3. disturbing the regular interface pattern in a stochastic manner.

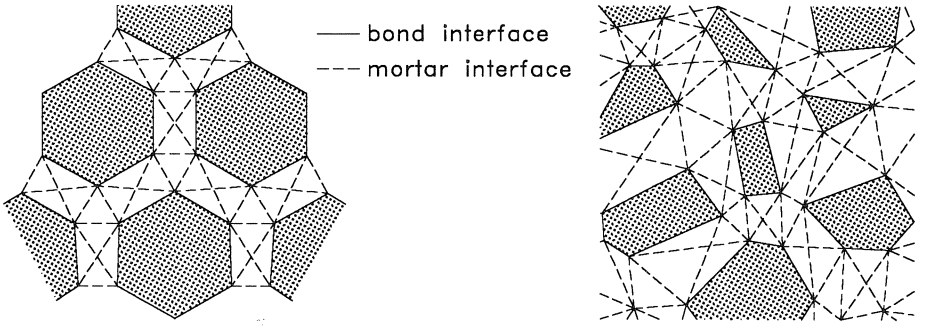

(a) (b)

Fig. 11. (a) Basic interface pattern and (b) randomly disturbed interface pattern.

As a result, the heterogeneous structure will determine the interfaces which will be activated during the failure process and those which will not.

Random mesh generator

The mesh generator allows the regular pattern of Fig. 11a to be disturbed in a random manner. The result is shown in Fig. 11b. The size of the aggregates is varied between the maximum aggregate size and approximately one third of this value. A random displacement of the aggregates away from their original position can be specified. The size and shape of the mortar layers between the aggregates can be varied. This results in a change of shape of the aggregates from a regular hexagon to an irregular polygon with six or less corners. Measures have been taken to prevent the formation of very small elements, which means that aggregates and mortar layers can disappear. A part, having the size and shape of the specimen, is cut out of the mesh at a randomly chosen position and angle of orientation. More details about the mesh-generation procedure can be found in Vonk [1992].

Finite element analysis

A finite element analysis was preferred to a simulation with a truss model because in finite element analysis the formation and behaviour of a crack can be modelled more naturally by means of an interface between the continuum elements. The truss models have been found to give good results for the simulation of tensile crack formation, but it was doubted whether phenomena like shear failure, friction and aggregate interlock could be easily simulated with such a model.

Choice of UDEC

To carry out the finite element analysis a choice was made in favour of the computer code UDEC (Universal Distinct Element Code, Itasca Consulting Group [1989]), as:

1. it has great capabilities in splitting up structures into continuum parts separated by interfaces, thus creating a discontinuum;

2. it is especially programmed to handle discrete cracking and mechanical interactions of continuum elements after complete separation and;
3. it takes into account the influence of large displacements on the mechanical interactions.

New constitutive model

Initially it was hoped that the interface behaviour could be described by means of brittle fracture and friction using a stochastic distribution for the characteristic properties. It appeared that this was not suitable for the model presented here. A highly brittle and irregular failure was found for specimens loaded in compression. Probably, this will not be found when the heterogeneous structure of concrete is modelled down to a smaller scale level. This was not done for the micromechanical model, because this would have resulted in extreme calculation times. Because UDEC dit not provide an interface model with softening for combinations of tensile and shear loading, a new constitutive model providing this feature was developed and implemented in UDEC.

2.3 *UDEC*

The computer program UDEC was written especially for the examination of mechanical problems of fractured media. UDEC has been applied extensively for modelling problems in rock mechanics. It is based on the Distint Element Method developed by Cundall [1971] and is formulated quite differently from the better-known Finite Element Method. The most characteristic features of UDEC are:

1. the division of structures into blocks and interfaces;
2. the allowance of large displacement and;
3. the explicit dynamic solution procedure.

Block system

Basically UDEC distinguishes 3 kinds of structural elements:

1. blocks;
2. zones;
3. interfaces.

They are shown in Fig. 12. A structure is split up in a number of blocks by creating a continuous pattern of interfaces through the structure. Blocks are the structural elements, which represent the continuum behaviour of the structure. They are not supposed to show localized cracking, but can have any linear or nonlinear continuum behaviour. Blocks may have any polygonal shape. For the calculation of stresses and strains, the blocks are divided into finite elements, which are called zones. UDEC only uses triangular constant-strain elements. The basic idea behind the Distinct Element Method is that failure is found in a limited number of weak planes. In UDEC these weak planes are modelled as interfaces between the blocks. Interfaces have their own constitutive behaviour, which is thought to be lumped in a number of contacts between the blocks (Fig. 12). The constitutive laws of the contacts are actually force-displace-

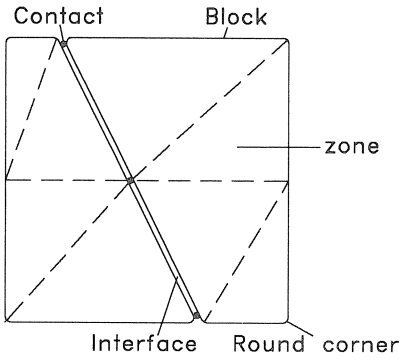

Fig. 12 Structure consisting of 2 blocks, 8 zones, 1 interface and 3 contacts.

ment relations, but can also be formulated as stress-displacement relations. Then the length of the interface represented by the contact is taken into account.

Large displacements

For micromechanical simulations, one of the most important properties of UDEC is that it can take into account the influence of large deformations on the interaction between the blocks. In micromechanical simulations, displacements of the size of the finite elements are found and it is important that the geometrical nonlinearity due to these displacements is treated correctly. In UDEC blocks are allowed to slip, separate, lose contact and displace over considerable distances. Contact points and contact lengths are continuously updated. UDEC even tracks new contacts which did not previously exist. Corners of blocks are rounded as is shown in Fig. 12.

Solution procedure

UDEC uses an explicit time-marching solution procedure. In this explicit approach for each time step the equations of motion for each separate element are solved neglecting the boundary conditions for the displacements. This is illustrated in Fig. 13. At time

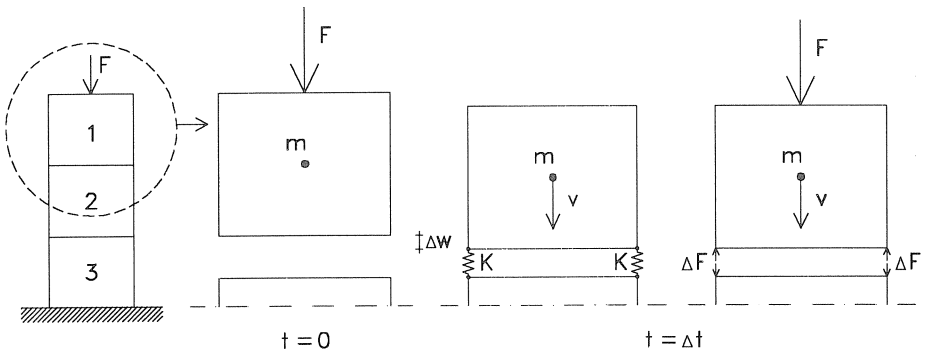

Fig. 13. Illustration of the explicit calculation procedure in UDEC.

$t = 0$, rigid block 1 with mass m is loaded with force F. Application of the law of motion gives an acceleration $a = F/m$. This results in a displacement increment Δw at the end of time increment Δt. Block 1 is connected to block 2 by 2 elastic springs with stiffness K. This means that the displacement Δw results in 2 reaction forces $\Delta F = K\Delta w$. In the next time increment Δt, the law of motion for block 1 is solved again taking also the 2 reaction forces ΔF into account. This is also done for block 2. In this way information travels through the structure. The basic calculation cycle is shown in Fig. 14. The law of motion and the constitutive laws are used alternating for each element for each time step. This procedure is not restricted to rigid blocks. The application of the constitutive laws can also include the application of constitutive laws for the continuum elements.

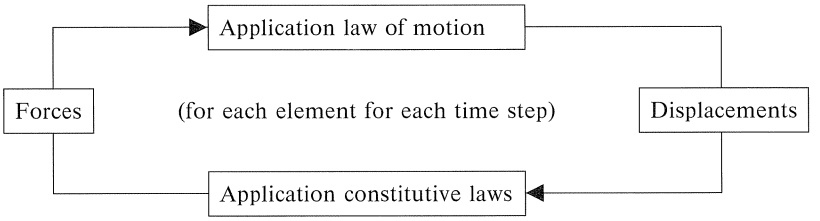

Fig. 14. Basic calculation cycle in UDEC.

Time step

For the explicit formulation used in UDEC, numerical stability and convergence to the exact solution are found only when a small enough time step is chosen. An algorithm is applied in UDEC which calculates a time step based on the speed of propagation of information through the mechanical system. The time step is chosen sufficiently small, so that information can not travel further than one structural element during a time step.

Quasistatic problems

UDEC also can solve quasistatic problems by following the nonlinear behaviour with small increments. Then, the time step is still used, but merely as a means of incrementation to reach the final solution. The kinetic energy is removed from the mechanical system by adding an artificial damping. UDEC uses an adaptive method dependent on the change in kinetic energy in the system that guarantees a critical damping. This method was developed by Cundall [1982], who showed it to be effective in several cases of structural failure.

Explicit method versus implicit method

For many problems, for instance linear-elastic problems, the implicit method of solving problems in most finite element methods is much more effective than the explicit method used in UDEC. This is due to the small time step needed in UDEC to obtain numerical stability. The explicit method of UDEC becomes competitive when:

1. the problem is highly nonlinear;

2. the constitutive behaviour is path dependent;
3. there are changes in connectivity of the elements.

The small calculation increments in the explicit method used in UDEC make it easy to follow highly nonlinear or path-dependent behaviour. In the implicit method this can lead to a dramatic increase in calculation time, because of the increase in increments and iterations needed to find a satisfactory convergence to the exact solution. This also happens in the implicit method when the physical or geometrical changes make it necessary to rebuild and invert the total structural matrix.

2.4 *Constitutive model describing interface behaviour*

A new constitutive model was formulated because no interface models were available in UDEC describing failure due to general combinations of tensile and shear loading, including softening for both (Vonk [1990, 1992]). The model was formulated with the intention of giving a simple description of the essentials of crack behaviour at micro-level to be used in the micromechanical simulations. The model was kept relatively simple for the reasons that:

1. many details modelled at the microlevel will probably hardly be recognized on the macrolevel due to an averaging process. It was thought better to make the model more complicated when the results of the simulations required it;
2. many details of crack behaviour at microlevel are not well known or not known at all;
3. it reduces calculation time.

Failure surface

The model is formulated linearly throughout. The initial failure surface is shown in Fig. 15. Tensile failure is governed by a tensile strength f_t and a reduction angle χ to take into account the presence of a shear stress. Shear failure is governed by a Mohr-Coulomb

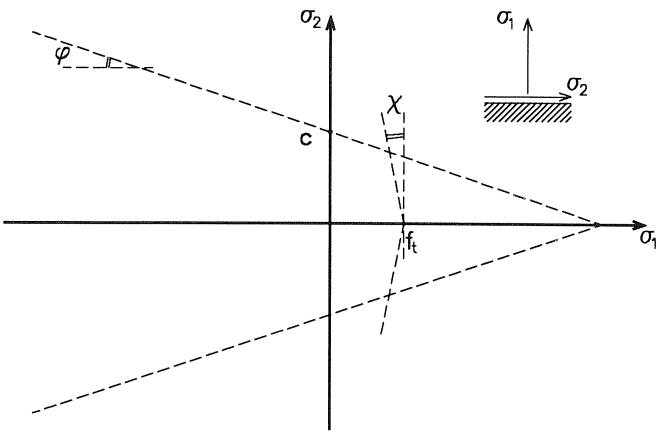

Fig. 15. Initial failure surface.

criterion applying a cohesion c and a friction angle φ. No failure is modelled for pure compressive loading.

Elastic deformations

Until the failure surface is reached, the behaviour is assumed to be linear elastic, depending on the two different moduli of elasticity K_1 and K_2 for normal and shear deformations, respectively. In the micromechanical simulations the moduli of elasticity are chosen very high to keep the interface deformations negligible until failure starts.

Softening

After the failure criteria are met, linear softening is modelled both for tensile and shear loading by reducing the tensile strength and the cohesion (Fig. 16). A plasticity formulation is used, which means that the deformations during softening are irreversible and unloading takes place according to the moduli of elasticity. The two kinds of softening are coupled, assuming that both tensile strength and cohesion decrease at the same time and at the same rate, depending on the damage to the interface. This results in an isotropic shrinkage of the failure surface, which is shown in Fig. 16. Residual tensile strength and residual cohesion are formulated as linearly decreasing functions of the parameter $\varkappa$ representing the state of damage. It varies from 0 in the undamaged state to 1 in the fully damaged state. It is assumed that $\varkappa$ increases linearly depending on the plastic deformations of the interface. The rate of increase differs between normal and shear deformations. Pure tensile softening ends after a plastic tensile deformation $w_{1\max}$, whereas pure shear softening ends after a plastic shear deformation $w_{2\max}$. This is shown in Fig. 16. Simultaneous softening due to tensile and shear deformations is treated as a linear combination. Completed softening sets the tensile strength and the cohesion to 0, which means that a pure friction model is left. During shear softening or frictional sliding it is assumed that the interface opens with a dilatancy angle ψ.

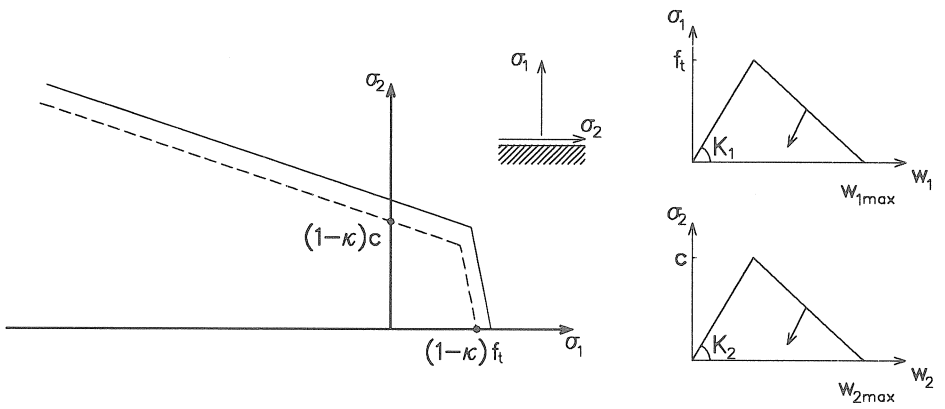

Fig. 16. Shrinkage of the failure surface due to softening.

2.5 *Simulation of softening with UDEC*

In UDEC a deformation controlled simulation can be carried out by:
1. applying the required deformation in large steps;
2. applying a constant velocity.

The last method was chosen because the material behaviour is path dependent. Also, it was found that the first method causes significant dynamic effects resulting in undesired damage. The application of a constant velocity means that a perfect state of equilibrium is virtually never found. UDEC gives an indication of the dynamic effects by continuously monitoring the maximum unbalance force in the mechanical system. During the micromechanical simulations this unbalance force was always very small compared to the total force in the system. Only incidentally it was more significant.

Tensile softening

Four calculations were carried out to investigate the ability of UDEC to simulate softening and localization of deformations. In these calculations the applied boundary velocity, the time step, the elastic stiffness, the fracture energy and the size of the specimen were chosen in the same order of magnitude as in the micromechanical simulations. A simulation of tensile softening was carried out for the specimen in Fig. 17a consisting of two blocks separated by one interface. The result is shown in Fig. 18. It shows the dynamic character of UDEC. Information is transmitted through the mechanical system by means of stress or deformation waves. The automatically applied damping in UDEC keeps the dynamic energy in the system low. It can be reduced further by decreasing the velocity of the boundaries. Due to the dynamic effects, the total energy dissipation was found to be 2% higher than the theoretical value for the fracture energy.

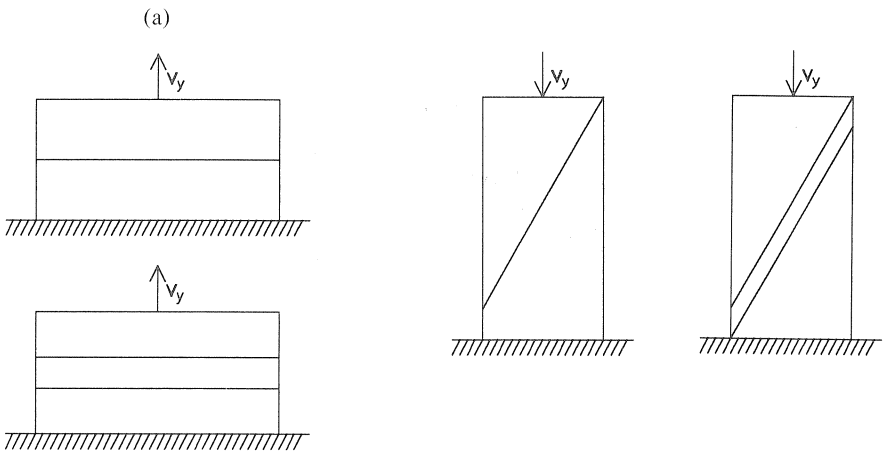

Fig. 17. Simple structures used for simulation of softening with UDEC.

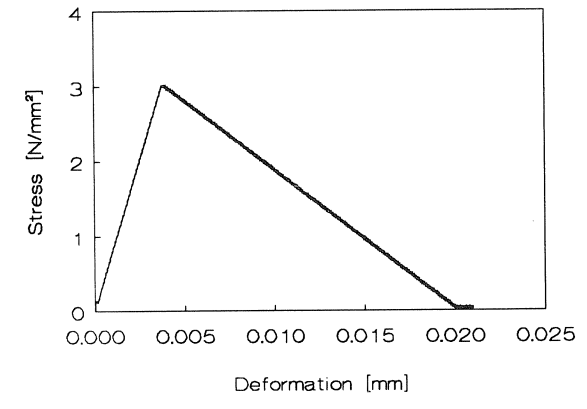

(a)

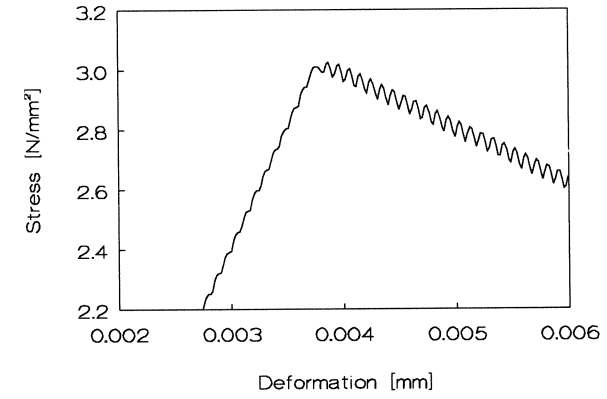

(b)

Fig. 18. (a) Result of a simulation of tensile softening with UDEC and (b) detail around peak stress.

Localization in tension

The ability to handle localization of deformations was shown by the second simulation of tensile failure of the specimen with two interfaces in series (Fig. 17b). Only the upper interface fractured, while the lower interface remained almost undamaged. The fact that the upper interface fractured was to be expected, because the stress waves are initiated at the upper boundary of the specimen. The simulation showed that UDEC is sufficiently selective to make only the upper interface fracture. The fracture energy was 1% higher than the theoretical value. This was due to a decrease of the dynamic effect. The size of the stress waves halved with respect to those in the first simulation. In the calculations with the micromechanical model the dynamic effects were also found to be much smaller. The simulation of the first tensile test in this paragraph is a critical case due to its homogeneity and symmetry.

Shear softening

Two simulations of shear softening due to uniaxial compressive loading were carried

out too. The specimens are shown in Figs. 17c+d. The simulations gave qualitatively the same results as those for tensile softening. The fracture energy for shear loading was found to be approximately 1% higher than the theoretical value and localization of deformations was found in the upper interface.

Softening simulated with the micromechanical model
It is hard to prove that localization of deformations is always predicted correctly by UDEC. The simulations presented in this work always show realistic results. When no perfect localization is found, but the cracking is more diffuse, this can be explained by the heterogeneity of the material.

To determine the influence of some UDEC calculation parameters on the micromechanical simulations, a sensitivity study was carried out for the simulation of a uniaxial compression test (Vonk [1992]). The maximum finite element size was chosen to be 5 mm. A complete simulation of a compressive softening test required 320000 to 400000 calculation steps ("time" steps). This took 4 days CPU time on an Alliant FX2600 minicomputer. Because of the large number of calculation steps, UDEC was changed to carry out the calculations in double precision instead of single precision.

3 Testing technique

3.1 *Loading technique*

Loading apparatus
All the compression tests have been carried out with the triaxial apparatus at Eindhoven University of Technology (Fig. 19, Van Mier [1984]). This apparatus consists of three identical loading frames with a capacity of 2000 kN each. One loading frame is shown in Fig. 20a. Each of the three frames is provided with its own hydraulic servomechanism, which can be used to load a specimen either in force control or in deformation control. For this purpose the load cell or the LVDTs attached to the loading platens are used to supply a feedback signal. All the tests have been carried out in deformation control to be able to measure softening. A constant strain rate of 1×10^{-5} l/s was used. The hinges of the frame were kept fixed for all the tests.

Loading platens
Four different loading platens have been used to investigate their influence on compressive softening (Vonk [1989]):
1. Short brush (BS);
2. Long brush (BL);
3. Teflon platen (T);
4. Dry platen (D).

Steel brushes
The short brush (Fig. 20b) is the same as that used by Van Mier [1984] in his triaxial

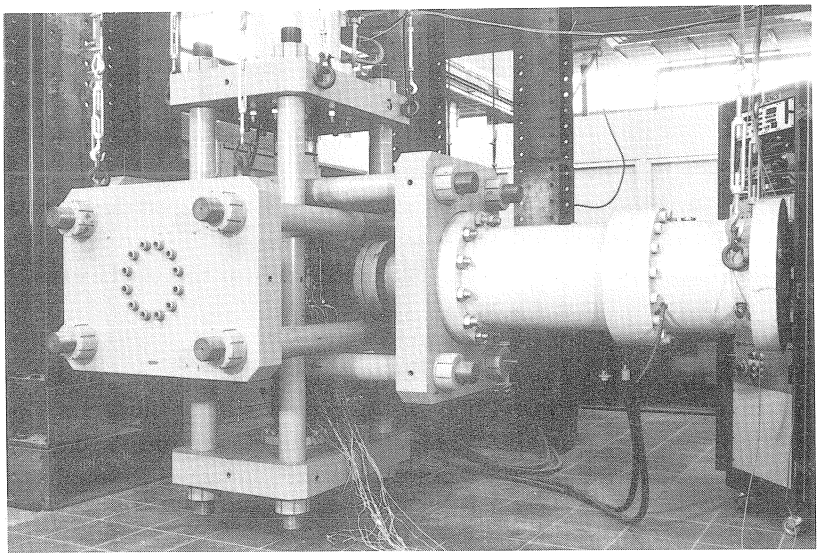

Fig. 19. Triaxial loading apparatus, Van Mier (1984).

tests. The brush rods (5×5 mm^2) are separated at the clamped side by means of a grid consisting of 0.2-mm-thick phosphor bronze strips. The rod packet is clamped to a solid steel block. The effective length of the rods is 84 mm. Steel brushes are used in compression tests, because their restraint to the lateral expansion of the concrete specimen is slight (Hilsdorf [1965], Linse [1978]). The brush rods can easily follow the lateral expansion of the specimen by bending. Peak stress in a compression test is not influenced significantly by steel brushes (Kotsovos [1983], Van Mier [1984]). The shear forces induced in the specimen can be minimized by increasing the length or decreasing the width of the brush rods. This is limited by the buckling load of the rods.

Calculation of shear stresses

The shear stress induced in the specimen and the buckling stress of the rod can be estimated with simple mechanical formulas. However, it is not clear what boundary conditions are present for the brushes used in the present experiments. Most researchers assume a complete fixation at the clamped side of the rod (Hilsdorf [1965], Linse [1978]). Whether this is true can be queried when inspecting the construction of the brush in Fig. 20b. The phosphor-bronze grid and the clamping system are relatively weak. At the rod end in contact with the concrete specimen a state between free rotation and a perfect fixation can be assumed. Due to an eccentricity of the force in the rod, a moment can be transferred by the brush-rod top. However, the stresses in the contacting area will become significant, which will cause a penetration of the rotating brush rod in the concrete surface and limit the moment transferred by the brush-rod top.

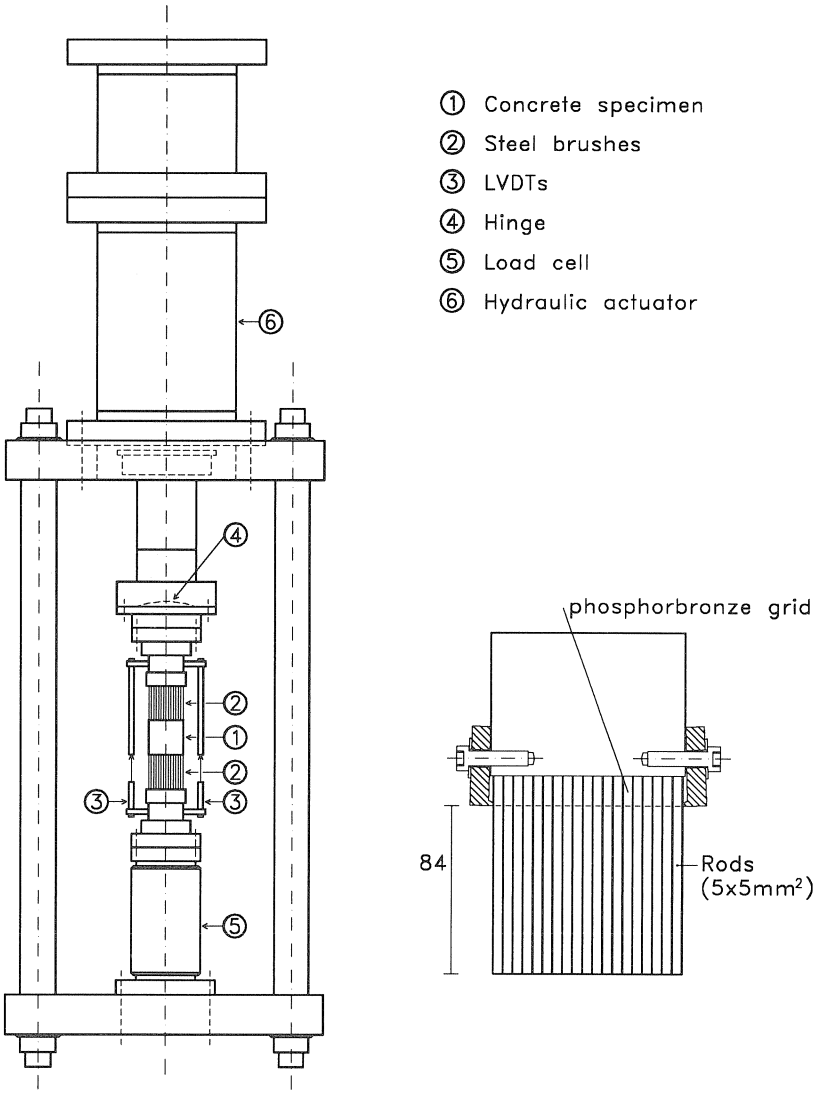

(a) (b)

Fig. 20. (a) Single loading frame of the triaxial apparatus and (b) short brush.

The aim was to measure the shear stress as a function of the lateral displacement of the brush-rod top. The tests showed that the initial stiffness lies somewhere between the theoretical value for a brush rod with one side fixed and one side hinged and the value for a brush rod with two sides fixed. The behaviour was found to be highly nonlinear and to be dependent on the preparation of the brush and the loading history in former tests. The use of a brush in compression tests on concrete resulted always in a certain amount of play in the clamping system due to the considerable lateral deformations of the specimens and consequently of the brushes.

To give an indication of the shear stresses induced in the concrete by the steel brushes, some values have been calculated for a zero normal stress. They are given in Fig. 21. The shear stress is proportional to the lateral displacement w of the brush-rod top. Also, the buckling stress is given, as the shear stress decreases gradually to zero when the normal stress increases from zero to the buckling stress. It has been assumed that one end of the rods is completely fixed. For the other end, two cases have been assumed: a free rotation and a complete fixation. The actual state in the compression tests will be somewhere in between.

Fig. 21. Calculated values for shear stress (as a function of the lateral displacement w of the rod top) and buckling stress for the steel brushes.

		σ_{shear} (N/mm^2)		$\sigma_{buckling}$ (N/mm^2)	
end condition		rotating	fixed	rotating	fixed
BS	$l = 84$ mm	2.00 w	7.99 w	138	552
BL	$l = 119$ mm	0.70 w	2.81 w	69	275

The shear stresses increase when the lateral deformations of a specimen increase. Compressive softening of concrete is accompanied by an acceleration of the lateral expansion. This means that the lateral shear stresses will increase significantly and that it is not certain whether the influence of the brushes is still negligible as it was in the behaviour up to peak stress. In order to estimate the influence of the short brush on compressive softening, it was decided to carry out tests not only with the brush used by Van Mier but also with a brush with longer rods. Fig. 21 shows that the long brush, with an effective rod length of 119 mm, gives a significantly less lateral restraint. The shear stress has been reduced to 35% and the buckling stress to 50%.

Frictional stresses

The restraint to lateral deformations due to friction is quite different from that due to the bending of brush rods. Frictional stresses rise quickly as a function of the shear deformation but are limited by a maximum which depends on the frictional properties of the surfaces of the loading platen and the specimen and the normal stress in their contact. Frictional stresses increase with an increase of the normal stress. This means that the restraining frictional stresses in a compressive softening test are maximal at peak stress and decrease with softening. The restraining shear stresses due to the bending of the brush rods grow more slowly but continuously as a function of the lateral deformations. This means that, when softening takes place and the lateral expansion accelerates, the lateral restraint due to the bending of brush rods will become greater than that due to friction. It was therefore decided to develop loading platens with a low coefficient of friction to investigate the effect on compressive softening of the platen and compare it to the effect of steel brushes.

Teflon platen

A loading platen with a very low coefficient of friction was developed for this research (Vonk [1989]). The surface of a loading platen was first tempered and then polished. This resulted in a surface roughness $R_a \simeq 0.05$ μm. Further, an additional sheet of teflon was applied. Teflon was chosen because it is the best solid lubricant. It is known that the use of intermediate layers of a soft material can make it impossible to carry out a stable softening test. Besides, there is the danger of introducing splitting stresses into the concrete specimen when using a soft intermediate layer (Kotsovos [1983]). To avoid these drawbacks, a very thin sheet of teflon 0.05-mm-thick was used. Further, it was found profitable to slightly grease the interface of loading platen and teflon. Only very little grease was added. The effect of several kinds of grease was tested. The lowest coefficient of friction was found for an ordinary bearing grease (Molykote BR2 plus).

Measurement of frictional stresses

A series of tests was carried out to determine the frictional properties of the teflon platen (Vonk [1989]). A concrete cube was loaded with a constant force in the vertical axes of the triaxial apparatus using two teflon platens. One of the horizontal axes was used to make the concrete cube slide between the two teflon platens. The sliding speed was about 1 μm/s, which is representative for the sliding speed in the compression tests on concrete. This is important because teflon shows some creep, which influences the measured friction. Fig. 22 shows a characteristic experimental result. Only a very small displacement is enough to activate the shear stresses. The peak value is already found for a displacement of few microns. Subsequently, a significant stick-slip behaviour takes place. This behaviour is known to be strongly influenced by the characteristics of the loading apparatus (Bartenev and Lavrentev [1981]). If a test setup of greater stiffness had been used, the stick-slip behaviour would have been smaller and a more gradual

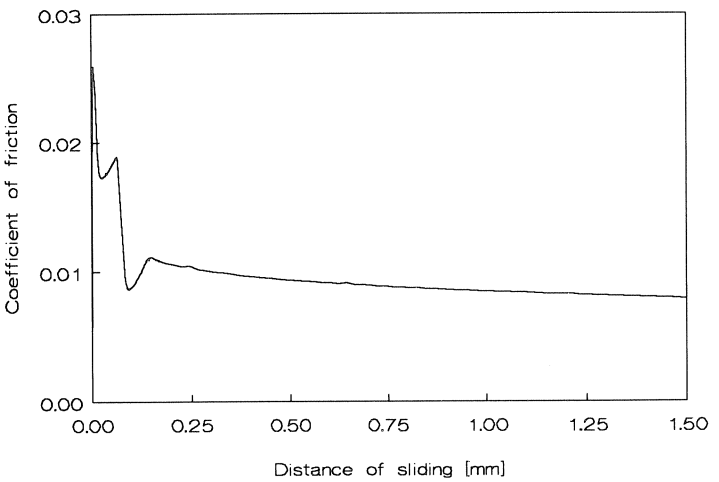

Fig. 22. Result of tests to determine the friction of a teflon platen.

curve would have been found. The shape of the curve during the stick-slip behaviour is not a material property, but a property of the testing technique. It is expected that this stick-slip behaviour will be less pronounced in compression tests on concrete because in those tests only very small parts of the surface will slip at one time over a short distance. The decrease in friction in Fig. 22 is considerably, which is probably due to the self-lubricating effect of teflon (Bartenev and Lavrentev [1981]).
Fig. 23 shows the coefficients of friction found in the tests with the teflon platens. The values vary from 0.026 to 0.048 for the first peak and from 0.008 to 0.013 after 1.5 mm of sliding. The normal stress was limited to -30 N/mm^2 because of the danger of failure of the concrete cube. No aluminium or steel specimens can be used instead of concrete specimens because it was found that they do not provide representative results. Those materials have a smoother surface, which influences the measurements of the friction significantly. In tests with a steel cube, coefficients of friction were found which were 50% lower than those found in the tests with concrete cubes (Vonk [1989]). The coefficients of friction are low compared to values mentioned by other researchers. Shah & Sankar [1987] report a coefficient of friction of 0.07 for teflon. Nojiri et al. [1984] also carried out friction tests. They report a coefficient of friction varying from 0.025 to 0.03 for a loading platen with two teflon sheets with some grease in between. The low values in the tests presented here are due to the great care given to polishing the surface of the loading platen, the addition of the grease and the low sliding speed, which allows for some creep.

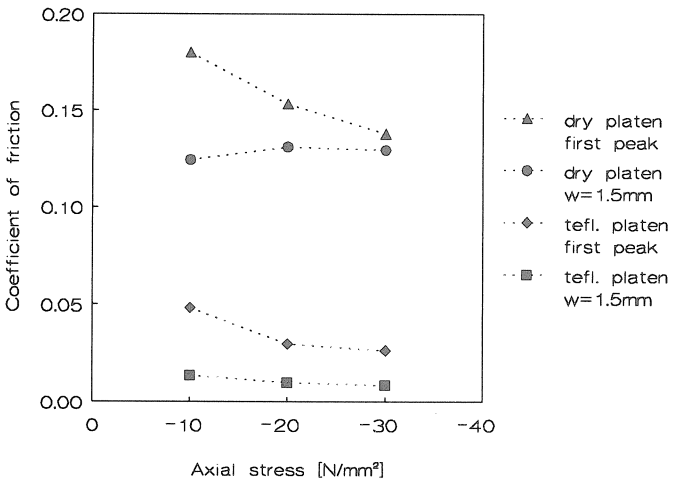

Fig. 23. Coefficients of friction for the teflon platen and the dry platen.

Dry platen
The dry platen was identical to the polished steel platen used for the teflon platen. Fig. 23 also gives coefficients of friction for the dry platen. This platen also shows a stick-slip behaviour. The coefficients of friction decrease from 0.138 to 0.180 for the

first peak to 0.128 to 0.132 after 1.5 mm of sliding. Values reported in literature are scarce. Nojiri et al. [1984] report a coefficient of friction of 0.18.

3.2 *Measuring technique*

Measurement of forces and deformations

The forces were measured by means of calibrated load cells with a range of 2000 kN (Fig. 20a). The axial deformations were measured by means of strain gauges and LVDTs. The strain gauges were glued to the four sides of the specimens as shown in Fig. 24. Their length was 30, 60 and 120 mm (TML, PL-30/60/120-11, maximum strain 2%) for the specimen heights of 50, 100 and 200 mm, respectively. Further, at each side of the specimen an LVDT (HBM, W10-K, range 10 mm) was attached to the loading platens. Fig. 24 shows how the LVDTs were attached to the steel brushes and the teflon platens. The separate readings of the 4 strain gauges and 4 LVDTs were recorded for information on the uniformity of deformations of a specimen during a test. Two extra LVDTs were always present to be used for the test control (Fig. 24b). The lateral deformations were measured by means of clip gauges. An example is shown in Fig. 25. The clip gauges were clamped along all four sides of a specimen. Often two or three clip gauges were used at one side at different heights of the specimen to investigate the uniformity of deformations of the specimen.

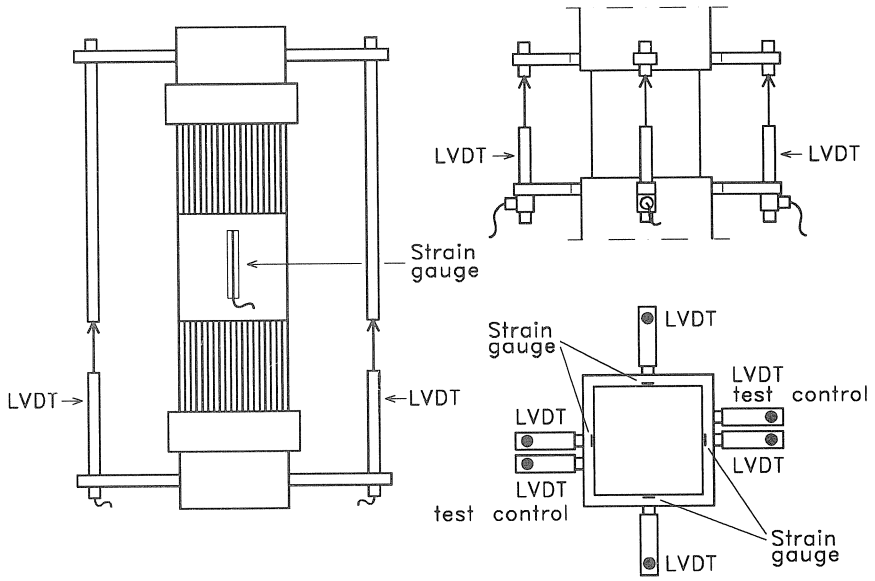

(a) (b)

Fig. 24. Positions of strain gauges and LVDTs.

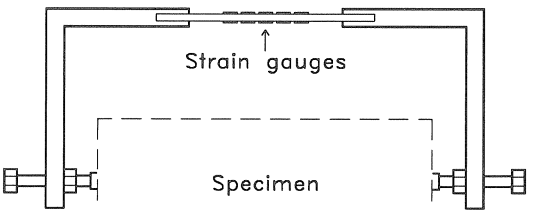

Fig. 25. Clip gauge attached to a specimen.

Correction of initial setting

The LVDT measurements had to be corrected for the deformations of the loading platen and for extra deformations due to the setting of the loading platen against the specimen (see also Schickert [1980], Van Mier [1984]). This setting is due to nonflatness of the specimen surface, nonparallelism of loading platen surface and specimen surface and internal setting of the loading platens. The corrections have been described extensively in Vonk [1989, 1992].

3.3 *Preparation of specimens*

Casting and hardening

The concrete mix proportions are given in Fig. 26. The concrete was cast in large moulds on a vibrating table (5000 Hz). Concrete 1 was used for the boundary condition tests and concrete 2 for the size effect tests. The maximum aggregate size for concrete 2 was reduced to 8 mm because the smallest specimen size in the size effect tests was 50 mm. For this concrete it was found necessary to use in addition an extra vibration needle with a higher frequency (15000 Hz) to obtain good compaction. Subsequently, the concrete in the moulds was placed in the laboratory for three days, keeping it wet and covered with plastic to prevent it from drying out. After demoulding, the concrete blocks were immersed in water.

Fig. 26. Concrete mix proportions.

	Concrete 1	Concrete 2
Portland cement A	330 kg/m^3	340 kg/m^3
Water	165 kg/m^3	170 kg/m^3
Gravel/Sand	1879 kg/m^3	1828 kg/m^3
0.0 - 0.25 mm	8%	8%
0.25- 0.5 mm	12%	10%
0.5 - 1.0 mm	12%	13%
1.0 - 2.0 mm	10%	16%
2.0 - 4.0 mm	14%	23%
4.0 - 8.0 mm	20%	30%
8.0 -16.0 mm	24%	-

Sawing
At an age of 28 days, the blocks were taken out of the water to be sawn to the required specimen size plus 3 mm. At least 1.5 times the maximum aggregate size was removed from the outer layers of the blocks to obtain specimens which are as homogeneous as possible. Due to a wall effect, the outer layers of cast concrete have a different structure, which influences the mechanical behaviour (Schickert [1980], Van Mier [1984]).

Direction of casting
The direction of casting was marked on the specimens in order to be able to apply the loading in tests parallel to the direction of casting. Concrete is an anisotropic material due to the process of casting. Significant differences in test results can be found for loading parallel and perpendicular to the direction of casting (Hughes and Ash [1970], Van Mier [1984]).

Grinding
Then the specimens were ground to their required size. Special attention was paid to the flatness and parallelism of the loading surfaces. This is necessary for uniform loading. In the first series the deviation of the ideal parallel surface was always found to be less than $\pm$ 15 μm. For the second series a grinding apparatus with a higher stiffness was used, which resulted in a maximum deviation of $\pm$ 5 μm. The lack of parallelism between concrete and loading-platen surface was minimized in the tests by loosening the hinges in the loading frame, when placing the loading platen against the specimen.

Storage
After grinding, the specimens of the first series were stored in sealed plastic bags with some water added. A few hours before testing, the specimens had to be in the open air to be prepared for testing. The second series was stored in a case with a constant relative humidity of 100% and taken out of this case only two hours before testing. This was done in order to keep the influence of drying shrinkage as slight as possible. The age of concrete at testing varied from 4 to 6 months. At that age, standard compression tests on 150 mm cubes, carried out according to the Dutch codes, resulted in compressive strengths of 51.9 N/mm^2 for concrete 1 and 56.6 N/mm^2 for concrete 2.

3.4 *Crack-detection technique*

In the present investigation both external and internal crack patterns were recorded at the end of a test to be used in the analysis of softening. The external crack patterns were recorded by simply tracing the macrocrack pattern on the specimen surface visible with the naked eye.

Recording of crack patterns after a test
The most detailed information about internal crack patterns can be acquired by sawing specimens open and recording the crack patterns directly. Good examples of this

technique are found in the investigations at Cornell University to establish a relation between the crack-formation process and the stress-strain curve. There internal crack patterns were analyzed by means of a dyeing technique and an x-ray technique of slices of concrete after a test (Hsu et al. [1963], Slate [1983]). For intensively cracked specimens this technique cannot be applied, because the process of sawing would damage the specimen totally. Recently, a petrographic technique inspecting thin slices of concrete impregnated with a fluorescent epoxy resin has been used to analyze the structure and microcracking of concrete (Knab et al. [1986], Soers & Meyskens [1987]). The fluorescent epoxy resin is impregnated in the cracks to stabilize the concrete during cutting and polishing and makes the cracks and pores visible under ultra violet light. This technique was only used for small sections.

It was decided to try to inspect the internal crack patterns by means of impregnating the specimens with a fluorescent epoxy resin because:
1. the epoxy resin stabilizes the intensively cracked specimens;
2. ultraviolet photography can give detailed pictures of the crack patterns and;
3. both impregnation technique and photographic technique are very simple.

Impregnation technique
At the end of a test the specimen was unloaded and carefully taken out of the loading apparatus. After a few weeks of drying in the laboratory, the specimen was placed in a plexiglas mould. Subsequently, the mould was filled with a low-viscous (110 mpas) fluorescent (fluorol green, BASF) epoxy resin (EP-IS, CIBA Geigy). Under vacuum (6.5 mbar) the air was removed from the cracks in the concrete and replaced by epoxy resin. After 30 minutes, atmospheric pressure was restored in order to let the epoxy resin penetrate even deeper into the cracks. The pot life of the resin was about 50 minutes. The epoxy resin easily filled all the macrocracks of cubes of 200 mm. After 8 hours of hardening, the epoxy resin reached a strength of approximately 60 N/mm^2. Subsequently, the specimen was carefully sawn into slices to be able to record the internal crack patterns. The introduction of additional cracks by the sawing had no influence on the recording of the cracks, because only cracks which were filled with epoxy resin before the sawing started are recorded.

Ultraviolet photography
The crack patterns were recorded by means of ultraviolet photography (Roleiflex SL66 technical camera and a Kodak professional plus-x-pan film, black-white 6 × 6 cm, 21 Din). The use of a yellow-green filter resulted in the best contrast between concrete and cracks.

The development of this technique is described extensively by Goudswaard & Vonk [1989]. It works very well for specimens with continuous patterns of macrocracks. It can also be extended to detect isolated microcracks by the techniques developed at Cornell University (Slate [1983], Goudswaard & Vonk [1989]). Recently this technique also has

been applied successfully for the detection of cracks in uniaxial tensile tests (Van Mier [1991]).

4 Process of softening

4.1 *Simulations of tensile tests*

In this chapter a few simulations of tensile tests are discussed to show that the micro-mechanical model is very well able to describe this type of concrete failure.

Specimen and boundary conditions

In these numerical simulations specimens of 50 × 100 mm are loaded in uniaxial tension subjecting the upper boundary to a constant velocity, while the lower boundary remains at rest. The lateral displacements of all the boundaries are kept unrestrained. Plane-stress conditions are assumed. The input for the mesh generator is chosen in such a way that a coarse aggregate (4–16 mm) content of approximately 31% is simulated, as was present in concrete 1 (Chapter 3.3). An example of the composite structure, the interface mesh and the finite element mesh are given in Fig. 27.

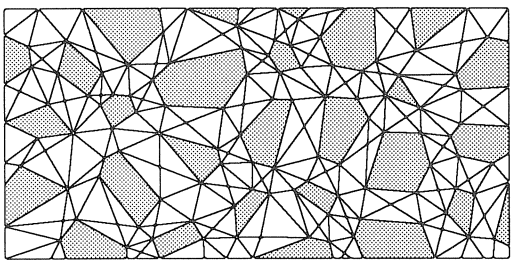

(a)

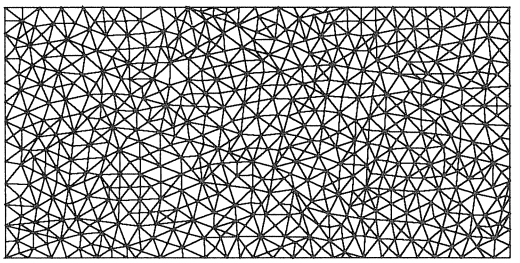

(b)

Fig. 27. (a) Example of a composite structure and interface mesh and (b) a finite element mesh used for the simulation of a tensile test.

Material properties

The material properties used in the simulations of both tensile and compressive softening tests are shown in Fig. 28. They were chosen so that the results obtained are

close to test results. Only very limited information is available in literature to determine their values. There was no attempt to fit the results of the simulations more closely to test results by adapting the material parameters, because this would have taken a considerable amount of time and would probably not have resulted in a better insight into the process of failure.

Fig. 28. Material parameters used in the simulations of tensile and compressive tests.

Continuum		Interface	
Aggregate	Mortar	Bond	Mortar
$E = 70000$ N/mm^2	$E = 25000$ N/mm^2	$f_t = 3.0$ N/mm^2 $c = 10.0$ N/mm^2	$f_t = 6.0$ N/mm^2 $c = 20.0$ N/mm^2
$\nu = 0.2$		$K_1 = 5 \times 10^5$ N/mm^3 $K_2 = 5 \times 10^5$ N/mm^3 $w_{1max} = 0.02$ mm $w_{2max} = 1.00$ mm	$\operatorname{tg} \varphi = 0.3$ $\operatorname{tg} \psi = 0.0$ $\operatorname{tg} \chi = 0.0$

For these simulations it is interesting to note that the heterogeneity of the simulated concrete is modelled by means of:

1. different moduli of elasticity for mortar ($E_m = 25000$ N/mm^2) and aggregate ($E_a = 70000$ N/mm^2);
2. a bond strength ($f_{tb} = 3$ N/mm^2, $c_b = 10$ N/mm^2), which is 50% of the mortar strength ($f_{tm} = 6$ N/mm^2, $c_m = 20$ N/mm^2).

The moduli of elasticity for the interfaces are chosen very high to make their elastic deformations as small as possible. These deformations are approximately 1% of the total elastic deformations of the specimen. The moduli were not increased further, because this would have had a negative influence on the stability of the UDEC calculations and consequently on the calculation time.

Total stress-deformation relation

Fig. 29 shows the stress-deformation relations found for the micromechanical simulations. They compare well with test results. The pre-peak behaviour of the different meshes is almost the same. Near peak stress differences occur, which grow in the softening regime. In the pre-peak regime the stress-deformation relation is determined by the average response of the total volume of the specimen. Due to the localization of cracking, a gradually smaller part of the random internal structure of the specimen determines its behaviour. This makes the stochastic variation in the heterogeneous structure more apparent during softening. This effect is stronger than in reality because the model is two-dimensional. An aggregate of a certain size has a greater influence on the behaviour of a specimen in two-dimensional model than on that in a three-dimensional model because in the first case it occupies a greater percentage of the total cross section than in the last case.

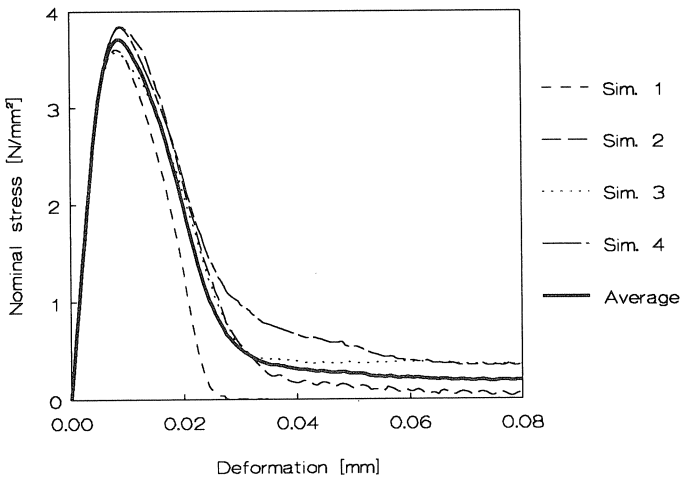

Fig. 29. Stress-deformation relations for 4 simulations of a tensile test.

Peak stress

Peak stress is found to be 3.7 N/mm^2. The work of Rüsch & Hilsdorf [1963] and Hordijk [1989] shows that this is a realistic value for the type of concrete used in the present research. The value obtained for peak stress shows it to be more influenced by the bond strength (3.0 N/mm^2) than by the mortar strength (6.0 N/mm^2). This can be explained by the brittleness of tensile failure of the interfaces. As a consequence, the weakest component has the greatest influence on peak stress.

Post-peak behaviour

In the post-peak regime the well-known softening curve with the long tail is found. The long tail is remarkable because it was not introduced in the material parameters. Apparently, it is a result of the heterogeneous composite structure. The material parameters were chosen so that localization in a straight-line crack parallel to the loaded boundaries would have resulted in the end of the softening process at a deformation of 0.02 mm. In Fig. 30, the final crack patterns for the different composite structures are shown. The cracks are tortuous and show overlaps. Comparison of the stress-deformation diagrams and the macrocrack patterns reveals that the post-peak stress is greater when the crack pattern is more tortuous and shows more overlaps. When no crack overlaps are found, as in simulation 1, no tail is found in the stress-deformation relation. When the crack overlaps grow in size and number, a more significant tail is found. The tail is most pronounced for simulation 4, which shows two of the largest crack overlaps.

Softening and heterogeneity

When it is assumed that a crack through the specimen consists of 50% bond cracks ($G_f = 30$ J/m^2) and 50% mortar cracks ($G_f = 60$ J/m^2), which is close to the results of the

simulations, the tensile-fracture energy for a straight-line crack can be estimated to be 45 J/m^2. By integrating the stress-deformation curves in Fig. 29, fracture energies of 54 up to 98 J/m^2 are found. The last value is lower than the actual value because the integration could only be carried out up to a deformation of 0.08 mm, where the simulation was terminated. The calculated values show that modelling the heterogeneity of the material increases the fracture energy substantially. This indicates that concrete behaviour can probably be described realistically by brittle behaviour at microlevel, when the heterogeneity is modelled down to a sufficiently low scale level. The results of the brittle truss model of Zubelewicz & Bazant [1987] and the brittle lattice models of Schlangen & Van Mier [1991, 1992] also point in this direction.

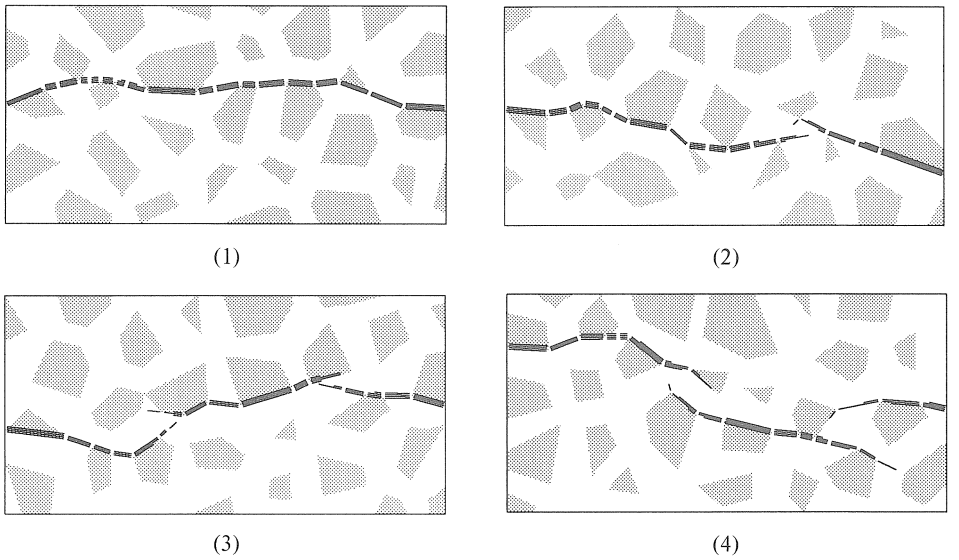

Fig. 30. Final crack patterns (interfaces with an opening > 0.02 mm) for the 4 simulations of a tensile test.

Growth of damage

Fig. 31 shows the growth of damage in simulation 4. The damage is represented by the damage parameter $\varkappa$ of the constitutive model (see Chapter 2.4). It varies from 0 in the undamaged state to 1 in the fully damaged, which means fractured, state. The thickness of the lines in Fig. 31 indicates the value of $\varkappa$. The thinnest lines indicate a $\varkappa$ value of between 0.0 and 0.2 and the thickest lines indicate a value of $\varkappa$ of 1.0.

Due to the heterogeneity, damage is already found in the bond interfaces for small deformations (Fig. 31a). Gradually the damage zones grow along the aggregate boundaries, but stay distributed (Fig. 31b). The higher strength of the mortar prevents the damage zones in the bond interfaces from connecting through the mortar. At peak stress the overall damage has grown to such a level that the damage zones connect through the mortar and become continuous. There the localization of damage and deformations starts. The state of damage just past peak stress is shown in Fig. 31c. The

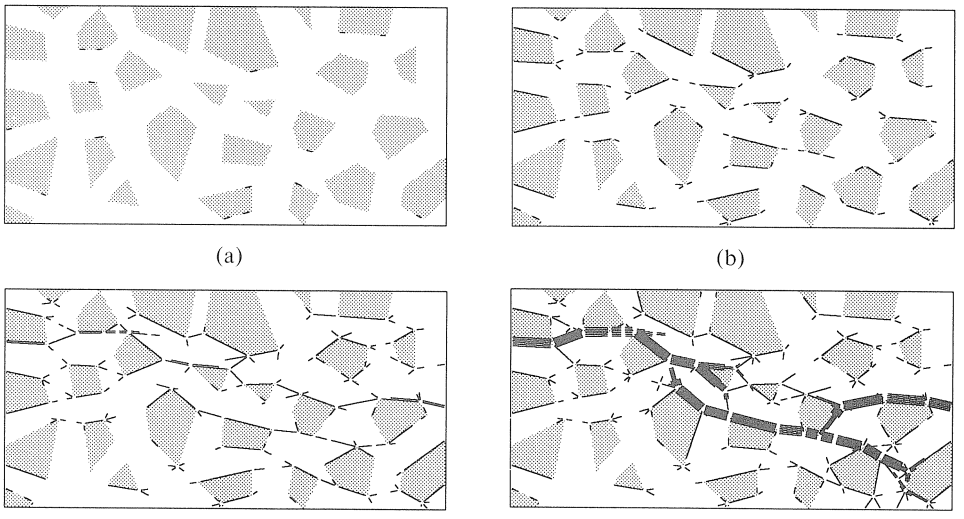

Fig. 31. Damage found in simulation 4 for a deformation of (a) 2.9 μm, (b) 5.8 μm, (c) 11.6 μm and (d) 86.7 μm.

final damage pattern is shown in Fig. 31d. The heterogeneity of the material causes some spread in damage. Forks and overlaps are found in the crack pattern. This makes the actual length of the crack pattern much greater than the width of the specimen, which explains the increase of the fracture energy for the specimen due to the heterogeneity. Modelling the material on a lower scale level will increase the length of the cracks further and introduce more forks and overlaps on this lower scale level. Making the material more heterogeneous by increasing the difference in bond and mortar strength will widen the zone of damage, thus also making the material more ductile.

Crack growth

The process of cracking can be followed more easily, when only the stress-free cracks ($\varkappa = 1$) are taken into account (Fig. 32). Due to the heterogeneity of the material the macrocracks are initiated at several places in the specimen (Fig. 32a + b). These cracks grow in each others direction, but also avoid each other (see also Simha et al. [1986]). After the crack tips have passed each other (Fig. 32c), a bending mechanism is created, which makes one crack-tip bend in the direction of the other crack (Fig. 32d). This mechanism, illustrated in Fig. 33, is very ductile and causes the long tail in the stress-deformation relation. It has been assumed that the tail is caused by friction between the two crack faces (Hordijk [1991], Duda [1991]). This is not confirmed by the micro-mechanical simulations.

Comparison with tests of Van Mier [1991]

The results of these simulations correspond well to recent test results of Van Mier [1991]. His tests show that only few continuous macrocracks are found at the beginning

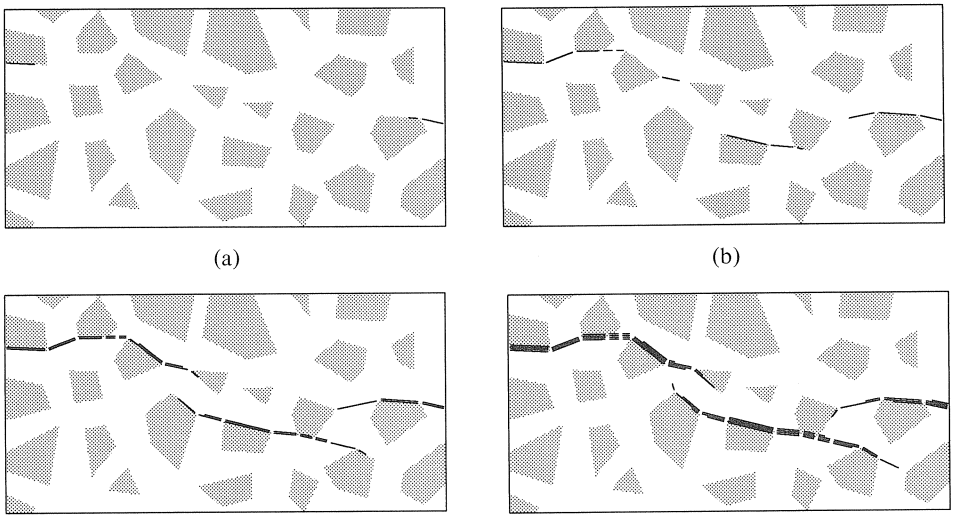

Fig. 32. Macrocrack patterns in simulation 4 at a deformation of (a) 21.7 μm, (b) 28.9 μm, (c) 57.8 μm and (d) 86.7 μm.

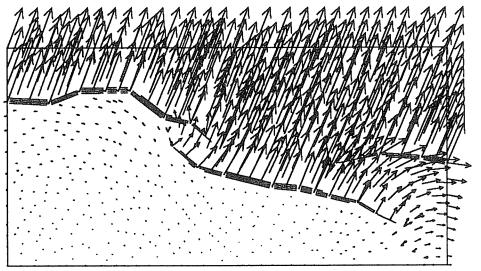

Fig. 33. Failure mechanism for simulation 4.

of softening. He reasons that the first steep drop in the softening diagram is due to isolated debonding of coarse aggregates as described here by the micromechanical model. His tests show further that, even at a deformation of 50 μm, the macrocrack does not go completely through the specimen. This has occurred at a deformation of 100 μm, but even then the macrocrack is still discontinuous, due to the fact that crack tips have missed each other and show overlaps.

4.2 *Simulation of a compression test*

Specimen, boundary conditions and material properties

A specimen of 100 × 100 mm is loaded in uniaxial compression giving the upper boundary a constant downward velocity, while the lower boundary remains at rest. The lateral displacements of all the boundaries are kept unrestrained. Plane stress

conditions are assumed. The input for the mesh generator and the material parameters are equal to those used in the simulations of the tensile tests in Chapter 4.1. The simulation in this chapter will be referred to further as simulation T1.

Stress-deformation relation

Fig. 34 shows the axial stress-deformation relation and the relation between the axial and the lateral deformation found in simulation T1. Qualitatively, the gradual softening and the increase of lateral expansion correspond well to what is found in experiments (Vonk [1992]). The irregular shape of the softening branch is caused by the heterogeneous structure, the process of localization and the two-dimensional character of the model. When a piece of concrete of the maximum-aggregate size fails, this has a

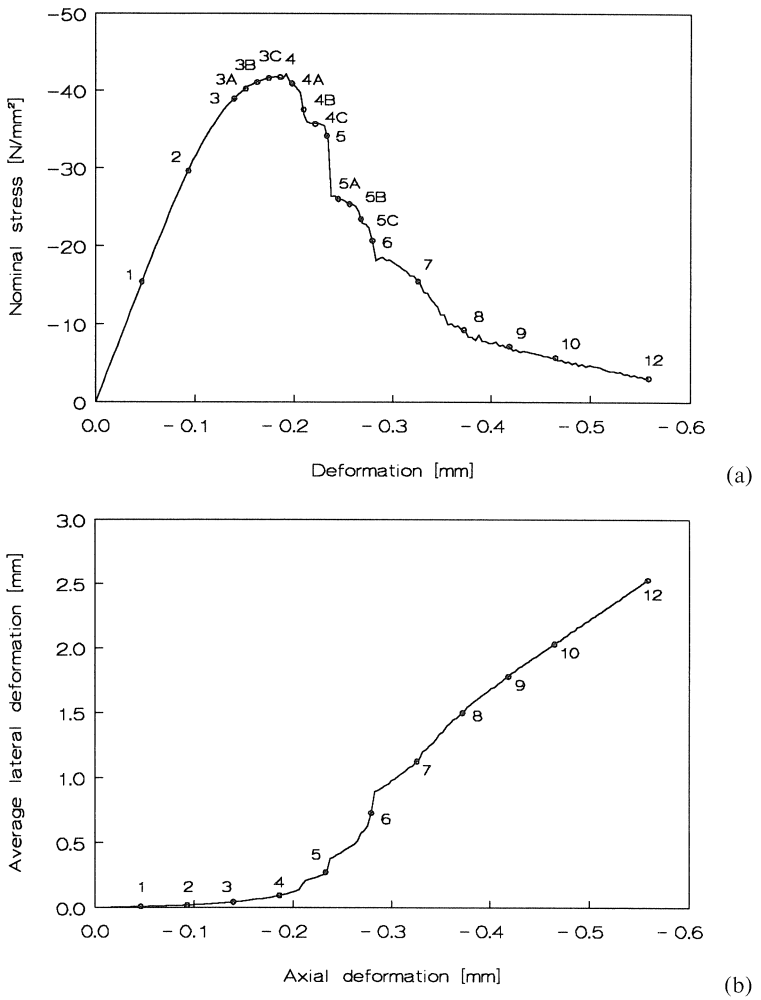

Fig. 34. (a) Axial stress-deformation relation and (b) relation between axial and lateral deformation for simulation T1.

significant influence on total resistance of the specimen. The steep drops in the stress-deformation relation show that this failure can have a brittle character.

Failure mode

Fig. 35 shows the predicted failure mode. Fig. 35a gives the interfaces with the largest normal and shear deformations. Only deformations larger than 0.1 mm are given. The thickness of the lines indicates the value of the deformations. The displacements of the corners of the finite elements are given as vectors. Fig. 35b gives the stress-free interfaces. The specimen is split up into a number of pieces which shear off. Localization of deformations is found. Each vertical line, the direction of the compressive loading, crosses approximately one inclined shear crack. The number of cracks crossed is sometimes larger than one due to the heterogeneity of the material, which causes some spread in the cracking. Additional cracks are found, which do not seem to be an essential part of the failure mechanism. They were created before the final failure mechanism was formed or were caused by stresses introduced by the sliding of the crack faces.

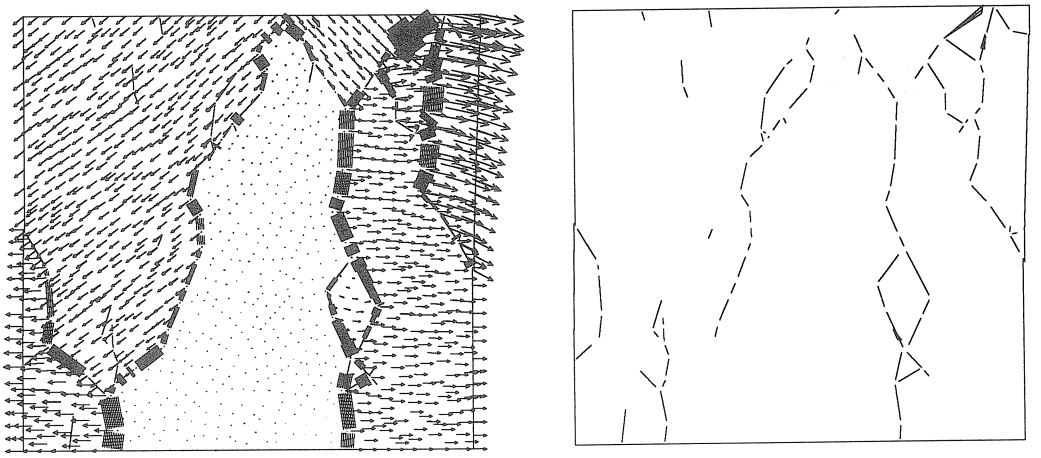

(a) (b)

Fig. 35. Failure mechanism for simulation T1: (a) interfaces with the largest normal and shear displacements (>0.1 mm) combined with displacement vectors of the finite elements and (b) stress-free interfaces.

Growth of damage

The growth of damage in the interfaces is shown in Fig. 36. The numbers of the pictures in this figure correspond to the stages in the failure process presented in Fig. 34. The thickness of the lines indicates the magnitude of the damage parameter $\varkappa$ of the interface model. Damage is already found for a low stress level (stage 1). The damage is found in the bond interfaces, more or less parallel to the direction of compressive loading. It is initiated by the combination of splitting and shear stresses caused by the composite structure of the concrete. During further deformation the damage zones

grow along the boundaries of the aggregates. At 75% of peak stress (stage 2) the damage zones start to extend through the mortar, connecting the damage zones around the aggregates. This corresponds closely to the observations in tests of Hsu et al. [1963]. The damage is still distributed. At peak stress the growth of damage accelerates (stage 4). The localization of damage starts from this moment on and is clearly shown at stage 12.

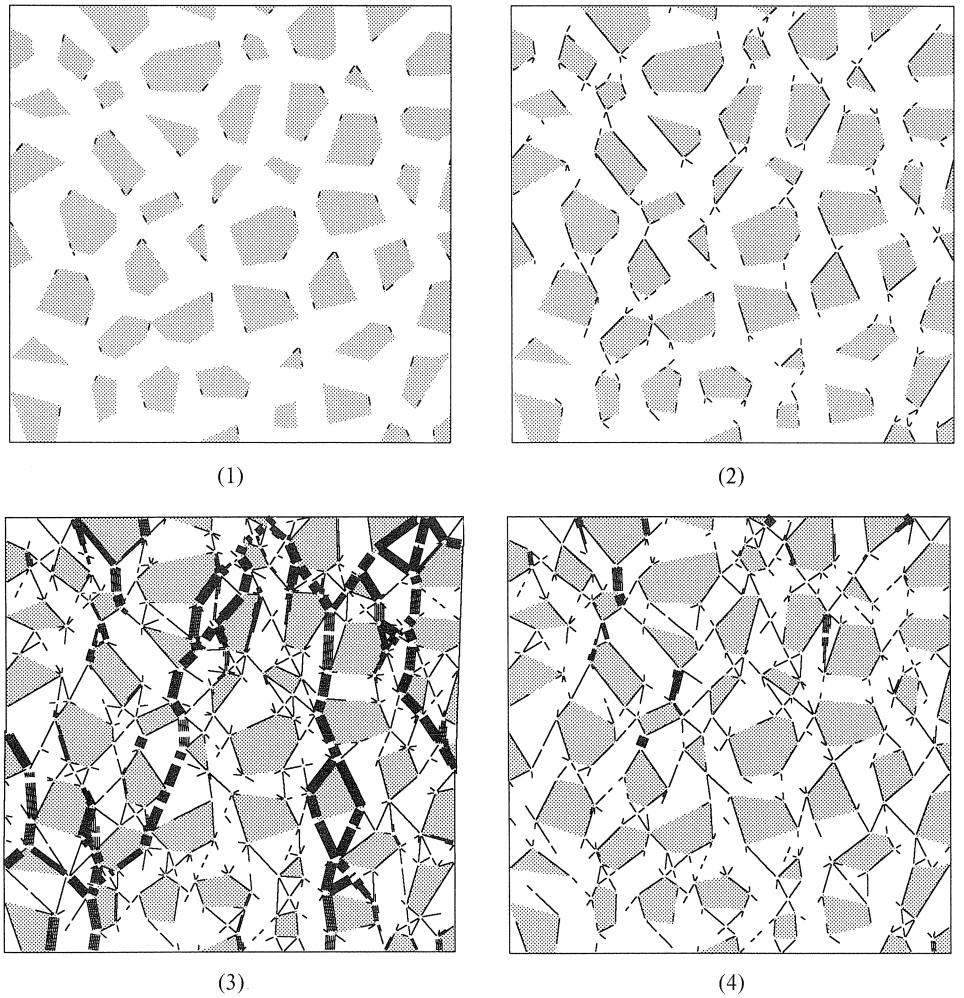

Fig. 36. Growth of damage in simulation T1. The numbers in this figure correspond with those in Fig. 34.

Failure process

The failure process, including localization of deformations, is illustrated best by the deformations of the interfaces and velocities of the finite elements. These are shown in Fig. 37. Both normal and shear deformations are shown, but the larger of the two is

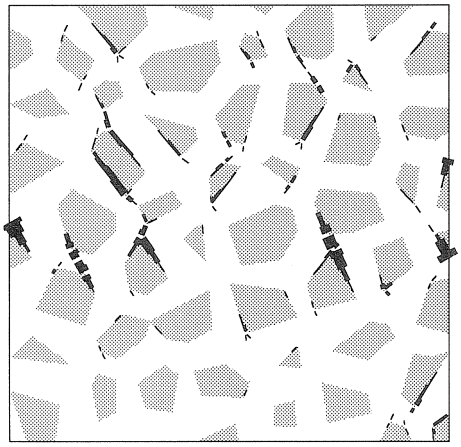

(2)

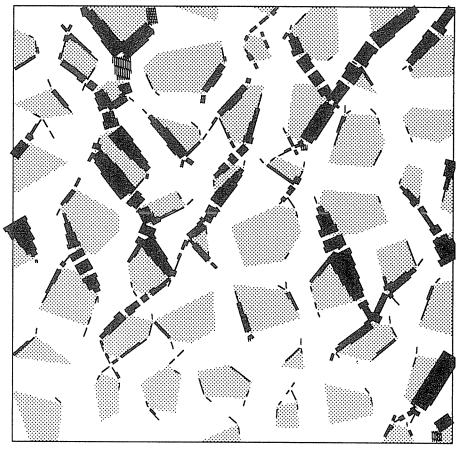

(3)

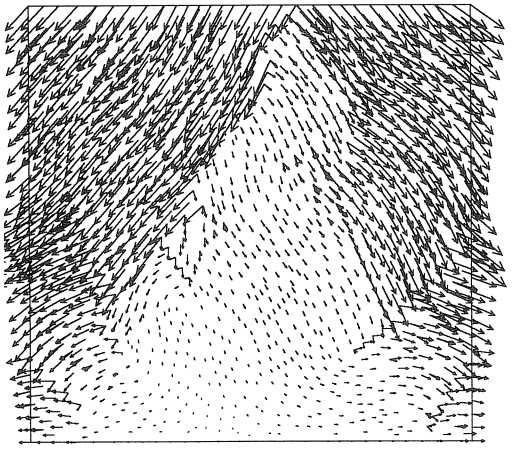

(4a)

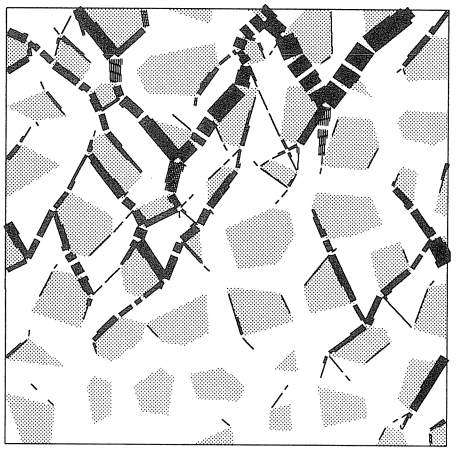

(4a)

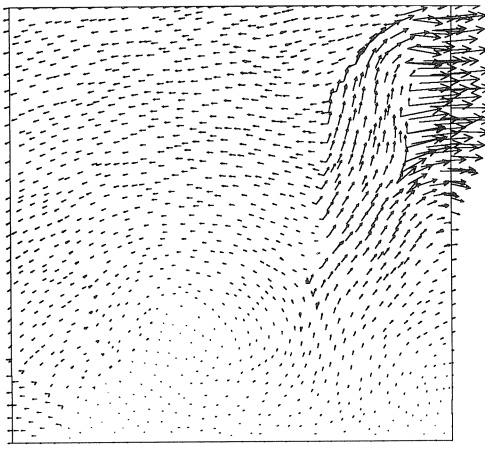

(4b)

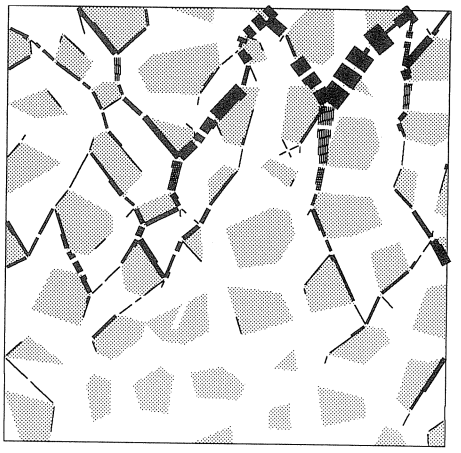

(4b)

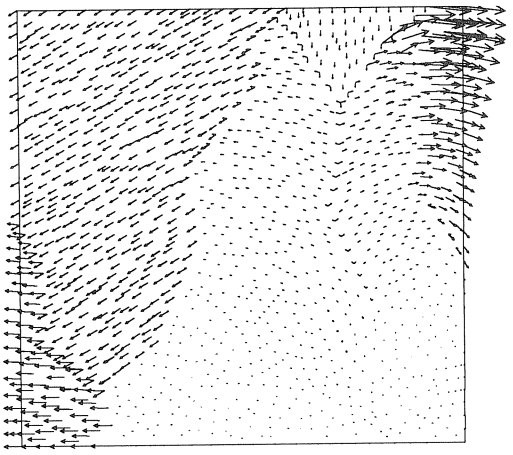

(5a)

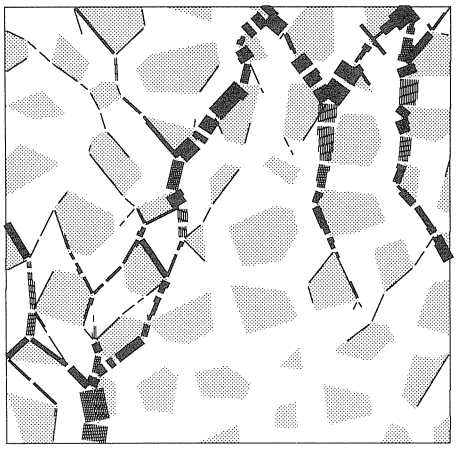

(5a)

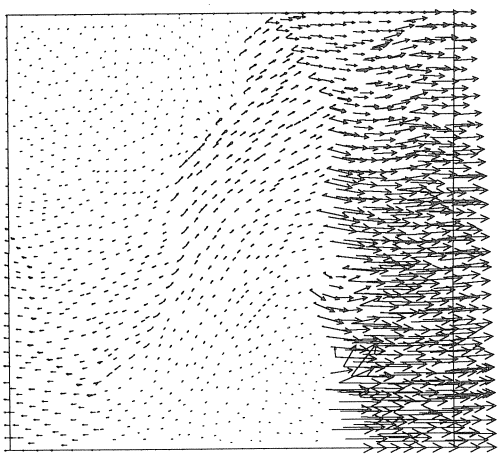

(6)

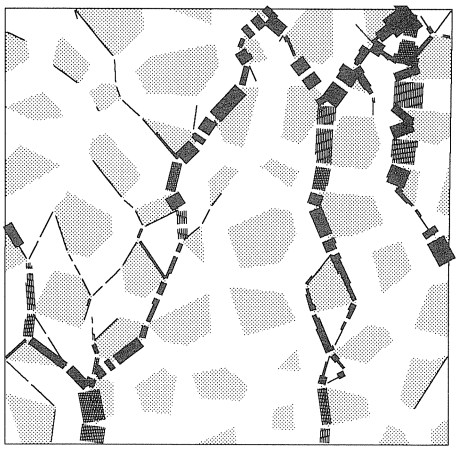

(6)

Fig. 37. Interface deformations and incremental displacements of finite element corners at several stages of simulation T1. The numbers in this figure correspond with those in Fig. 34.

visible for each interface. The thickness of the lines is proportional to the size of the deformations. It should be noted that the scale of deformations is different for the different pictures in Fig. 37. To simplify the discussion, groups of interfaces, which deform significantly more than the other interfaces, will be called cracks.

At stage 2, at 75% of peak stress, a number of small cracks is found which are isolated and do not seem to influence each other. At stage 3, at 90% of peak stress, the length of the cracks has increased considerably. They have started to influence each other, but have not yet formed a continuous pattern. The cracks are arrested by zones of higher strength, i.e. mortar and aggregate, or by cracks in other directions. As in the simula-

tions of tensile tests, crack overlaps are found. Overlapping cracks seem to be quite stable, probably because it takes a considerable amount of energy for these cracks to connect by means of a curved crack path.

At peak stress, some of the larger cracks connect in the upper-middle part of the specimen and form a continuous pattern. The result is shown at stage 4A. This is beginning of the growth of the final crack pattern in which the localization of deformations takes place. The first steep drop in the stress-deformation curve is due to the failure of the upper-right corner of the specimen, which is shown at stage 4B. This corner is split off in a brittle mode. Further crack growth is mainly determined by the two triangular pieces in the upper part of the specimen, which are pushed downward. This causes the growth of two splitting cracks. The second steep drop in the stress-deformation curve is due to the failure of the bottom-left corner of the specimen, when the left splitting crack reaches this area. The result is shown at stage 5A. The crack pattern is completed when the right splitting crack reaches the bottom of the specimen at stage 6. This causes the last drop in the stress-deformation curve. The final part of the softening curve is not due to crack growth, but to a decrease in resistance of the contacts (shear softening) and a decrease in the number of contacts due to opening of the crack pattern. Fig. 34b shows that at this stage, when the failure mechanism has been completed, the ratio between the axial and the lateral deformations becomes constant.

Localization of deformations

It is shown above that localization of cracking and deformations is found in a uniaxial compression test as the result of a continuous crack-growth process. Fig. 38 shows what this means for the deformations of the pieces of concrete between the macrocracks. Soon after the peak is passed, the deformations of these pieces decrease. The results compare quite well with the measurements of strain gauges in real tests (Vonk [1989, 1992]).

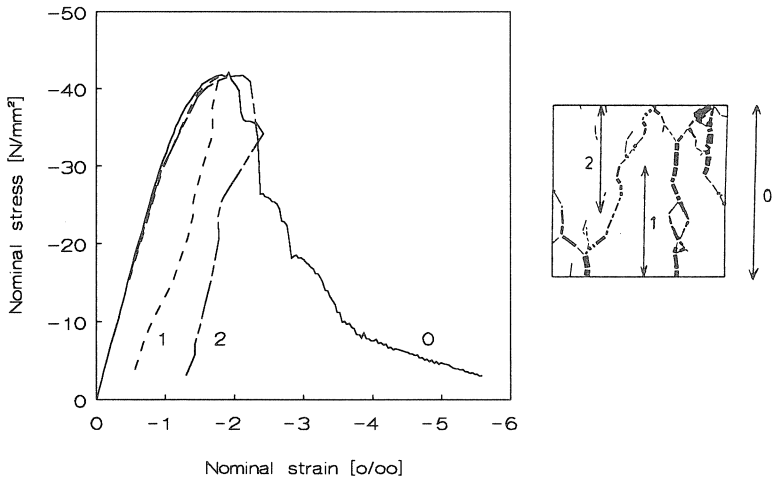

Fig. 38. Overall and continuum deformations for simulation T1.

4.3 *Sensitivity study*

Random composite structure

To investigate the influence of the random generation of the composite structure, three more simulations with different meshes, but generated with the same set of parameters as used for simulation T1, were carried out.

Stress-deformation relations

The nominal stress-deformation relations and the relations between axial and lateral deformations in Fig. 39 agree very well up to peak stress. Post peak, the differences in the composite structures result in significant differences in softening, as was found in Chapter 4.1 for the tensile tests. This scatter has to be taken into account when the results of micromechanical simulations are interpreted.

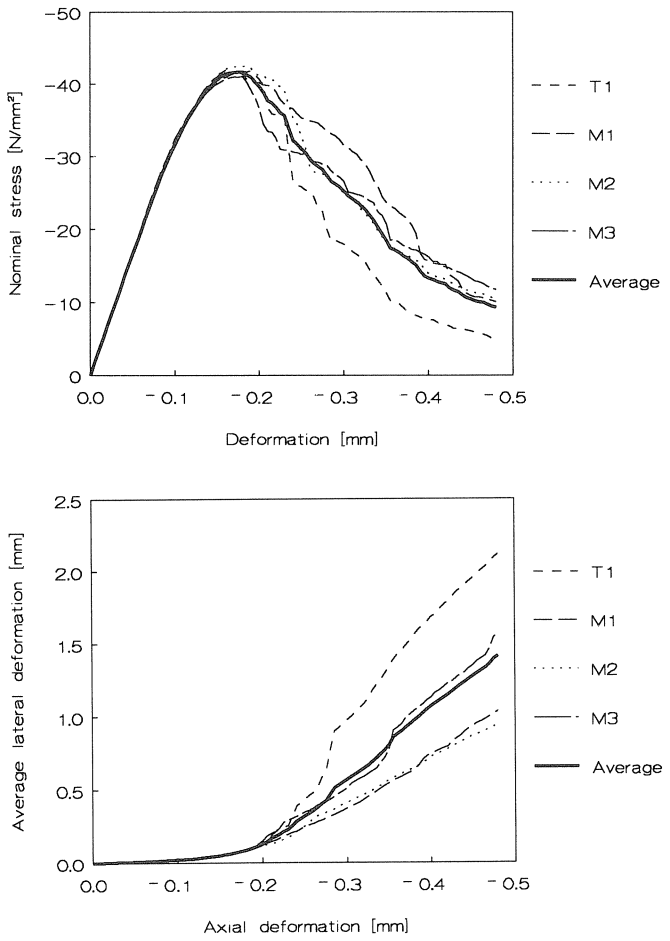

Fig. 39. (a) Stress-deformation relations and (b) relation between axial and lateral deformation for 4 different composite structures.

Crack patterns

Due to the heterogeneous material structure and the unconstrained lateral boundary conditions, a significant variation in crack patterns is found in Fig. 40. All the specimens are split up into pieces which shear off, but shape and size of the pieces differ significantly. The continuous cracks, which are combinations of more or less vertical splitting cracks and inclined shear cracks, make an angle of 20° to 30° with the direction of compressive loading. Where the continuous cracks reach the boundaries of the specimen or are arrested, the cracking become more irregular and spreads out.

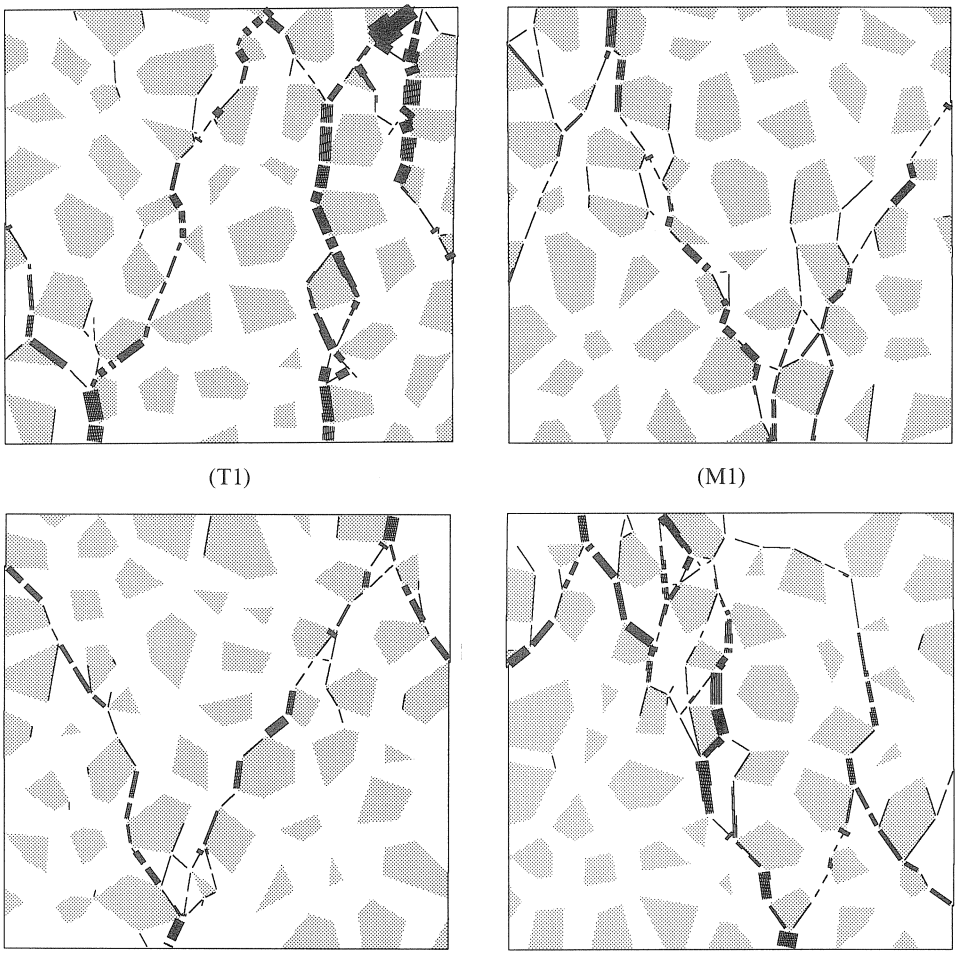

Fig. 40. Failure modes found for 4 different simulations.

Variation in material parameters

Fig. 41 gives a summary of the variation of material parameters used to study the sensitivity of the micromechanical model with respect to their values. First, the

parameter values are given for the default case T1 (see also Fig. 28). Next the modified parameter values are given, which are substituted in the default case to test their influence on the results. One parameter is substituted each time, except in the case of the strength parameters. The values for the cohesion c_b and c_m are replaced in pairs, keeping the ratio between bond and mortar strength constant at 0.5 (variation code C). The same is done for the values of the tensile strength f_{tb} and f_{tm} (variation code FT). The ratio between bond and mortar strength (variation code RBM) is varied from 0.25 to 1.0 for both cohesion and tensile strength at the same time. The values for the mortar strength are kept constant, while the values for the bond strength are varied.

Fig. 41. Summary of parameter variation.

Default case T1		Variation				
Parameter	Value	Code	Value 1	Value 2	Value 3	
c_b	10	C	5	15		N/mm^2
c_m	20		10	30		N/mm^2
$tg\chi$	0.0	CHI	0.15	0.3		-
E_m	25000	EM	10000	20000	30000	N/mm^2
$tg\varphi$	0.3	FI	0.2	0.4		-
f_{tb}	3.0	FT	2.0	4.0		N/mm^2
f_{tm}	6.0		4.0	8.0		N/mm^2
$tg\psi$	0.0	PSI	0.15	0.3		-
f_b	3.0	RBM	1.5	4.5	6.0	N/mm^2
c_b	10		5	15	20	N/mm^2
w_{1max}	0.02	W1M	0.01	0.03		mm
w_{2max}	1.0	W2M	0.5	2.0	1×10^6	mm

The codes for the variations given in this table will be used further on in the discussion in this chapter. The results are presented in Fig. 42 by means of the nominal stress-deformation relations combined with the crack patterns and the relations between axial and lateral deformations. They are also denoted by the codes for the variations of the specific parameters.

Peak stress

The most important change in the nominal stress-deformation relation is found, when peak stress changes significantly. The peak stress is mainly determined by the cohesion (Fig. 42-C), the friction angle (Fig. 42-FI) and the ratio between bond and mortar strength (Fig. 42-RBM). When peak stress changes, the deformation at peak stress also changes. It seems that this change in deformation is mainly due to an elastic shift caused by the change in stress level at the peak. The inelastic part of the deformations at peak stress seems not to be influenced significantly by these parameters. As a consequence of the shift of peak stress and deformations at peak stress, the brittleness of the post-peak behaviour changes because the deformation due to which the softening ends is unaffected by a change in the above mentioned parameters.

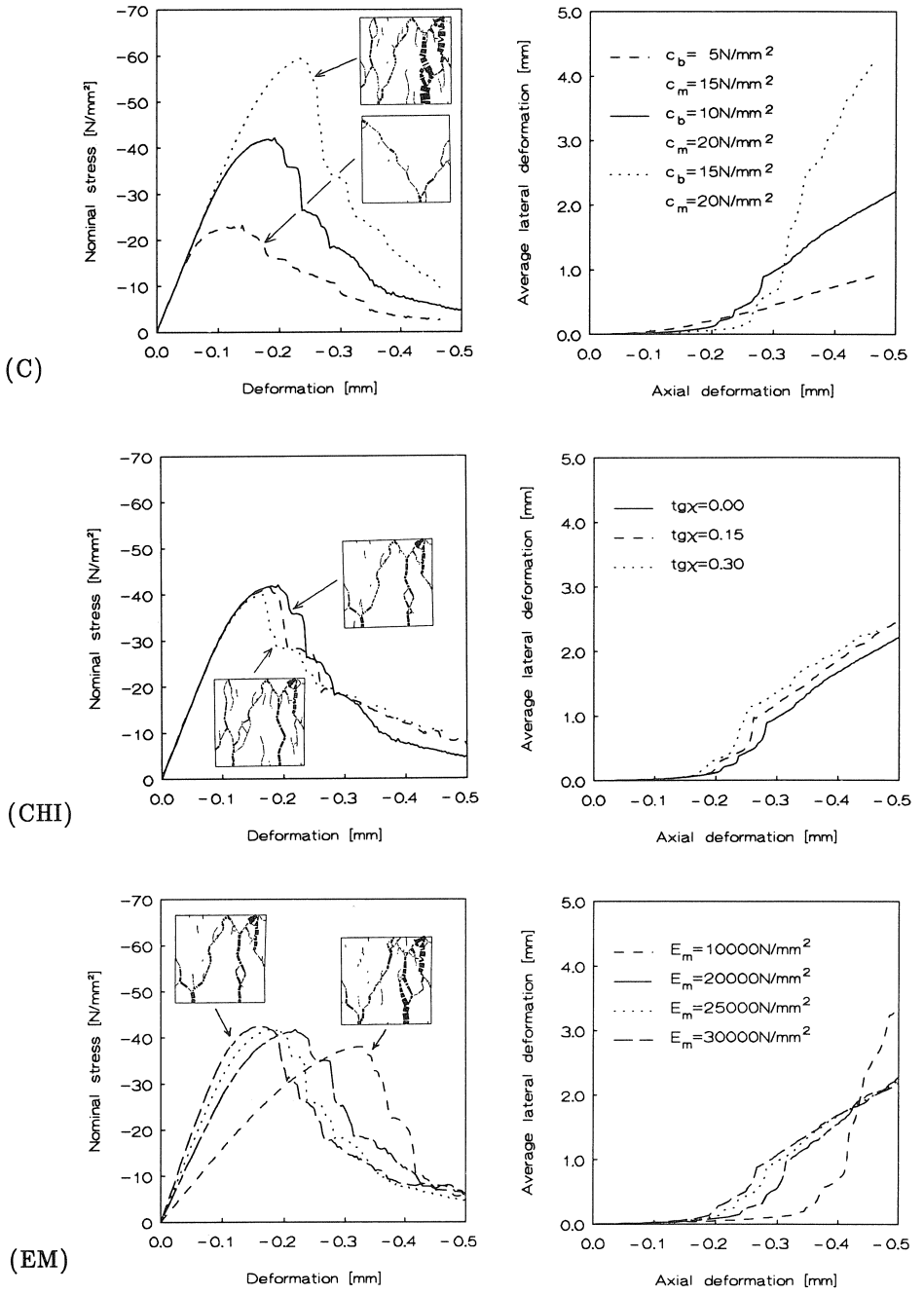

Fig. 42. Results of a variation of the cohesion (C), the reduction factor for tensile strength (CHI) and the modulus of elasticity of mortar (EM).

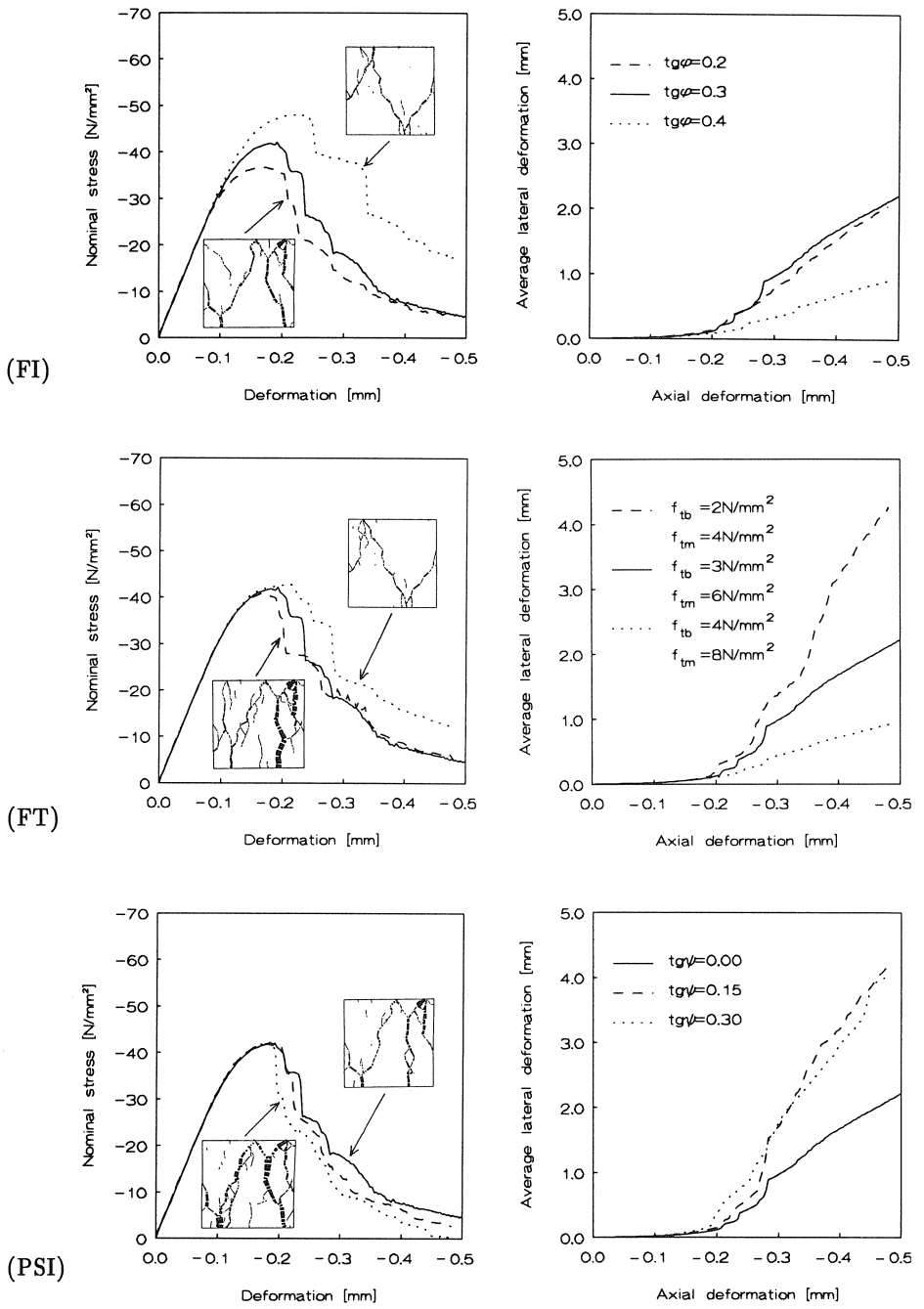

Fig. 42. Results of a variation of the friction (FI), the tensile strength (FT) and the dilatancy (PSI).

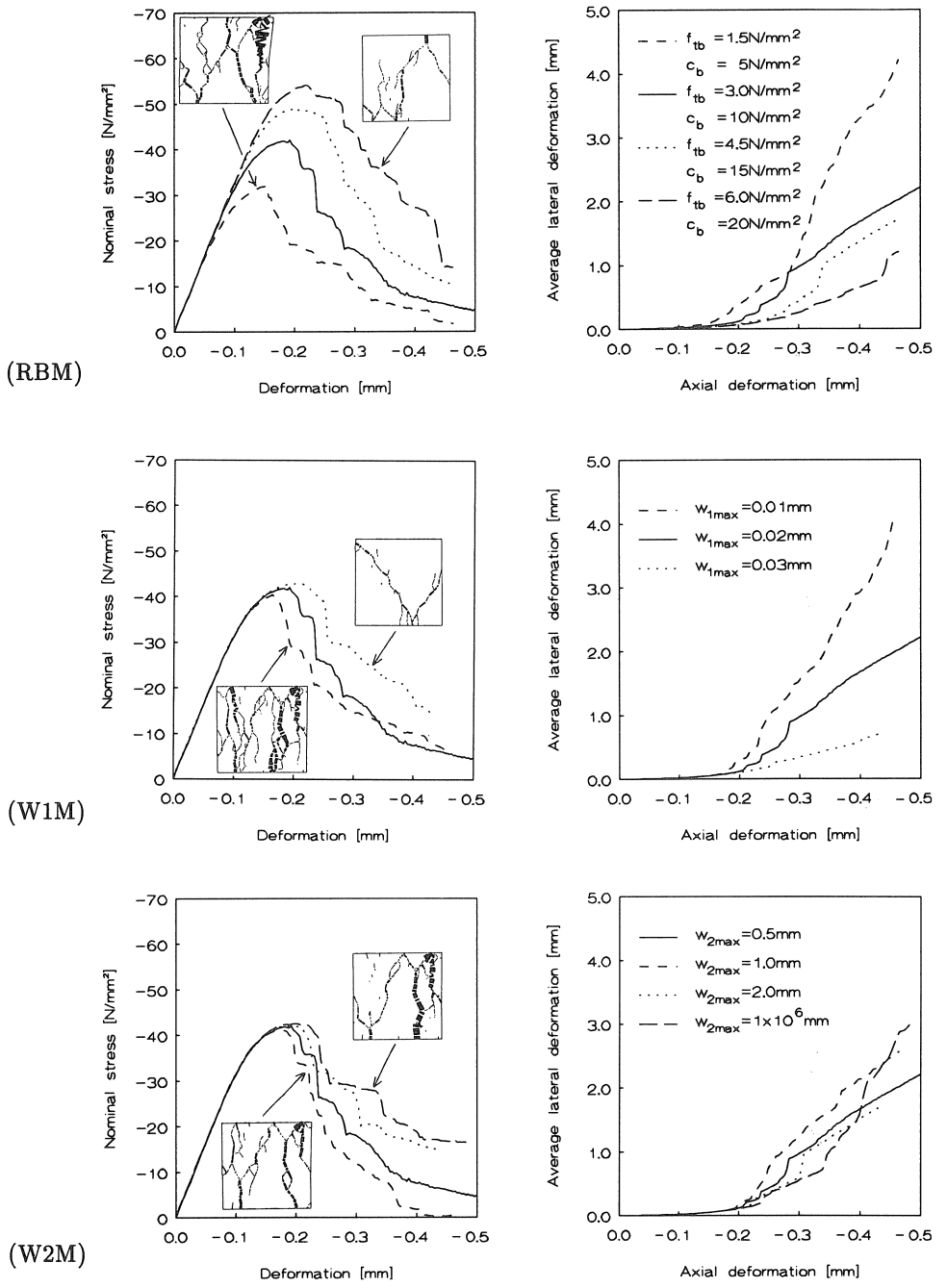

Fig. 42. Results of a variation of the ratio between bond and mortar strength (RBM), the maximum crack opening (W1M) and the maximum crack shear displacement (W2M).

End of softening

The maximum shear displacement w_{2max} for the interface behaviour is the parameter that determines the end of compressive softening (Fig. 42-W2M). What is interesting, is that an increase in maximum shear displacement to infinity does not make the softening disappear. This indicates that compressive softening in the model is not only due to shear softening of the interfaces, but also to a reduction of contact length caused by a gradual opening and shearing of the cracks.

Tensile fracture energy

The figures for the influence of the tensile strength (Fig. 42-FT) and the maximum crack opening (Fig. 42-W1M) indicate that an increase of the tensile fracture energy ($0.5 f_t w_{1max}$) has a positive influence on the fracture energy of the specimen under compressive loading. This influence is less than that of the parameters mentioned above. It modifies the compressive softening of the specimen, because it influences the opening and shearing of the crack pattern in which splitting cracks and shear cracks are combined.

Heterogeneity

A change in the modulus of elasticity of the mortar causes an elastic shift in the total stress-deformation relation (Fig. 42-EM). The failure mode is not changed. When the modulus of elasticity of the mortar decreases, slightly more damage is found in the pre-peak regime due to the larger stresses caused by the composite structure. The influence of the increase of these stresses is limited. The damage caused by these stresses, corresponding to the formation of splitting cracks, seems a stable process which does not influence the final failure process significantly. Also, the influence of the ratio between bond and mortar strength is less than expected (Fig. 42-RBM). The shape of the stress-deformation curve changes only slightly. The slight influence of the difference in moduli of elasticity and strength suggests that the heterogeneity introduced by the configuration of the mesh of interfaces determined by the composite structure plays a more important role in the simulation of uniaxial compression than the other factors. Actually, the acceptance of cracking in the interface elements alone is the most significant factor determining the heterogeneity in the model.

Lateral deformation and crack pattern

A general trend, which seems to be present, is that the lateral deformations increase when more vertical splitting cracks are present. This also makes the combined cracks steeper due to the fact that more splitting cracks are combined with inclined shear cracks. More splitting cracks are found when the tensile facture energy decreases due to a decrease of the tensile strength (Fig. 42-FT) or the maximum crack opening (Fig. 42-W1M). The same is found for an increase of the cohesion, which means a relative decrease of the tensile strength (Fig. 42-C). More splitting cracks are found too, when the bond strength decreases (Fig. 42-RBM). An increase of the dilatancy also increases the lateral deformations (Fig. 42-PSI). This causes faster opening of the cracks during sliding.

4.4 *Discussion and conclusions*

Comparison with experimental results

Comparing the average results of the 4 simulations in Chapter 4.3 to the results of experiments where the specimens were loaded with teflon platens (Vonk [1992]), which cause only a slight restraint to the lateral deformations of the specimen, it can be concluded that:

1. the total stress-deformation relation found in the simulations compares well with the experimental results (Fig. 43a);
2. the lateral expansion is described well by the simulations, although it is finally a little underestimated (Fig. 43b);

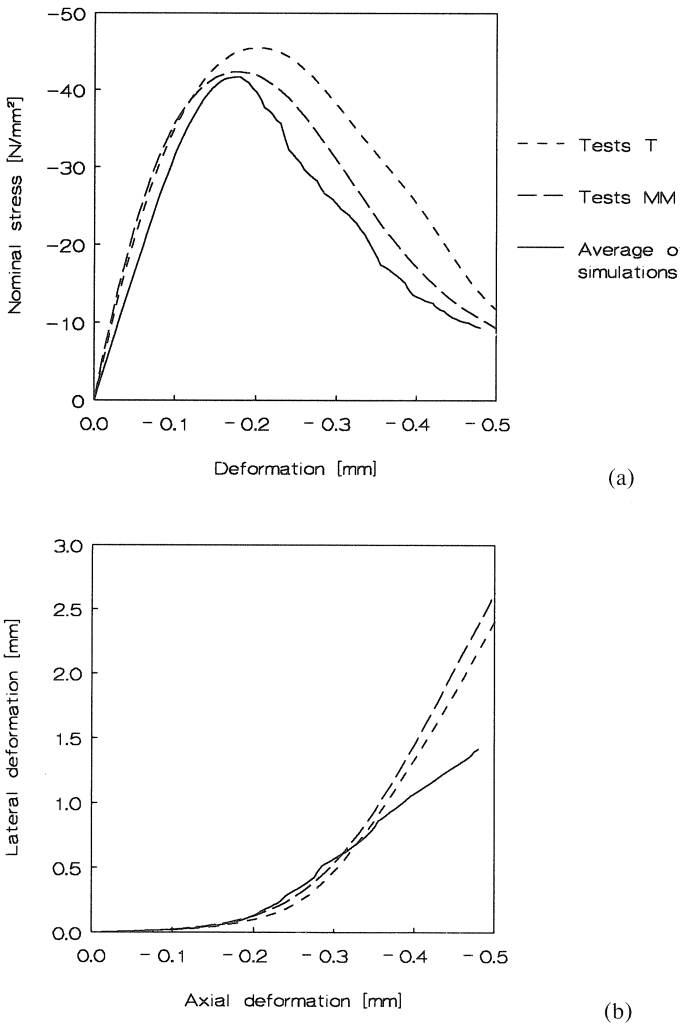

Fig. 43. Comparison of average simulation results and results of tests with teflon platens.

3. the failure mechanism observed in experiments (Van Mier [1984] is described well, but the number of splitting cracks is underestimated (compare Fig. 44a with Fig. 40);
4. the crack-growth process as described by the model compares well to the observations by Hsu et al. [1963].

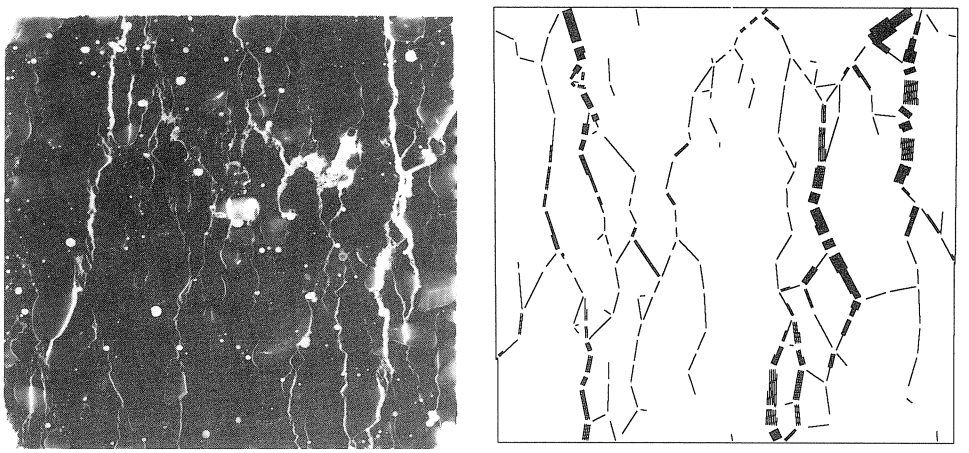

(a) (b)

Fig. 44. Comparison of crack patterns found in (a) a test with a low restraint to the lateral deformations (Vonk [1992]) and (b) a simulation with the micromechanical model with a low tensile fracture energy (simulation W1M, $G_{fb}=15\,J/m^2$, $G_{fm}=30\,J/m^2$).

Softening and localization in a compression test

According to the model cracks gradually grow in size in the pre-peak regime. Just past peak stress during the first softening localization of cracking is found and the macrocrack pattern forming the mechanism develops through the specimen. The final softening is for the most important part due to a decrease in resistance of the already existing macrocrack pattern.

Influence of tensile fracture energy

The compressive failure energy in the model is mainly dependent on the parameters describing shear failure. Shear failure is essential to the formation of the failure mechanism and requires a significant amount of energy. The compressive failure energy is only slightly influenced by the tensile fracture energy, because this failure mode requires only a relatively small amount of energy compared to that for shear failure. However, the tensile fracture energy influences strongly the number of splitting cracks and the lateral expansion. Fig. 44b shows that a reduction of the tensile fracture energy results in very realistic crack patterns.

Influence of heterogeneity

The sensitivity study has shown that the micromechanical model is less sensitive to the parameters determining the heterogeneity than was expected. In Vonk [1992] it was

shown that the model is also relatively insensitive to initial stresses in the model due to shrinkage of the mortar and to a stochastic distribution over the specimen of the strength parameters. This is probably caused by the presence of softening in the interface behaviour and the allowance of cracking only in the interfaces and not in the continuum. This basic property of the model is justified by the observations of crack formation in compression tests by Hsu et al. [1963]. It reflects the important role the large aggregates in normal strength gravel concrete play in the crack formation process.

Softening at the microlevel
Initially it was tried to describe concrete behaviour by introducing only brittle failure and friction in the interfaces on the microlevel of the micromechanical model. This resulted in highly irregular and brittle behaviour on the macrolevel. Therefore, softening was introduced at the microlevel. Brittle behaviour can probably be introduced at the microlevel, when the heterogeneous structure of concrete is modelled further down to a sufficiently small scale level. However, one has to realize that it is attempted to describe a three-dimensional process by a two-dimensional model. Failure of each interface in the two-dimensional model represents a complex three-dimensional process of crack growth, which is represented by softening. This means that it would be incorrect to model failure of these interfaces as brittle as long as the geometrical heterogeneity is not modelled in finer detail and in three dimensions. One should realize that a two-dimensional heterogeneous model is still homogeneous in the third dimension. Modelling concrete softening realistically by a two-dimensional model with brittle failure at the microlevel can probably only be done by making the geometrical heterogeneity more extreme than it is so as to compensate for the missing heterogeneity in the third dimension.

The above indicates that it is necessary to translate three dimensional properties and three-dimensional nonlinear processes into two-dimensional ones in order to obtain a quantitatively correct description of three-dimensional processes by a two-dimensional model. Whether this is possible without restrictions is a question which cannot yet be answered.

It is not easy to get a better fit of the model results with experimental results. This is a complex process of trial and error, which should be carried out for all kinds of tests. As stated above, it should also be borne in mind that a two-dimensional model will probably have its limitations in simulation of three-dimensional processes. In the present work, optimization of the model parameters will not be pursued further. It has been shown that the model is able to provide a good qualitative insight into the process of concrete failure and gives a reasonable description of a uniaxial compression test with a low restraint to the lateral deformations of the specimen by the loading platens. In the next two chapters it will be investigated what the performance of the micromechanical model is in the case of a varying restraint of the lateral deformations by the loading platens and in the case of a variation of the height of the specimen.

5 Influence of lateral boundary restraint

5.1 *Introduction*

Influence of lateral boundary conditions

Lateral expansion is essential to find failure in a compression test. A confining stress slows down the lateral expansion and makes a concrete specimen stronger and more ductile. A confining stress in the order of magnitude of 1 N/mm^2 already influences concrete compressive failure significantly (Jamet et al. [1984]). A partial confinement of a specimen is caused by the restraint of lateral expansion by the loading platens in a compression test. Tests carried out by Kotsovos [1983] (Fig. 45) show that when the influence of the lateral restraint by the loading platens on pre-peak behaviour is negligible, this does not have to mean that the influence on softening is neglibible. Obviously, softening is more sensitive to the lateral boundary restraint than pre-peak behaviour. Therefore it is necessary to take always into account the lateral boundary conditions when analysing compressive softening tests.

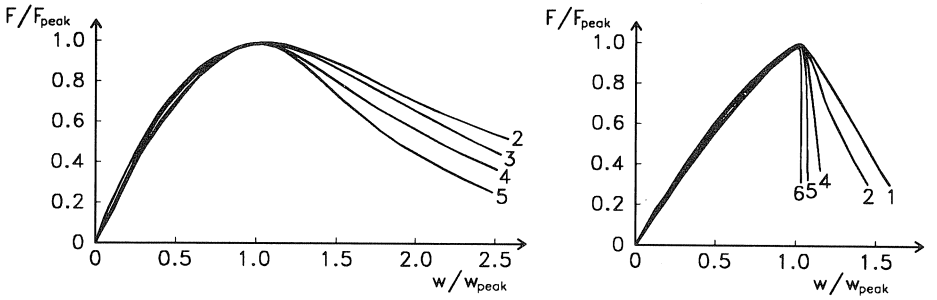

(a) (b)

Fig. 45. Influence of lateral boundary restraint on softening of (a) a low-strength and (b) a normal-strength concrete: the restraint increases when the number in the figure decreases (Kotsovos [1983]).

Tests with a varying lateral boundary restraint

In this chapter the influence of the lateral restraint by loading platens in a uniaxial compression test is investigated further by discussing a series of experiments with different loading platens. Subsequently a series of micromechanical simulations of the experiments will be discussed and compared to the experimental results in order to get a better understanding of the structural behaviour that is found in these experiments and to show that the micromechanical model is able to describe this behaviour and its dependency on the lateral boundary restraint.

The behaviour of 100 mm concrete cubes is analysed. They are loaded with dry platens, teflon platens and two types of steel brushes (see Chapter 3.1). The dry platens and teflon platens are used to investigate the considerable change in structural behaviour of a specimen subjected to these extremes of frictional boundary restraint. The two types

of brushes are used to investigate their different influence on softening, while their influence on pre-peak behaviour is negligible. Further it is interesting to compare the influence of steel brushes and teflon platens on the uniaxial compressive behaviour, as it is known that the influence of steel brushes on pre-peak behaviour is negligible, but that during softening the influence of the teflon platens becomes smaller than that of the steel brushes.

5.2 *Test results*

The most important test results are given in Figs. 46 and 47. To support the interpretation of the test results, Fig. 48 gives the estimated values for the average shear stresses induced in the specimen by the loading platens. The frictional stresses induced by the teflon platens and the dry platens have been calculated, interpolating or extrapolating the results of the tests carried out to measure the frictional properties of these platens (see Chapter 3.1 and Vonk [1989]). The shear stresses induced by the steel brushes have been calculated, taking the average value for a rod with two ends fixed and a rod with one end fixed and the other hinged. This average value was taken, because the end condition is not known exactly and is difficult to measure.

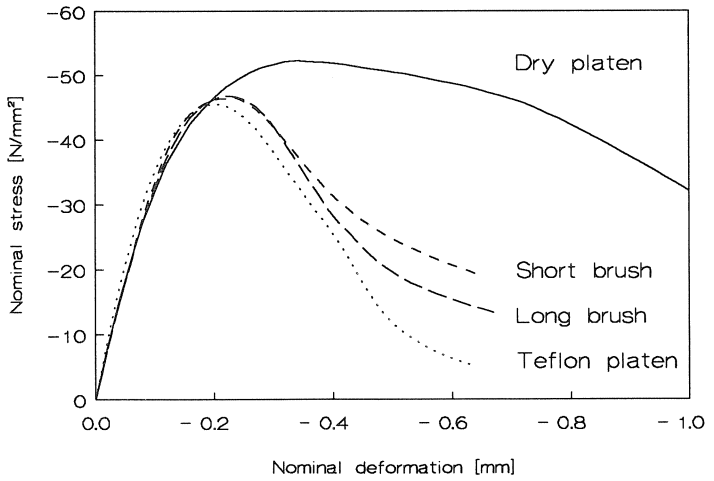

Fig. 46. Axial stress-deformation relations for tests with different loading platens.

High boundary restraint

Due to the high boundary restraint, the results of the tests with the dry platens differ significantly from the test results with the other loading platens. Peak stress is higher, post-peak behaviour is significantly more ductile and the lateral deformations are smaller for this type of test than for the others with a lower boundary restraint. Due to the frictional restraint, significant confining stresses are built up in the specimen near the loading platen. Fig. 48 shows that the average shear stress induced in the concrete

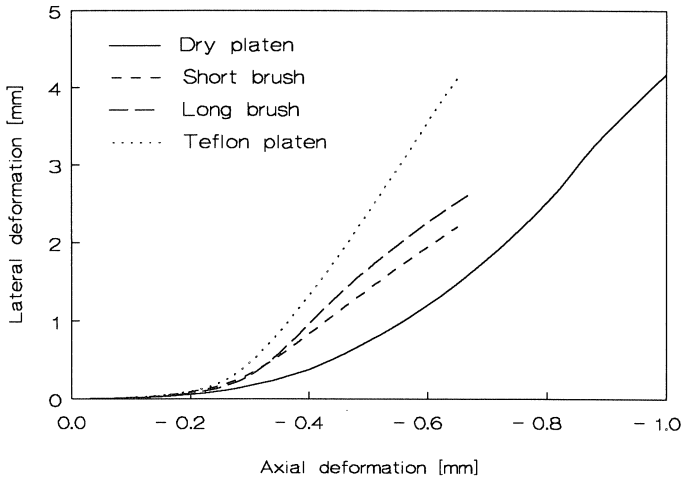

Fig. 47. Relations between axial and lateral deformation for tests with different loading platens.

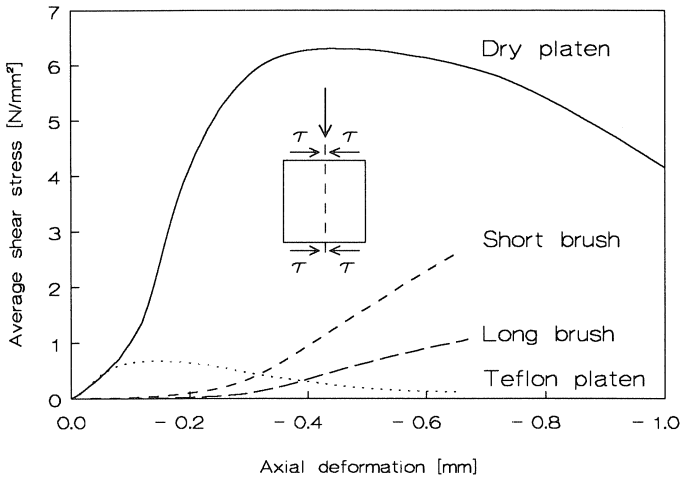

Fig. 48. Average shear stresses induced in the concrete specimens by the different loading platens.

by the dry platens is more than 6 N/mm^2, which means that the average confining stress in the middle vertical cross-section of the specimen is also more than 6 N/mm^2. This prevents crack formation in this part of the specimen, as is shown in Figs. 49 and 50. Cracking starts from the more uniaxially stressed sides of the specimen, which split off. This process results in the well-known hour-glass failure mode. Softening in this test is caused by a decreasing load-carrying capacity of a more or less intact core of the specimen, which reduces gradually in size. Compressive failure in this test is dominated

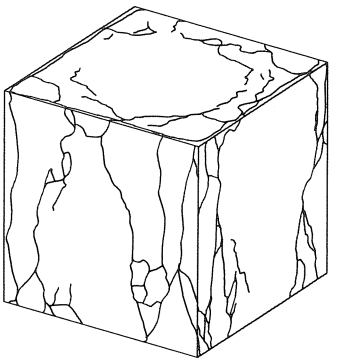

Fig. 49. External crack patterns for a test with dry platens.

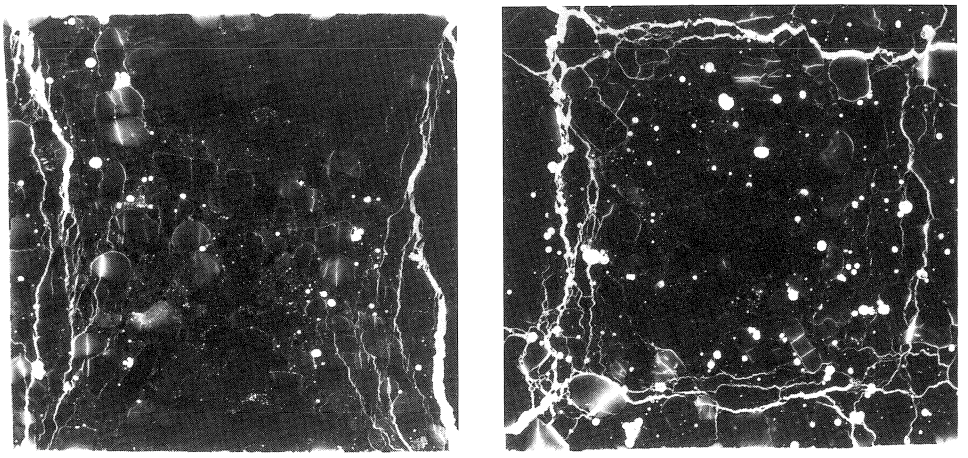

(a) (b)

Fig. 50. Internal crack patterns for tests with dry platens: (a) vertical plane, (b) horizontal plane.

by a nonuniform triaxial stress state, which causes a typical structural behaviour. It gives the impression that concrete loaded in uniaxial compression is ductile, what is not always true.

Low boundary restraint

Due to the low boundary restraint, the tests with the brushes and the teflon platens show a lower peak stress, a more brittle post-peak behaviour and a larger lateral deformation than the tests with the dry platens. Due to the reduction of the boundary restraint, peak stress reduces by 12% and the deformation at peak stress decreases from -0.34 mm ($-3.4‰$) to -0.23 mm ($-2.3‰$) for the brushes and -0.20 mm ($-2.0‰$) for the teflon platens. This agrees well with results of other tests. It should be noted that the reduction of strength is by no means a constant, but depends significantly on the

type of concrete and the test set-up. The compressive strength of a slender specimen is found to be 10 to 27% lower than the cube strength (Schickert [1980], Kotsovos [1983], FIP/CEB [1990]).

The axial stress-deformation curves for the brushes and the teflon platens show no significant differences until halfway along the softening branch, where curves start to diverge. Fig. 50 shows that then the shear stresses induced in the specimen by the brushes become greater than those induced by the teflon platens. This causes the softening of the specimens loaded with the brushes to slow down. This is not found for the tests with the teflon platens due to the decrease in shear stresses found for these tests. The smaller lateral boundary restraint by the teflon platens is also reflected in the lateral deformations in Fig. 47, which are greater at the end of the tests for the teflon platens than for the brushes.

It is shown that for larger deformations the softening stress is for an important part due to the restraint of the lateral deformations by the brushes, which have been used. No conclusions can be drawn from the differences around peak stress, because there the scatter in test results is too great to make the differences meaningful.

For all tests with brushes and teflon platens, qualitatively the same crack patterns were found at the end of the test. A characteristic example of the crack patterns found in these tests was shown in Figs. 44a. It shows a random configuration of splitting and shear cracks, which reveals no clear influence of the boundary restraint as found for the tests with the dry platens. It seems that the higher shear stresses induced by the teflon platens around peak stress did not have a significant influence on the configuration of the crack pattern. The divergence of the softening curves is probably due to the fact that the already been formed cracks cannot open and shear off easily due to the restraining shear stresses induced by the loading platens.

5.3 *Micromechanical simulations*

Frictional restraint

To be able to simulate the frictional restraint, two loading platens were modelled together with the specimen. The two loading platens were assumed to be infinitely stiff. The load was applied in deformation control, giving the upper loading platen a downward velocity. The frictional restraint is modelled by prescribing a coefficient of friction $\mathrm{tg}\,\varphi$ for the interface between loading platen and specimen. The elastic normal and shear stiffness of the interface was 2×10^5 N/mm^3. The high value for the shear stiffness means that the shear deformations were negligible until the maximum frictional stress was reached. Then, plastic slip was assumed to take place. Plane-stress conditions were assumed in the simulations. For these simulations the same material properties were used as for simulation T1 (see Fig. 28).

Simulation results

The results of the simulations are given in Figs. 51 to 53 inclusive. The coefficient of friction tg φ was varied from 0 to ∞. The coefficient of friction tg $\varphi = \infty$ means that all lateral deformations along the loaded boundaries were prevented completely. The axial stress-deformation relations in Fig. 51 show that compressive softening is highly sensitive to the frictional restraint along the loaded boundaries. A coefficient of friction of 0.01 to 0.05 already has a significant influence. This is also reflected in the lateral deformations in Fig. 52, which are slowed down considerably by the presence of friction along the loaded boundaries.

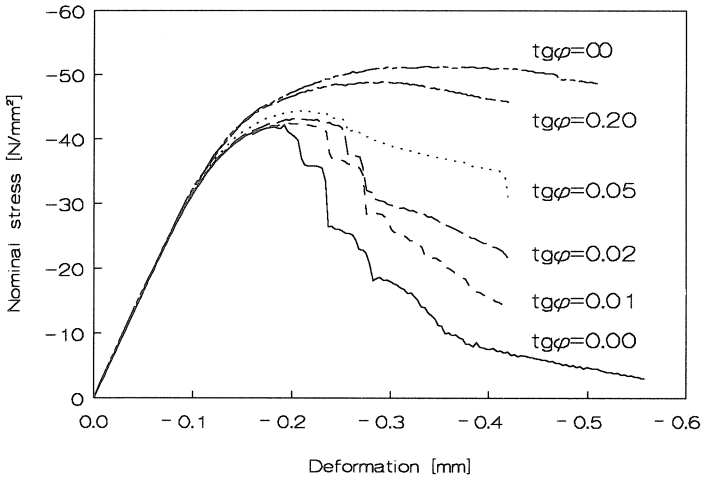

Fig. 51. Axial stress-deformation relations for the micromechanical simulations of the influence of the frictional boundary restraint.

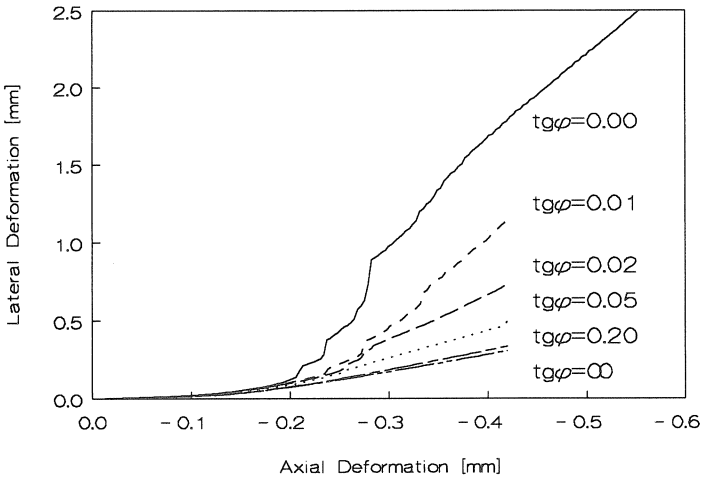

Fig. 52. Relations between axial and lateral deformation for the micromechanical simulations of the influence of the frictional boundary restraint.

For a low frictional restraint the crack pattern does not change in a qualitative sense. This is shown in Fig. 53. In the case of a low boundary restraint, opening and shearing of the cracks are delayed. This results in a slower reduction in the number of contact points in the crack pattern. An example of how the lateral boundary restraint influences the number and length of contacts in the crack pattern is shown in Fig. 54. This figure shows the stress-free interfaces for the simulations with coefficients of friction of 0.01

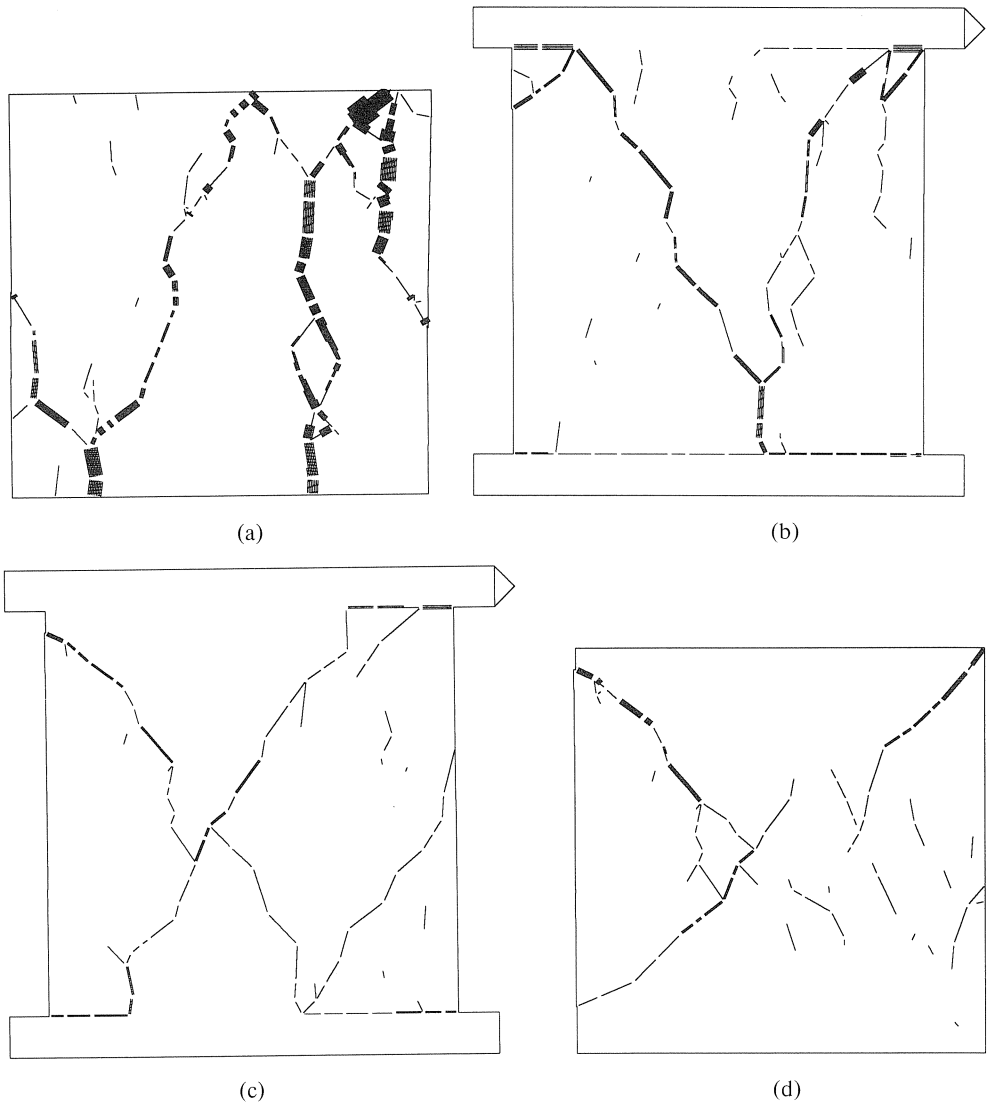

Fig. 53. Change in crack pattern for an increase of the frictional boundary restraint:
(a) $\mathrm{tg}\varphi = 0.00$ ($w = -0.465$ mm, $\sigma = -5.6$ N/mm^2),
(b) $\mathrm{tg}\varphi = 0.02$ ($w = -0.422$ mm, $\sigma = -21.6$ N/mm^2),
(c) $\mathrm{tg}\varphi = 0.05$ ($w = -0.422$ mm, $\sigma = -30.4$ N/mm^2),
(d) $\mathrm{tg}\varphi = \infty$ ($w = -0.464$ mm, $\sigma = -50.2$ N/mm^2).

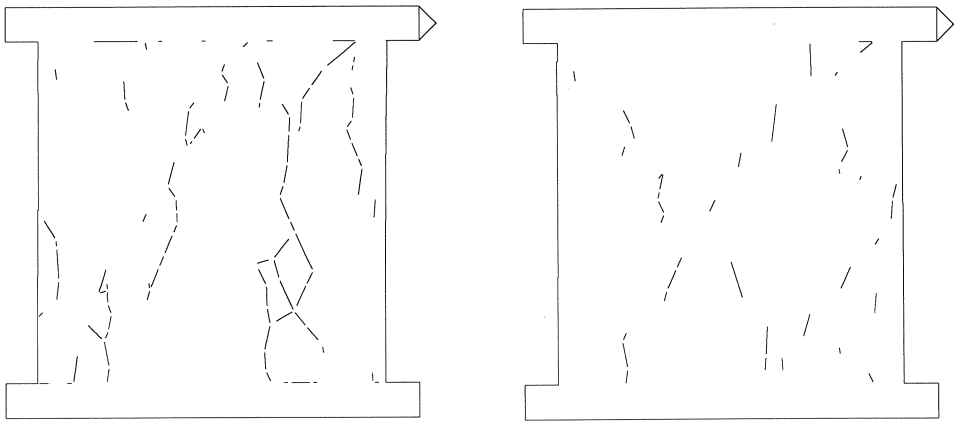

(a) (b)

Fig. 54. Stress-free interfaces for simulations with (a) $\mathrm{tg}\varphi = 0.01$ ($\sigma = -14.4$ N/mm^2) and (b) $\mathrm{tg}\varphi = 0.05$ ($\sigma = -30.4$ N/mm^2) at a deformation $w = -0.422$ mm.

Fig. 53 shows that, when the frictional restraint increases, the crack pattern changes gradually to the well-known hourglass shape. The crack pattern in the specimen can no longer have a random shape governed by the heterogeneous material structure, but is forced into a pattern determined by the nonhomogeneous state of stress in the specimen.

Due to the significant confining stress near the loading platen, this part of the specimen stays free of cracks, while the more uniaxially stressed sides of the specimen are forced to split off. To illustrate the failure mode, Fig. 55 shows the principal stresses in the specimen at the end of the simulation with the coefficient of friction $\mathrm{tg}\,\varphi = \infty$. It is shown clearly how the uncracked core of the specimen carries almost all the load. The creation of this failure mode takes considerably more energy than the failure mode with the zero boundary restraint. In the last case the crack pattern can search for the weakest links in the specimen to combine with them in a failure mode. In the first case the stress state determines what interfaces have to fail, regardless of the energy it takes to cause their failure. For an increase of the coefficient of friction from 0 to ∞, peak stress increases by 23% and the deformation at peak stress increases from -0.185 mm (-1.85‰) to -0.335 mm (-3.35‰), which is in good agreement with test results.

Influence of steel brushes

The lateral restraint by steel brushes has been modelled by giving the elastic shear stiffness in the interface between loading platen and specimen the appropriate value (see Fig. 21). In Chapter 3.1 it was shown that the shear stiffness of the long brush varies between $k = 0.70$ N/mm^3 and $k = 2.80$ N/mm^3 and that of the short brush between $k = 2.00$ N/mm^3 and $k = 7.99$ N/mm^3. Simulations have been carried out for all these values, Figs. 56 to 58 inclusive show the results of the simulations of the tests with the steel brushes. The influence of the steel brushes on compressive softening grows

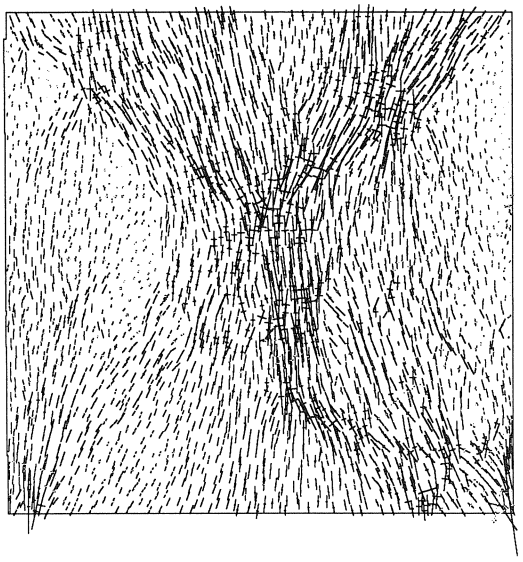

Fig. 55. Principal stresses at the end of the simulation with $\mathrm{tg}\varphi = \infty$ ($\sigma = -49.8$ N/mm^2, $w = -0.526$ mm).

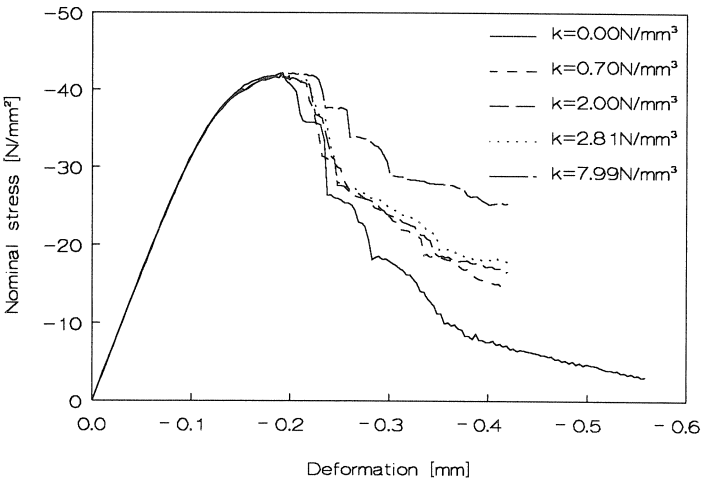

Fig. 56. Axial stress-deformation relations for the micromechanical simulations of the tests with steel brushes.

gradually. Peak stress is almost uninfluenced by the presence of the brushes because the shear stresses are still very low around peak stress. Post-peak the softening is slowed down more and more due to the growing shear stresses. This agrees well with the test results. Fig. 57 shows that the lateral deformations also become smaller and smaller when the lateral shear stresses increase. These differences in softening are not due to differences in the crack pattern. The crack patterns found for $k = 0.70$ N/mm^3 and

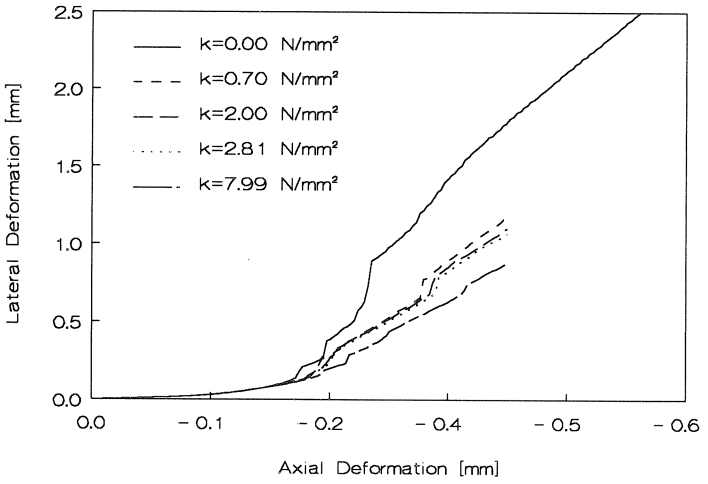

Fig. 57. Relations between axial and lateral deformation for the micromechanical simulations of the tests with steel brushes.

$k = 7.99$ N/mm^3 in Fig. 58 do not differ significantly from the crack pattern found for simulation T1 with $k = 0$ N/mm^3, which is shown in Fig. 53a. As for the tests with the low frictional restraint, the softening is mainly influenced by to the fact that opening and sliding of the already existing crack pattern is slowed down by the restraining shear stresses.

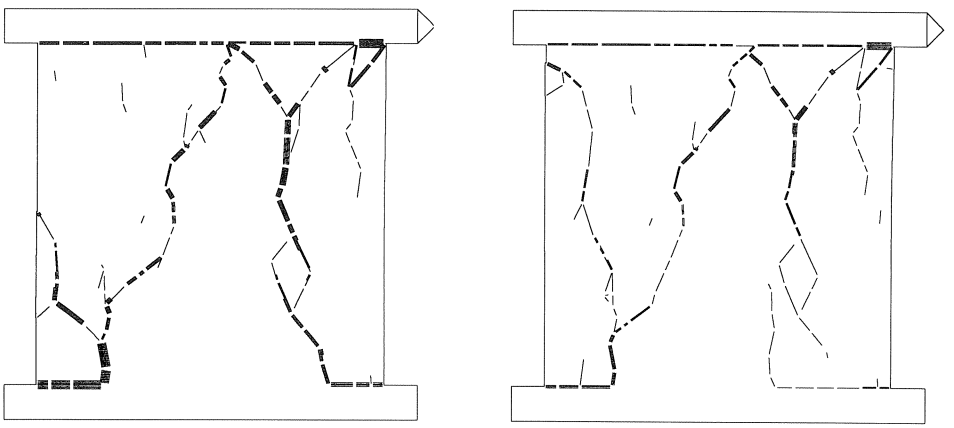

(a) (b)

Fig. 58. Crack patterns found in the simulations of the tests with the steel brushes for (a) $k = 0.70$ N/mm^3 and (b) $k = 7.99$ N/mm^3.

6 Influence of size

6.1 *Introduction*

Localization of cracking causes that the softening response of a specimen becomes dependent on its size. Continuum mechanics is no longer applicable, but fracture mechanics has to be used to be able to give a reliable description of the behaviour. For a long time it was not recognized that localization and consequently a size effect are present for compressive softening. The first indication was found in the test results of Van Mier (1984), who found a size effect in the softening response of specimens of different height loaded in compression. Investigating the post-peak behaviour he found a striking resemblance with the response found in tensile tests. This was surprising, because his test specimens did not show clearly a localized fracture like found in tensile tests. The specific crack patterns, which suggest a more distributed nature of cracking, have been the cause that it has not been recognized for a long time that a size effect should be present for compressive softening.
In Chapter 5 it was shown that the steel brushes used by Van Mier can have a significant influence on the softening response of a 100 mm cube, when the lateral expansion increases. This must also have caused a size effect, besides that due to localization of cracking, since lateral restraint by the brushes has a smaller influence on the softening response of a specimen when its slenderness increases. Therefore, a new series of size-effect tests on specimens of different height was carried out to investigate this phenomenon further, using teflon platens instead of steel brushes, because the teflon platens were shown to induce smaller shear stresses in a softening specimen than steel brushes. In this test series, the width of the specimens was varied too to get some indication of the influence of the lateral boundary restraint by the teflon platens, which is possibly still not negligible. In addition a series of micromechanical simulations of the tests has been carried out to investigate the abilities of the model to simulate the tests and describe the present size effect.

6.2 *Test results*

Test setup
The different specimen geometries used in the size-effect tests are shown in Fig. 59. Three different heights, 50, 100 and 200 mm, and two different widths, 50 and 100 mm, were used. All tests were carried out with teflon platens. A constant strain rate of 1×10^{-5} 1/sec was applied in all the tests irrespective of the height of the specimen. Further details about the testing technique can be found in Chapter 3.

Axial stress-strain curves
The nominal stress-strain curves for the different specimen geometries are shown in Fig. 60. This figure confirms that there is a size effect in compressive softening. The post-peak stress is less for a certain strain, the greater the height of the specimen. The differences are statistically significant (Vonk [1992]). It seems that the width of the

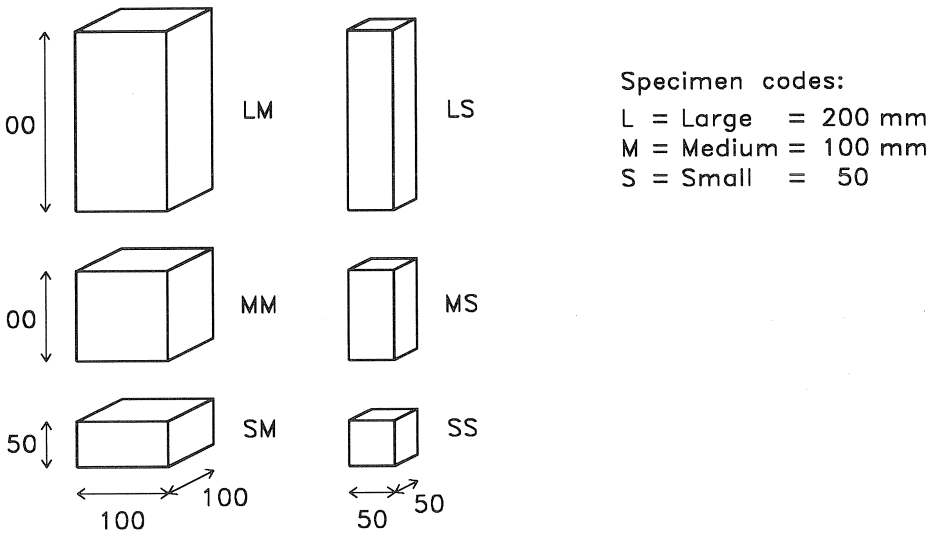

Fig. 59. Specimen geometries used in the size-effect tests.

specimen has also a slight influence on the stress-strain relation, but that this influence is less significant. Further, it is found that the influence of the specimen geometry on the stress-strain relation extends into the pre-peak regime. This results in an increase in peak stress as the height or the width of the specimen decreases.

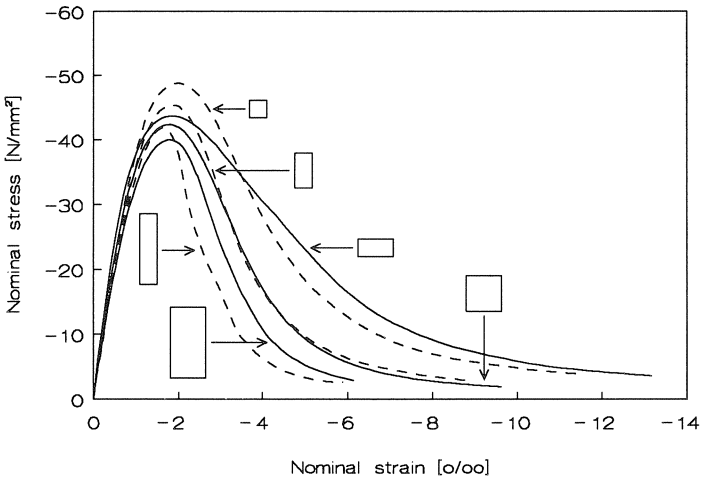

Fig. 60. Nominal stress-strain relations for the different specimen geometries.

Fig. 61 shows the dependence of the fracture energy per unit of volume on specimen geometry. The fracture energies have been calculated by integrating the stress-strain curves up to a softening stress of -2.9 N/mm^2. Estimating the energy in the tail of the

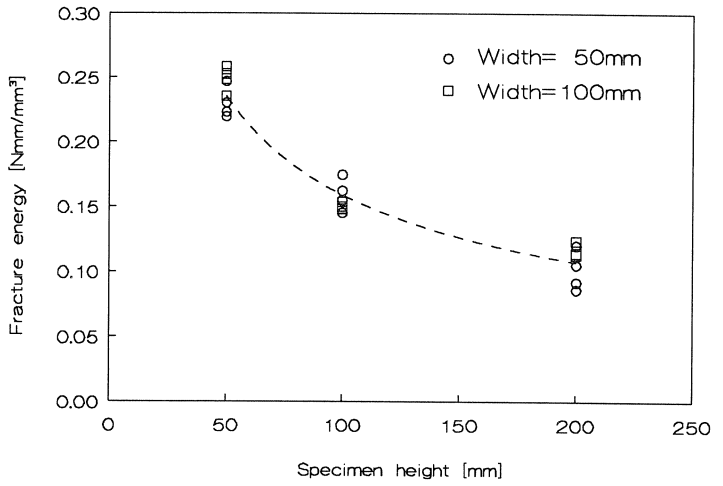

Fig. 61. Fracture energies per unit of volume for all specimens.

stress-strain relation was not attempted. This can not be done with any degree of accuracy. Theoretically the tail will extend to a strain of -1 ($= -1000‰$).

Lateral deformations

The lateral deformations of the specimens with a height-width ratio ≤ 1 showed a more or less uniform lateral expansion. The scatter in lateral deformations was significant. The relations between axial and lateral strains did not differ significantly for the

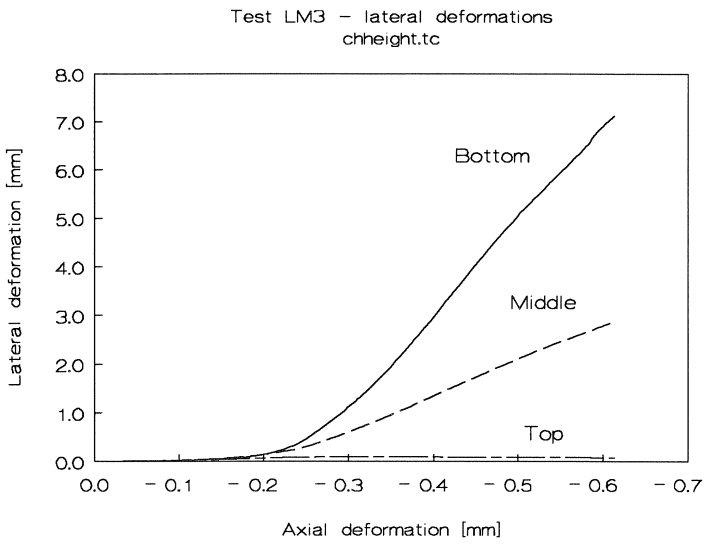

Fig. 62. Average lateral deformations in test LM3 for the bottom, middle and top of the specimen.

different specimen types. The measurements of the lateral deformations of all the slender specimens with a height-width ratio ≥ 2 showed a localization of deformations. An example is given in Fig. 62 for test LM3. The bottom of the specimen shows a significant lateral expansion during softening, while the top of the specimen stays almost passive and even shows a decrease in deformations. This indicates that it is mainly the bottom of the specimen that fails, while the top of the specimen stays more or less intact.

Crack patterns

Examples of internal crack patterns, recorded with ultraviolet photography after the tests, are shown in Figs. 63 and 64. There is a clear difference between the crack patterns for specimens with a height-width ratio ≤ 1 and a height-width ratio ≥ 2. The specimens with a height-width ratio ≤ 1 show crack patterns distributed over the whole specimen, while specimens with a height-width ratio ≥ 2 show parts which are free of macrocracks. In other words, these tests show localization of cracking. This agrees with the localization of lateral deformations for test LM3 shown in Fig. 63.

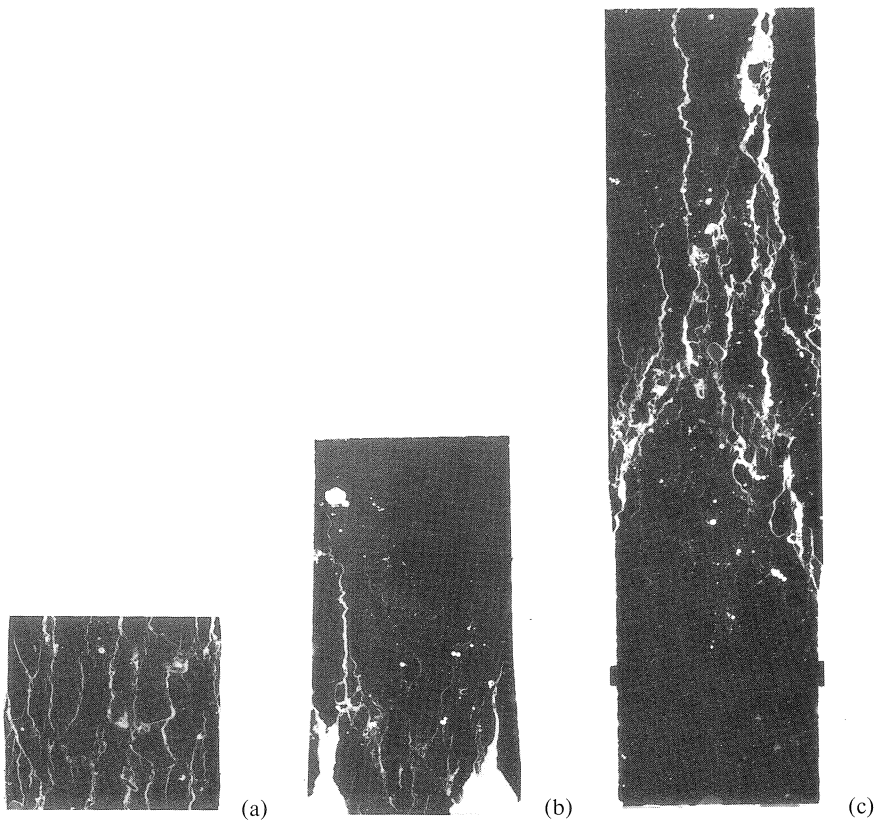

Fig. 63. Internal crack patterns (middle sections) for specimens with a width of 50 mm:
(a) test SS4 ($\sigma = -3.56$ N/mm^2, $\varepsilon = -12.35$‰)
(b) test MS3 ($\sigma = -2.76$ N/mm^2, $\varepsilon = -\ 9.62$‰)
(c) test LS2 ($\sigma = -2.57$ N/mm^2, $\varepsilon = -\ 5.71$‰).

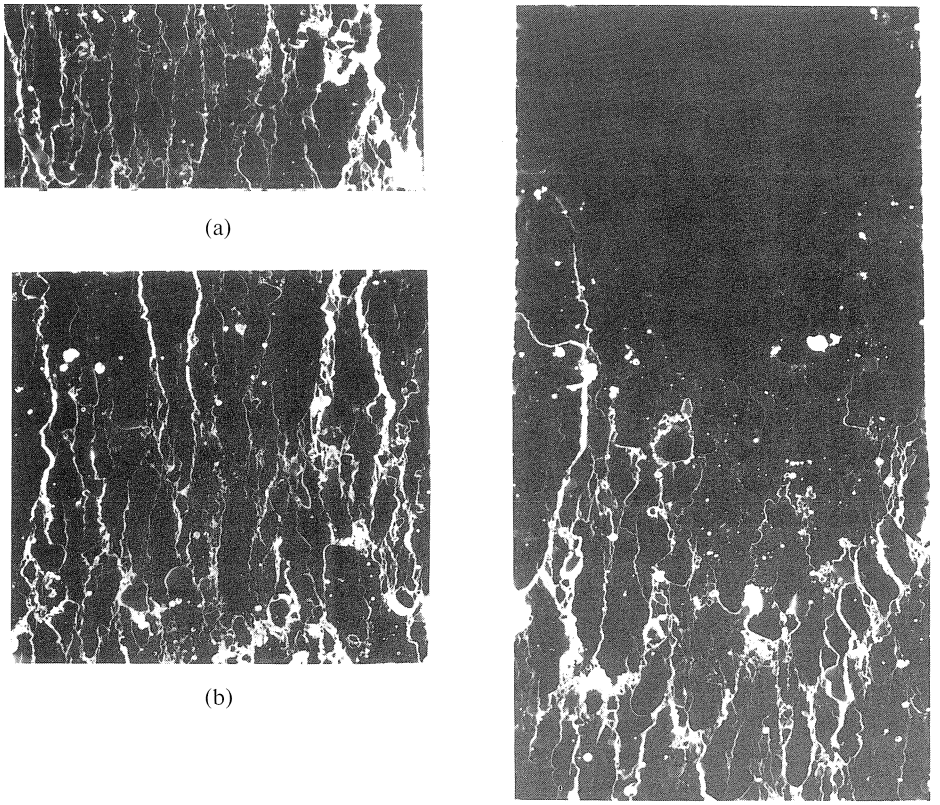

(a)

(b)

(c)

Fig. 64. Internal crack patterns (middle sections) for specimens with a width of 100 mm:
(a) test SM3 ($\sigma = -2.76$ N/mm^2, $\varepsilon = -9.62‰$)
(b) test MM4 ($\sigma = -1.87$ N/mm^2, $\varepsilon = -9.63‰$)
(c) test LM3 ($\sigma = -3.52$ N/mm^2, $\varepsilon = -6.13‰$).

Furthermore the crack patterns are qualitatively the same. The concrete is split up into many pieces which shear off. The more or less vertical splitting cracks, which are best visible, are distributed and have a spacing of approximately the size of the largest aggregate fraction (4–8 mm). However, little energy is required to create these splitting cracks. The inclined shear cracks, which are less well visible, are essential to the formation of the failure mechanism. Their formation and sliding requires more energy. Localization in the direction of compressive loading for these shear cracks is not easy to detect. For the specimens with a height of 50 mm it can be found that the number of inclined shear cracks crossed by a vertical line is limited, but is regularly greater than one. This indicates some localization, but not perfectly in one shear crack. However, for

the higher specimens, the crack patterns become more complex and the number of inclined shear cracks crossed by a vertical line is regularly greater than 1 or 2. A parallel shows up with the shear bands found for of granular materials.

Size effect in peak stress

Fig. 60 indicates that peak stress increases as the height of the specimen decreases. This effect was shown to be statistically significant. In Vonk [1992] some possible causes are discussed briefly. It seems not likely that the lateral restraint by the loading platens or differential shrinkage caused the observed effects. An interesting possibility is thought to be an extension of the size effect from the post-peak regime into the pre-peak regime.

Discussion of size effect in softening

Fig. 60 shows that a similar size effect on softening is found for the present tests with the teflon platens as was found by Van Mier [1984]. A comparison of the post-peak curves of the specimens with a width of 100 mm with the post-peak curves found by Van Mier for the specimens of the same width is given in Fig. 65. To facilitate comparison of the results the stresses have been normalized by dividing them by peak stress. Corresponding to the findings in Chapter 5, the tests with the steel brushes carried out by Van Mier show a more ductile post-peak behaviour than the present tests with teflon platens. Fig. 65 shows that the difference is larger as the height of the specimen decreases. Assuming that localization of deformations takes place at peak stress, analogous to tensile failure, Van Mier compared the post-peak stress-deformation curves for the different specimen heights and found a striking resemblance (see Fig. 3b). The post-peak curves for the present tests are shown in Fig. 66. These curves were determined by subtracting not just the deformation at peak stress, but by subtracting the inelastic pre-peak deformations as shown in Fig. 67. This was done to take into account elastic unloading of the continuum due to softening.

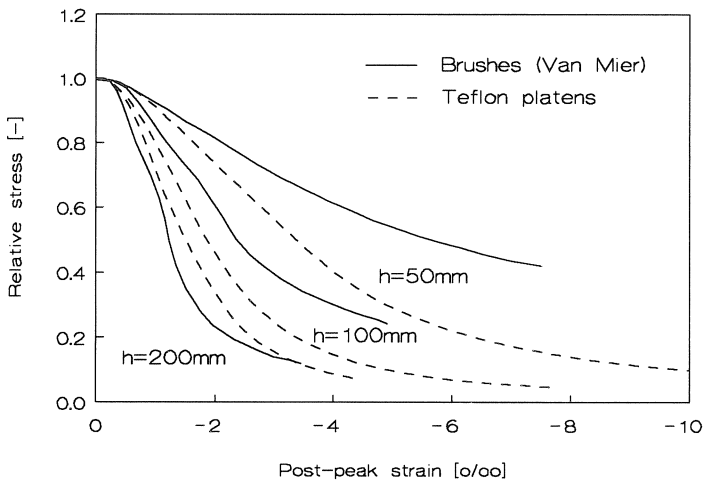

Fig. 65. Comparison of softening curves found by Van Mier [1984] with the present test results.

Fig. 66 shows that the post-peak curves are not equal, as found by Van Mier, due to the fact that the influence of the boundary restraint has been reduced. Here it is found that the post-peak resistance for a certain deformation increases as the height of the specimen increases. This indicates that the post-peak resistance is not only a result of a local process, but also depends on a diffuse process, which makes that the height, and thus

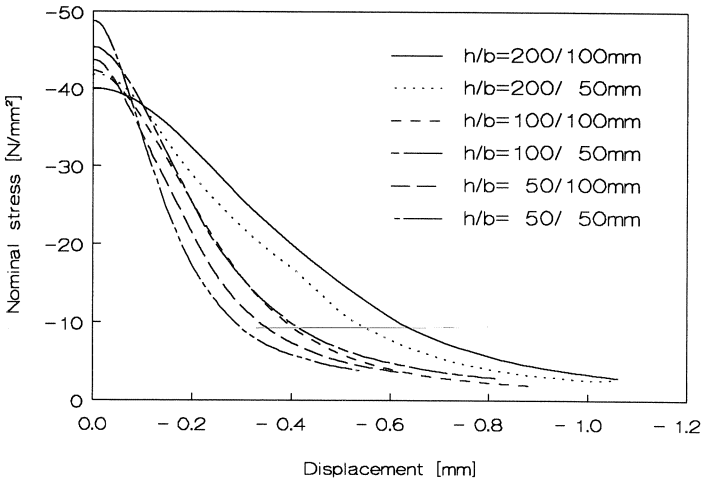

Fig. 66. Post-peak stress-displacement curves for all specimen geometries.

the volume, of the specimen has an influence. The same is observed when the estimated local fracture energy per unit of area is compared for all the different specimens (Fig. 68). The local fracture energy has been estimated by integrating the post-peak curves of Fig. 66 to a softening stress of $-2.9\ N/mm^2$, as is shown in Fig. 67b. If localization of cracking was perfect, the fracture energy would not depend on the height of the

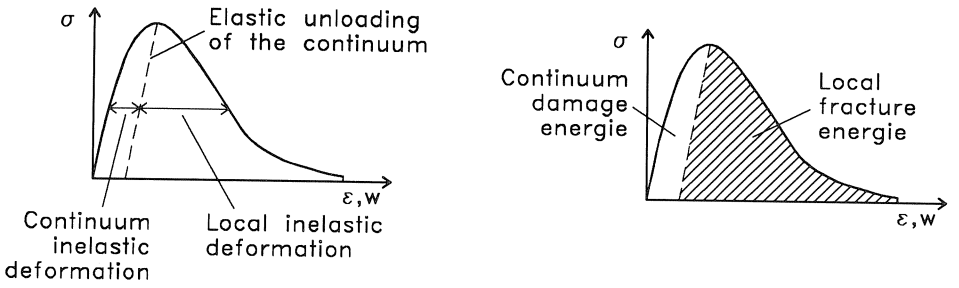

Fig. 67. Determination of continuum and local components of deformations and energies.

specimen as is found in Fig. 68. This indicates that compressive fracture is a mixture of a local and a diffuse process. A possible division into local and volumetric components is shown in Fig. 68.

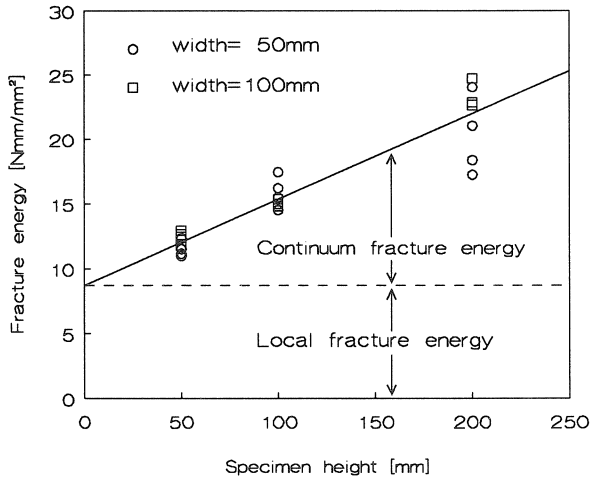

Fig. 68. Post-peak fracture energies for all different specimen geometries.

Influence of the specimen volume on softening

How can the influence of the specimen volume on the post-peak behaviour be explained? It seems that the diffuse cracking should be taken into account. Especially, the specimens with a height-width ratio ≤ 1 show a significant amount of almost vertical cracks distributed over the entire volume. The more slender specimens with a height-width ratio ≥ 2 also show a significant number of vertical cracks, but they are often not distributed over the entire volume. The many vertical cracks are probably a result of the forces introduced into the specimen by the shearing of the concrete pieces.

The average distance between the vertical cracks is approximately equal to the size of the largest aggregate fraction (4–8 mm). When it is assumed that the vertical cracks go completely through the specimen (area = b × h) in two directions, the energy needed for the formation of these vertical cracks can be estimated by

$$E = 2 \frac{b}{0.75 d_{\max}} bh\, G_f = \frac{8}{3} \frac{b^2 h}{d_{\max}} G_f$$

or

$$E/b^2 = \frac{8}{3} \frac{h}{d_{\max}} G_f$$

Here, $d_{\max}$ is the maximum aggregate size. The tensile fracture energy per unit of area G_f can be estimated as 0.12 Nmm/mm^2 for a normal-strength gravel concrete with a water-cement ratio of 0.5 and a maximum aggregate size of 8 mm (Hordijk [1991]). Then above equation results in fracture energies per unit area of 2, 4 and 8 Nmm/mm^2 for specimens with a height of 50, 100 and 200 mm, respectively. Comparing these fracture

energies to the values found in Fig. 68, it shows that this phenomenon can not be neglected and can explain the dependence of the fracture energy on the volume of the specimen. In the more slender specimens, the splitting cracks were not distributed over the total volume. However, in these specimens more inclined cracks are found of which the creation requires a significant amount of energy.

6.3 *Micromechanical simulations*

Details of the micromechanical simulations

Three tests on specimens with a width of 50 mm and a height of 50, 100 and 200 mm were simulated. The tests on specimens with a width of 100 mm were not simulated because of the limitations in computer time. The parameters for the mesh generation were chosen in such a way that the procedure resulted in a large-aggregate content (2–8 mm) of 0.375. This was equal to the large-aggregate content in the concrete used for the size-effect tests (concrete 2, Chapter 3.3). The stochastic parameters to disturb the interface mesh were kept equal to those used earlier.

The material parameters used in the simulations were approximately equal to those used in the previous simulations. They are summarized in Fig. 69. The moduli of elasticity were increased slightly, because in the previous simulations it was found that the actual modulus of elasticity of the concrete was underestimated. Also the values for the cohesion of bond and mortar were slightly increased, because the tests on the 50 mm wide specimens showed a higher peak stress than the boundary condition tests. Furthermore, a small dilatancy of 0.15 was introduced in the interfaces.

Fig. 69. Material parameters used for the simulations of the size-effect tests.

Continuum		Interface	
Aggregate	Mortar	Bond	Mortar
$E = 75000$ N/mm^2	$E = 30000$ N/mm^2	$f_t = 3.0$ N/mm^2	$f_t = 6.0$ N/mm^2
		$c = 11.0$ N/mm^2	$c = 22.0$ N/mm^2
$\nu = 0.2$			
		$K_1 = 5 \times 10^5$ N/mm^3	tg $\varphi = 0.3$
		$K_2 = 5 \times 10^5$ N/mm^3	tg $\psi = 0.15$
		$w_{1max} = 0.02$ mm	tg $\chi = 0.0$
		$w_{2max} = 1.00$ mm	

All specimens were loaded by moving the upper loading platen downwards in deformation control. The properties of the teflon platens were simulated as closely as possible with the interface model. Fig. 70 shows the interface parameters and the fit of the model parameters to the results of the friction tests on teflon platens (see also Chapter 3.1). The reduction of friction during the first sliding was modelled by introducing softening for the first 0.115 mm of sliding.

Interface parameters		
K_1	$=5\times10^5$	N/mm^3
K_2	$=200$	N/mm^3
f_t	$=0.0$	N/mm^2
c	$=0.39$	N/mm^2
tg φ	$=0.0115$	
tg ψ	$=0.0$	
tg χ	$=0.0$	
w_{1max}	$=0.0$	mm
w_{2max}	$=0.115$	mm

(a)

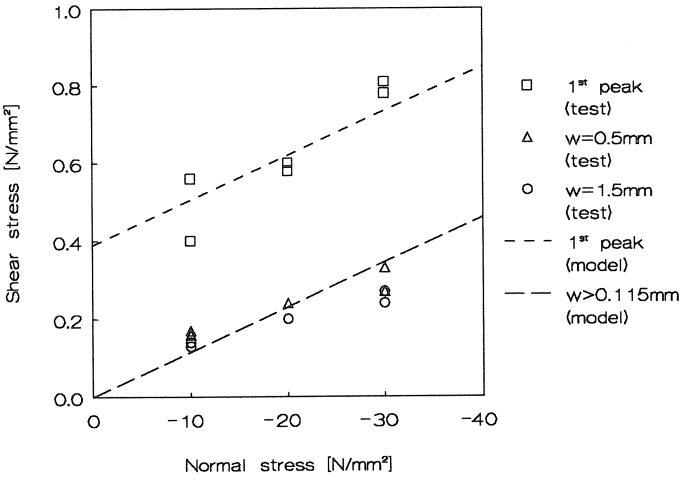

(b)

Fig. 70. (a) Interface properties to simulate the frictional properties of the teflon platens and (b) comparison of the interface properties and the results of the tests on teflon platens.

Results of simulations

The calculated nominal stress-strain curves are given in Fig. 71. A significant size effect for softening is predicted by the micromechanical simulations. On comparing the post-peak stress-deformation curves in Fig. 72, which are corrected for the inelastic pre-peak deformations, it is found that the micromechanical model, with the present set of material parameters, predicts an almost perfect localization after peak stress has been passed. This does not agree with the test results, which showed an influence of the continuum on the fracture process.

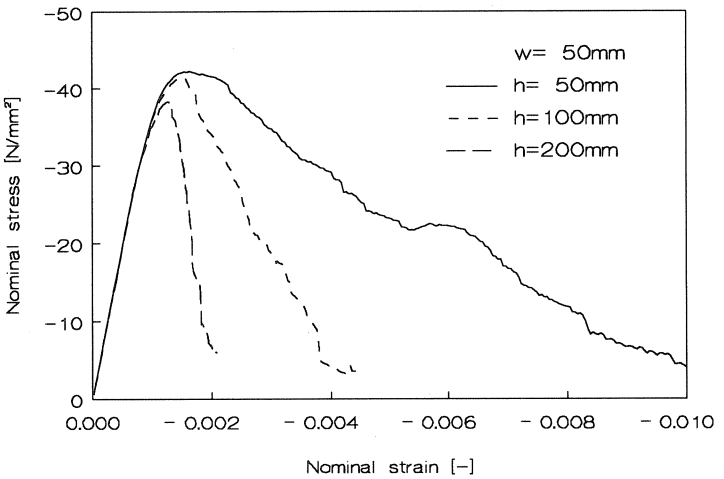

Fig. 71. Stress-strain curves found for the micromechanical simulations.

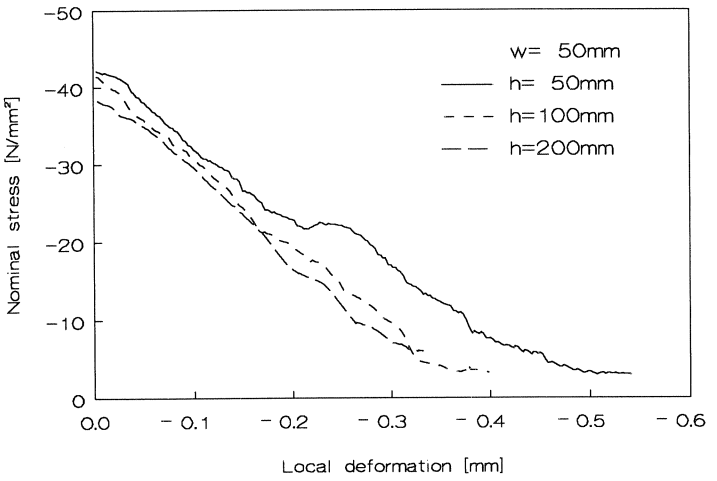

Fig. 72. Post-peak stress-deformation curves, which are corrected for the pre-peak inelastic deformations.

Fig. 73 shows the distribution of damage, the damage parameter $\varkappa$ of the interface model, for the different specimens at the end of the simulations. All specimens fail due to the formation of continuous patterns of inclined shear cracks, which are incidentally connected by more vertical splitting cracks.

Localization of cracking and deformations is most clearly found for the 200-mm-high specimen, which fails due to the formation of one crack band. The bottom half of the specimen shears off to the left, which allows the axial deformation of the specimen during softening. The forces introduced into the parts of the specimen which shear off, cause secondary cracks to be formed and the crack band to be widened. The same can be found in the specimens with a height of 50 and 100 mm, but it can not be recognized as easily, because the shear cracks zigzag through the specimen and are surrounded by the secondary cracks.

There is a tendency in the simulations to a more distributed crack formation, but it is less than what is observed in the test results. The 50-mm-high specimen shows the most significant spread in cracking. This is reflected by the slightly more ductile post-peak behaviour. In this simulation, the left part of the shear crack pattern locked up during shearing, which resulted in the increase of the post-peak toughness observed in Fig. 71 and the splitting cracks in Fig. 73. This was due to the fact that new contacts were created as a result of the shearing of the cracks and that a piece of mortar was torn loose and got stuck in the shearing crack. This caused a redistribution of forces, which resulted in additional cracking in the left part of the specimen. It shows that taking geometrical nonlinearity into account is an essential aspect of this type of calculation. It shows further that it will be necessary to increase the geometrical heterogeneity in the model to find a cracking and failure process which comes closer to the test results. A more significant heterogeneity will stimulate the formation of additional cracks

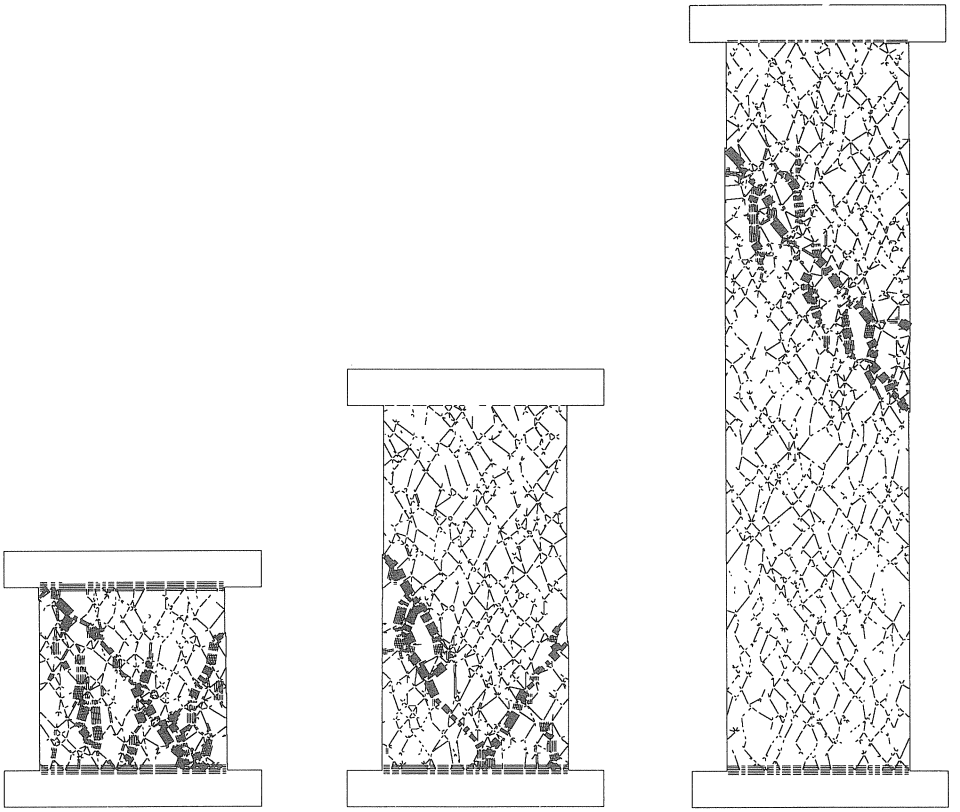

(a) (b) (c)

Fig. 73. Distribution of damage (damage parameter $\varkappa$ of the constitutive model) for the different specimens at the end of the simulations:
(a) h = 50 mm, $\sigma = -2.99$ N/mm^2, $\varepsilon = -11.4$ ‰
(b) h = 100 mm, $\sigma = -3.28$ N/mm^2, $\varepsilon = -4.5$ ‰
(c) h = 200 mm, $\sigma = -5.95$ N/mm^2, $\varepsilon = -2.1$ ‰

and will make the influence of the volume of a specimen on the failure process more significant. It is not unlikely that a part of the necessary increase in the heterogeneity can be found in extending the model to the third dimension. Also an increase of the coefficient of friction and the dilatancy can help too. It was shown by Hobbs & Ord [1990] that the size of a shear band in a heterogeneous material increases when the friction or the dilatancy are increased.

7 Restrospective view

Subject of research

In this work softening of concrete specimens loaded in uniaxial compression was investigated. Softening is caused by a crack-growth process. It is a property of a struc-

ture and not of a material. Due to the localization of cracking, which is the most salient feature connected to softening, the response of a softening specimen is a combined response of a local and a continuous process. Therefore it depends on the size of the specimen or structure. It can not be described by a simple continuum model, but additionally fracture mechanics have to be used to describe the local behaviour of the cracks causing the softening. The process of cracking causing compressive softening is complex and not well known. Is is highly sensitive to the boundary conditions applied in tests. Their role is often not easy to estimate. Therefore a micromechanical model using fracture mechanics was used to investigate the phenomenon of compressive softening. Such a model provides the opportunity to investigate the crack growth in a concrete specimen as it is influenced by the composition, the dimensions and the boundary conditions. It describes softening as the response of a structure. To verify the model results, a comparison was made to experimental results. A special crack-detection technique was developed to be able to investigate the internal crack patterns in the tested concrete specimens.

Micromechanical model

The micromechanical model developed in this research describes concrete as a two-phase material consisting of large aggregates in a mortar matrix. Its mechanical behaviour is analysed by means of finite element analysis and fracture mechanics. Most characteristic of the model is its randomly generated continuous mesh of interface elements between the continuum elements of which the geometry depends on the large aggregates in the concrete. It describes all potential crack paths. No cracking is allowed in the continuum elements. A new constitutive law was developed to describe the failure of the interfaces under combinations of tensile and shear loading. The heterogeneity of concrete is further modelled by different moduli of elasticity for aggregate and mortar and different strengths for interfaces between aggregate and mortar and interfaces in the mortar.

Process of softening

For compressive failure, the axial stress-deformation relation, the lateral expansion and the crack-growth process are described well by the micromechanical model. The crack growth in the pre-peak regime is described by the model as it is described by Hsu et al. [1963]. First, microcracks gradually grow in size along the interfaces between the aggregates and the mortar. They stay distributed. At 75% of peak stress, the cracks start to grow through the mortar and the rate of crack growth accelerates. The cracks grow further in size. At peak stress the growth of the final macrocrack pattern starts. Then, the size of the cracks jumps from the microlevel to the structural level. Localization of cracking and deformations is found. The first softening past peak stress is mainly due to the formation of the final macrocrack pattern necessary to have a failure mechanism. The specimen is split up in a number of irregularly shaped pieces which shear off. Further softening is mainly due to a reduction of the mechanical resistance of the already existing macrocrack pattern, which is caused by the opening and shearing of the cracks.

Importance of shear cracking

Not the splitting cracks but the shear cracks are most important for compressive failure because they are essential to the failure mechanism and their formation takes relatively more energy than that of the splitting cracks. Many splitting cracks are prominently visible, but only modify compressive failure. Shear cracks are often not well visible, because their length is relatively small and because they do often not open far. This explains why splitting cracks are not seldom mentioned to be the cause of compressive failure. However, the kinematics of such a failure mode are not very clear. The relative importance of the splitting cracks is shown by the fact that there are examples of uniaxial and multiaxial compression tests that show failure due to the formation of shear cracks only. The simulations with the micromechanical model support the postulate that shear failure is the most important cause of compressive failure. Compressive failure in the model is mainly determined by the material parameters describing shear failure, while the tensile parameters only modify it.

Tensile failure

The micromechanical model is also able to give a realistic description of tensile failure. The results of the simulations compare well with the test results of Van Mier [1991]. The model shows that the long tail of the stress-deformation relation is due to the formation of overlaps between cracks, which are caused by the heterogeneous structure of concrete.

Lateral boundary restraint

Due to the fact that lateral expansion is essential to the formation of a failure mechanism, a lateral confinement has also a great influence on compressive failure. As a consequence, the restraint to the lateral expansion of a concrete specimen by the loading platens can also have a great influence and should never be neglected when analysing experimental results. Depending on the boundary restraint, the behaviour of a cubic specimen can vary from ductile to brittle. The micromechanical model can very well describe this change in structural behaviour due to a varying lateral boundary restraint.

Steel brushes slow down compressive softening more and more when the lateral expansion of the specimen increases. This is not so in the case of teflon platens, where the restraining shear stresses decrease during softening. Then a more brittle failure is found. It is difficult to estimate how brittle concrete behaviour is for a zero boundary restraint. This is of relative importance. A model should be able to describe concrete failure under the complete range of lateral boundary conditions.

Size-effect

Due to localization of cracking a size effect is present in the softening response of concrete specimens under uniaxial compressive loading. This size effect is more complex than that for tensile loading. Similarity was indicated by test results of Van Mier [1984]. In the present work it was shown that in the test results of Van Mier,

besides a size effect due to localization of cracking, an additional size effect was present due to the lateral boundary restraint by the steel brushes that he used in his tests. Therefore new tests were carried out using teflon platens which were shown to slow down softening less than steel brushes do and thus introduce a smaller size effect due to their presence. The results of these tests show that compressive softening is more complex than tensile softening. The fracture process is not only determined by a local component, as in tension, but also by a continuum component. This is confirmed by the crack patterns. In high specimens the splitting cracks start to play a more important role, because their length increases with the length of the specimen. The micromechanical model predicts the size effect in compressive softening well, but overestimates it for the default set of parameters. This is due to the fact that it overestimates the localization of cracking, or thus underestimates the spread in cracking.

Evaluation of the micromechanical model

It was shown that the proposed micromechanical model can be used well to investigate softening of concrete in order to get a better understanding of the process causing it. The two-phase structure of aggregates in a mortar matrix combined with the continuous mesh of interfaces seems to be sufficient to simulate qualitatively the most important features of the structural behaviour of a softening concrete specimen loaded in tension or in compression. Comparison with test results indicates that, in order to get a closer fit to test results, it will be necessary to increase the geometrical heterogeneity. This wil increase the spread in cracking. It can be done by modelling the microstructure down to a smaller scale level than was done up to now or by changing the model from two-dimensional to three-dimensional. It was shown in this work that modelling of the heterogeneity increases the post-peak ductility. This means that the softening introduced on the microlevel has to be reduced when the modelling of the heterogeneous structure is extended further. It points at the possibility that concrete softening can probably be modelled adequately by modelling it brittle at the microlevel.

One thing should be kept in mind when using a two-dimensional heterogeneous model and that is that it is still homogeneous in the third dimension. This means that three-dimensional properties and processes have to be translated to equivalent two-dimensional ones. This will certainly have its limitations and can be the cause that not all features of the three-dimensional process can be described with the desired accuracy.

Acknowledgements

The author wishes to express his thanks to prof. dr. ir. H. S. Rutten, dr. ir. J. G. M. van Mier and ir. H. J. Fijneman for their support and stimulating discussions during the research. Prof. dr.-ing. K. Willam is also thanked for discussions and comment.
The author is indebted to all co-workers of the Department of Structural Design, the co-workers of the Pieter van Musschenbroek Laboratory and the computer experts of the university for their valuable assistance.
The financial support of the Netherlands Technology Foundation (STW) is gratefully acknowledged.

Notations

c	cohesion
d_{max}	maximum-aggregate size
E	modulus of elasticity
F	force
f_t	tensile strength
h	height
G_f	fracture energy
K	stiffness
l	length
m	mass
t	time
v	velocity
w	displacement
ε	strain
$\varkappa$	damage parameter
υ	Poisson's ratio
τ	shear stress
σ	normal stress
φ	friction angle
χ	reduction angle of tensile strength in the presence of a shear stress
ψ	dilatancy angle

subscripts

a	aggregate
b	bond
m	mortar
1	normal
2	tangential

References

ACI committee 446 (1990), Fracture mechanics of concrete: concepts, models and determination of material properties, Concrete International, 12 (12), 67–70.

Bartenev, G. M. and Lavrentev, V. V. (1981), Friction and Wear of Polymers, Tribology series 6, eds. L. H. Lee & K. C. Ludema, Elsevier, Amsterdam.

Bazant, Z. P. (1976), Instability, ductility and size effect in strain-softening concrete, Journal of the Engineering Mechanics Division, ASCE, 102 (EM2), 331–344.

Bazant, Z. P. (1983), Comment on orthotropic models for concrete and geomaterial, Journal of Engineering Mechanics, ASCE, 109 (3), 849–865.

Bazant, Z. P. (1986), Mechanics of distributed cracking, Applied Mechanics Review, 39 (5), 675–705.

Bazant, Z. P. and Gambarova, P. G. (1984), Crack shear in concrete: crack band microplane model, Journal of Structural Engineering, ASCE, 110 (9), 2015–2035.

Bazant, Z. P. and Oh. B. H. (1985), Microplane model for progressive fracture of concrete and rock, Journal of Engineering Mechanics, ASCE, 111 (4), 559–582.

Bazant, Z. P., Bishop, F. C. and Chang, T. P. (1986), Confined compression tests on cement paste and concrete up to 300 ksi, ACI Journal, 83 (48), 553–560.

Bazant, Z. P., Tabbara, M. R., Kazemi, M. T. and Pijaudier-Cabot, G. (1990), Random particle model for fracture of aggregate or fiber composites, Journal of Engineering Mechanics, ASCE, 116 (8), 1686–1705.

Bieniawski, Z. T. (1967), Mechanism of brittle fracture of rock, part I, II and III, International Journal of Rock and Mining Science, 4, 395–430.

Carrasquillo, R. L., Slate, F. O. and Nilson, A. H. (1981), Microcracking and behavior of high strength concrete subject to short-term loading, ACI Journal, 78, 179–186.

CEB-FIP (1991), CEB-FIP Model Code 1990, Final draft, Bulletin d'information No. 203, 204 and 205, CEB, Lausanne.

Cornelissen, H. A. W., Hordijk, D. A. and Reinhardt, H. W. (1986), Experiments and theory for the application of fracture mechanics to normal and lightweight concrete, in Fracture Toughness and Fracture Energy of Concrete, ed. F. H. Wittman, Elsevier Science Publishers, Amsterdam, 565–575.

Cundall, P. A. (1971), A computer model for simulating progressive large scale movements in blocky rock systems, in Proceedings of the Symposium of the International Society of Rock Mechanics, Nancy, France, 1 (II-8).

Cundall, P. A. (1982), Adaptive density scaling for time-explicit calculations, in Proceedings of the 4th International Conference on Numerical Methods in Geomechanics, Edmonton, 23–26.

Cundall, P. A. and Strack, O. D. L. (1979), A discrete numerical model for granular assemblies, Géotechnique, 29 (1), 47–65.

De Borst, R. (1986), Non-linear Analysis of Frictional Materials, PhD Thesis, Delft University of Technology, The Netherlands.

De Borst, R. (1989), Analysis of spurious kinematic modes in finite element analysis of strain-softening solids, in Cracking and Damage, eds. J. Mazars & Z. P. Bazant, Elsevier Applied Science, London, 335–345.

De Borst, R. (1991), Continuum models for discontinuous media, in Fracture Processes in Concrete, Rock and Ceramics, RILEM Proceedings 13, eds. J. G. M. Van Mier, J. G. Rots & A. Bakker, E. & F. N. Spon, London, 601–618.

Di Tomasso, A. (1984), Evaluation of concrete fracture, in Fracture mechanics of concrete, eds. A. Carpinteri & A. R. Ingraffea, Martinus Nijhoff Publishers, The Hague, 31–65.

Duda, H. (1991), Grain model for the determination of the stress-crack-width-relation, in Analysis of Concrete Structures by Fracture Mechanics, RILEM Proceedings 6, eds. L. Elfgren & S. P. Shah, Chapman & Hall, London, 88–96.

El-Rahman, M. and Shrive, N. G. (1984), Crack initiation in multiaxial compressive stress fields, in Proceedings of RILEM-CEB Symposium on Concrete under Multiaxial Conditions, INSA, Toulouse, 220–229.

ELFGREN L. (ed.) (1989), Fracture Mechanics of Concrete Structures, RILEM Report 3, Chapman & Hall, London, 1989.

GERSTLE, K. H., LINSE, D. L., BERTACCHI, P., KOTSOVOS, M. D., KO, H. Y., NEWMAN, J. B., ROSSI, P., SCHICKERT, G., TAYLOR, M. A., TRAINA, L. A., ZIMMERMAN, R. M. and BELLOTTI, R. (1978), Strength of concrete under multiaxial stress states, in Concrete and Concrete Structures, Proceedings of the Douglas McHenry International Symposium, SP 55-5, ACI, 103-131.

GERSTLE, K. H., ASCHL, H., BELLOTTI, R., BERTACCHI, P., KOTSOVOS, M. D., KO, H. Y., LINSE, D., NEWMAN, J. B., ROSSI, P., SCHICKERT, G., TAYLOR, M. A., TRAINA, L. A., WINKLER, H. and ZIMMERMAN, R. M. (1980), Behavior of concrete under multiaxial stress states, Journal of the Engineering Mechanics Division, ASCE, 106 (EM6), 1383-1403.

GOPALARATNAM, V. S. and SHAH, S. P. (1985), Softening response of plain concrete in direct tension, ACI Journal, 82, 310-323.

GOUDSWAARD, I. and VONK, R. A. (1989), A detection method for internal cracks in concrete specimens, Report TUE-BKO-89.12, Eindhoven University of Technology, The Netherlands (in Dutch).

HILLERBORG, A. (1988), Rotational capacity of reinforced concrete beams, Nordic Concrete Research, 7, Norske Betonforening, Oslo, 121-134.

HILLERBORG, A. (1991), Size dependency of the stress-strain curve in compression, in Analysis of Concrete Structures by Fracture Mechanics, RILEM Report 6, eds. L. Elfgren & S. P. Shah, Chapman & Hall, London, 171-178.

HILLERBORG, A. and ROTS, J. (1989), Crack concepts and numerical modelling, Chapter 5 in Fracture Mechanics of Concrete Structures, ed. L. Elfgren, RILEM Report 3, Chapman & Hall, London, 128-146.

HILLERBORG, A., MODÉER, M. and PETERSSON, P. E. (1976), Analysis of crack formation and crack growth in concrete by means of fracture mechanics and finite elements, Cement and Concrete Research, 6, 773-782.

HILSDORF, H. (1965), Die Bestimmung der Zweiachsiger Festigkeit des Betons, Deutscher Ausschuss für Stahlbeton, 173, Berlin.

HOBBS, B. E. and ORD, A. (1989), Numerical simulation of shear band formation in a frictional-dilational material, Ingenieur-Archiv, 59, 209-220.

HORDIJK, D. A. (1989), Deformation-Controlled Uniaxial Tensile Tests on Concrete, Report 25.5-89-15/VFA, Stevin Laboratory, Delft University of Technology, The Netherlands.

HORDIJK, D. A. (1991), Local Approach to Fatigue of Concrete, PhD Thesis, Delft University of Technology, The Netherlands.

HORDIJK, D. A., REINHARDT, H. W. and CORNELISSEN, H. A. W. (1987), Fracture mechanics parameters of concrete from uniaxial tensile tests as influenced by specimen length, in preprints of Proceedings of the SEM-RILEM International Conference on Fracture of Concrete and Rock, Houston, USA, eds. S. P. Shah & S. E. Swartz, 138-149.

HORDIJK, D. A., VAN MIER, J. G. M. and REINHARDT, H. W. (1989), Material properties, Chapter 4 in Fracture Mechanics of Concrete Structures, RILEM Report 3, ed. L. Elfgren, Chapman & Hall, Londen, 67-127.

HORII, H. and NEMAT-NASSER, S. (1985), Compression-induced microcrack growth in brittle solids: axial splitting and shear failure, Journal of Geophysical Research, 90 (B4), 3105-3125.

HORII, H. and NEMAT-NASSER, S. (1986), Brittle failure in compression: splitting, faulting and brittle-ductile transition, Philosophical Transactions, Royal Society of London, A319, 337-374.

HSU, T. T. C., SLATE, F. O., STURMAN, G. M. and WINTER, G. (1963), Microcracking of plain concrete and the shape of the stress-strain curve, ACI Journal, 60 (14), 209-224.

HUDSON, J. A., BROWN, E. T. and FAIRHURST, C. (1972), Shape of the complete stress-strain curve for rock, in Stability of Rock Slopes, Proceedings of the 13th Symposium on Rock Mechanics, 1971, University of Illinois, Urbana, ed. E. J. Cording, ASCE, 773-795.

HUGHES, B. P. and ASH, J. E. (1970), Anisotropy and failure criteria for concrete, Materials and Structures, RILEM, 3 (18), 371-374.

INGRAFFEA, A. R. and PANTHAKI, M. J. (1985), Analysis of shear fracture tests of concrete beams, in Proceedings of Seminar on Finite Element Analysis of Reinforced Concrete Structures, Tokyo, 1, 71-91.

INGRAFFEA, A. R. and SAOUMA, V. (1985), Numerical modelling of discrete crack propagation in reinforced and plain concrete, in Fracture Mechanics of Concrete, eds. G. Sih & A. Di Tomasso, Martinus Nijhoff Publishers, Dordrecht, The Netherlands, 171–225.

Itasca Consulting Group, Inc. (1989), UDEC (Universal Distinct Element Code), Volume 1, Software Summary, Topical Report 006-01-T12, Minneapolis Minnesota, USA.

JAMET, P., MILLARD, A. and NAHAS, G. (1984), Triaxial behaviour of a microconcrete – complete stress-strain curves for confining pressures ranging from 0 to 100 MPa, in Proceedings of RILEM-CEB Symposium on Concrete under Multiaxial Conditions, INSA Toulouse, session 4, experimental results, 1, 133–140.

KNAB, L. I., JENNINGS, H., WALKER, H. N. and CLIFTON, J. R. (1986), Techniques to observe the fracture zone in mortar and concrete, in Fracture Toughness and Fracture Energy of Concrete, ed. F. H. Wittmann, Elsevier Science Publishers B.V., Amsterdam, 241–247.

KOTSOVOS, M. D. (1983), Effect of testing techniques on the post-ultimate behaviour of concrete in compression, Materials and Structures, RILEM 16 (91), 3–12.

LINSE, D. (1978), Lösung Versuchstechnischer Fragen bei der Ermittlung des Festigkeits und Verformungsverhaltens von Beton unter dreiachsiger Belastung, Deutscher Ausschuss für Stahlbeton, 292, Berlin.

LORIG, L. J. and CUNDALL, P. A. (1989), Modeling of reinforced concrete using the distinct element method, in Fracture of Concrete and Rock, Proceedings of SEM-RILEM International Conference, Houston, Texas, USA, 1987, eds. S. P. Shah & S. E. Swartz, Springer-Verlag, New York, 276– 287.

NEWMAN, K. and SIGVALDASON, O. T. (1965–1966), Testing machine and specimen characteristics and their effect on the mode of deformation, failure and strength of materials, in Proceedings of the Institution of Mechanical Engineers, 180 (3A), 399–410.

NOJIRI, Y., KOTANI, K. and ABE, Y. (1984), Failure envelope of concrete subjected to multiaxial compressive stresses, in Proceedings of RILEM-CEB Symposium on Concrete under Multiaxial Conditions, INSA Toulouse, 141–148.

OZBOLT, J. and BAZANT, Z. P. (1991), Cyclic microplane model for concrete, in Fracture Processes in Concrete, Rock and Ceramics, RILEM Proceedings 13, eds. J. G. M. Van Mier, J. G. Rots & A. Bakker, E. & F. N. Spon, London, 639–650.

OZBOLT, J. and ELIGEHAUSEN, R. (1991), Analysis of reinforced concrete beams without shear reinforcement using non-local microplane model, in Fracture Processes in Concrete, Rock and Ceramics, RILEM Proceedings 13, eds. J. G. M. Van Mier, J. G. Rots & A. Bakker, E. & F. N. Spon, London, 919–930.

PATERSON, M. S. (1978), Experimental Rock Deformation – The Brittle Field, Springer-Verlag, Berlin.

PRAMONO, E. and WILLAM, K. (1989), Fracture energy-based plasticity formulation of plain concrete, Journal of Engineering Mechanics, 115 (6), 1183–1204.

READ, H. E. and HEGEMIER, G. A. (1984), Strain softening of rock, soil and concrete – a review article, Mechanics of Materials, 3, 271–294.

ROELFSTRA, P. E. (1989), Simulation of strain localization processes with numerical concrete, in Cracking and Damage, eds. J. Mazars & Z. P. Bazant, Elsevier Applied Science, London, 79–90.

ROELFSTRA, P. E. and SADOUKI, H. (1986), Fracture process in numerical concrete, in Fracture Toughness and Fracture Energy of Concrete, ed. F. H. Wittman, Elsevier Science Publishers BV, Amsterdam, 105–116.

ROKUGO, K. and KOYANAGI, W. (1992), Role of compressive fracture energy of concrete on the failure behaviour of reinforced concrete beams, in Applications of Fracture Mechanics to Reinforced Concrete, ed. A. Carpinteri, Elsevier Applied Science, London, 437–464.

ROTS, J. G. (1988), Computational Modeling of Concrete Fracture, PhD thesis, Delft University of Technology, The Netherlands.

RÜSCH, H. and HILSDORF, H. (1963), Verformungseigenschaften von Beton unter zentrischen Zugspannungen, Bericht Nr. 44, Materialprüfungsamt für das Bauwesen der Technischen Hochschule München.

SCHICKERT, G. (1980), Schwellenwerte beim Betondruckversuch, Deutscher Ausschuss für Stahlbeton, 312, Berlin.

SCHLANGEN, E. and VAN MIER, J. G. M. (1991), Boundary effects in mixed mode I and II fracture of concrete, in Fracture Processes in Concrete, Rock and Ceramics, RILEM Proceedings 13, eds. J. G. M. Van Mier, J. G. Rots & A. Bakker, E & F. N. Spon, London, 705-716.

SCHLANGEN, E. and VAN MIER, J. G. M. (1992), Experimental and Numerical Analysis of Micromechanisms of Fracture of Cementbased Composites, Cement and Concrete Composites, 14, (2), 105-118, Report 25.5-91-1/VFC, Stevin Laboratory, Delft University of Technology, The Netherlands.

SHAH, S. P. and SANKAR, R. (1987), Internal cracking and strain softening response of concrete under uniaxial compression, ACI Materials Journal, 84 (3), 200-212.

SIMHA, K. R. Y., FOURNEY, W. L., BARKER, D. B. and DICK, R. D. (1986), Dynamic photoelastic investigation of two pressurized cracks approaching one another, Engineering Fracture Mechanics, 23, 237-249.

SLATE, F. O. (1983), Microscopic observation of cracks in concrete, with emphasis on techniques developed and used at Cornell University, in Fracture Mechanics of Concrete, ed. F. H. Wittmann, Elsevier Science Publishers BV, Amsterdam, 75-93.

SOERS, E. and MEYSKENS, M. (1987), Concrete petrography - microscopic investigation of concrete, Cement, 11, 16-22, The Netherlands (in Dutch).

STANKOWSKI, T. (1990), Numerical Simulation of Progressive Failure in Particle Composites, PhD thesis, University of Colorado, Boulder, USA.

STEINMANN P. and WILLAM, K. (1991), Finite elements for capturing localized failure, Applied Mechanics, Springer-Verlag, 61, 259-275.

STROEVEN, P. (1973), Some Aspects of the Micromechanics of Concrete, PhD thesis, Delft University of Technology, The Netherlands.

TORRENTI, J. M., DESRUES, J., ACKER, P. and BOULAY, C. (1989), Application of stereophotogrammetry to the strain localization in concrete compression, in Cracking and Damage, eds. J. Mazars & Z. P. Bazant, Elsevier Applied Science, London, 30-41.

VAN MIER, J. G. M. (1984), Strain-softening of Concrete under Multiaxial Loading Conditions, PhD thesis, Eindhoven University of Technology, The Netherlands.

VAN MIER, J. G. M. (1986a), Multiaxial strain-softening of concrete, part I: fracture, part II: load-histories, Materials and Structures, RILEM, 19, (111), 179-200.

VAN MIER, J. G. M. (1986b), Fracture of Concrete under Complex Stress, Heron, 31 (3).

VAN MIER, J. G. M. (1991), Mode I fracture of concrete: discontinuous crack growth and crack interface grain bridging, Cement & Concrete Research, 21 (1), 1-15.

VONK, R. A. (1989), Influence of boundary conditions on softening of concrete loaded in compression, Report TUE-BKO-89.14, Eindhoven University of Technology, The Netherlands.

VONK, R. A. (1990), Constitutive Model describing Interface Behaviour with Tensile and Shear Softening, Report TUE-BKO-90.12, Eindhoven University of Technology, The Netherlands.

VONK, R. A. (1992), Softening of Concrete loaded in Compression, PhD thesis, Eindhoven University of Technology, The Netherlands.

VONK, R. A., RUTTEN, H. S., VAN MIER, J. G. M. and FIJNEMAN, H. J. (1989), Influence of boundary conditions on softening of concrete loaded in compression, in Fracture of Concrete and Rock: Recent Developments, eds. S. P. Shah, S. E. Swartz & B. Barr, Elsevier Applied Science, London, 711-720.

VONK, R. A., RUTTEN, H. S., VAN MIER, J. G. M. and FIJNEMAN, H. J. (1990), Size effect in softening of concrete loaded in compression, in Fracture Behaviour and Design of Materials and Structures, ed. D. Firrao, EMAS, United Kingdom, 767-772.

VONK, R. A., RUTTEN, H. S., VAN MIER, J. G. M. and FIJNEMAN, H. J. (1991), Micromechanical simulation of concrete softening, in Fracture Processes in Concrete, Rock and Ceramics, eds. J. G. M. Van Mier, J. G. Rots & A. Bakker, RILEM Proceedings 13, E & F. N. Spon, London, 129-138.

WALRAVEN, J. C. (1980), Aggregate Interlock; a Theoretical and Experimental Analysis, PhD thesis, Delft University of Technology, The Netherlands.

WILLAM, K., STANKOWSKI, T., RUNESSON, K. and STURE, S. (1989), Simulation issues of distributed and localized failure computations, in Cracking and Damage, eds. J. Mazars and Z. P. Bazant, Elsevier Applied Science, London, 363–378.
WISCHERS, G. (1978), Aufnahme und Auswirkungen von Druckbeanspruchungen auf Beton, Betontechnische Berichte, 19, 31–56.
ZUBELEWICZ, A. and BAZANT, Z. P. (1987), Interface element modeling of fracture in aggregate composites, Journal of Engineering Mechanics, ASCE, 113, 1619–1630.